Summer 2016

An experimental examination of combustion of isolated liquid fuel droplets with polymeric and nanoparticle additives

Mohsen Ghamari
University of Iowa

AN EXPERIMENTAL EXAMINATION OF COMBUSTION OF ISOLATED LIQUID FUEL DROPLETS WITH POLYMERIC AND NANOPARTICLE ADDITIVES

by
Mohsen Ghamari

A thesis submitted in partial fulfillment
of the requirements for the Doctor of Philosophy
degree in Mechanical Engineering
in the Graduate College of
The University of Iowa

August 2016

Thesis Supervisor: Associate Professor Albert Ratner

Graduate College

The University of Iowa

Iowa City, Iowa

CERTIFICATE OF APPROVAL

_____

PH.D. THESIS

_____

This is to certify that the Ph.D. thesis of

Mohsen Ghamari

has been approved by the Examining Committee for the thesis requirement for the Doctor of Philosophy degree in Mechanical Engineering at the August 2016 graduation.

Thesis Committee: _____
Albert Ratner, Thesis Supervisor

_____
Ching-Long Lin

_____
H.S. Udaykumar

_____
James H.J. Buchholz

_____
Jennifer Fiegel

ACKNOWLEDGEMENTS

First and foremost, I would like to thank my advisor, Associate Professor Albert Ratner, for his continuous support and guidance during my Ph.D. study. His patience and the great amount of flexibility he provided allowed me to explore different aspects of my research. This study would not have come to fruition if it was not because of him being motivational and encouraging especially during tough times in my Ph.D. pursuit.

I would like to express my sincere gratitude to my thesis committee members, Professors Ching-Long Lin, H.S. Udaykumar, James Buchholz and Jennifer Fiegel for their time, interest, and insightful questions and comments.

The members of the Thermal-Fluid lab in the Department of Mechanical and Industrial Engineering have contributed immensely in my personal and professional life and have been a source of friendship as well as technical advice and collaboration. I appreciate them all especially Yunye Shi, Jianan Zhang, Matt Panzer, Majid Emadi and Xinhui Zhang.

In regards to designing the experimental arrangement and performing measurements, I thank Jared Becker and Shreshtee Yadav who were of great help especially in the first round of our my data analysis in Summer 2013. I also appreciate Daniel Schenck from Professor Fiegel's group in the University of Iowa College of Pharmacy and Dr. Gary Aurand from Department of Chemical and Biochemical Engineering for their time and guidance during my measurements of surface tension and viscosity.

Lastly, I wish to express my love to my mother for her unconditional love and support during all these years. And most of all for my loving, supportive, encouraging, and patient wife Nasibeh whose faithful support during all stages of this Ph.D. is so appreciated. Thank you.

Mohsen Ghamari
University of Iowa
August 2016

ABSTRACT

In spite of recent attention to renewable sources of energy, liquid hydrocarbon fuels are still the main source of energy for industrial and transportation systems. Manufactures and consumers are consistently looking for ways to optimize the efficiency of fuel combustion in terms of cost, emissions and consumer safety. In this regard, increasing burning rate of liquid fuels has been of special interest in both industrial and transportation systems. Recent studies have shown that adding combustible nano-particles could have promising effects on improving combustion performance of liquid fuels. Combustible nano-particles could enhance radiative and conductive heat transfer and also mixing within the droplet. Polymeric additive have also shown promising effect on improving fire safety by suppressing spreading behavior and splatter formation in case of crash scenario. Polymers are also known to have higher burning rate than regular hydrocarbon fuels. Therefore adding polymeric additive could have the potential to increase the burning rate.

In this work, combustion dynamics of liquid fuel droplets with both polymeric and nanoparticle additives is studied experimentally. High speed photography is employed and the effect of additive concentration on droplet burning rate, burning time, extinction and soot morphology is investigated.

Polymer added fuel was found to have a volatility controlled combustion with four distinct regimes. The first three zones are associated with combustion of base fuel while the polymer burns last and after a heating zone because of its higher boiling point. Polymer addition reduces the burning rate of the base fuel in the first zone by means of increasing viscosity and results in nucleate boiling and increased burning rates in the second and third stages. Overall, polymer addition resulted in a higher burning rate and shorter burning time in most of the scenarios. Colloidal suspensions of carbon-based nanomaterials in liquid fuels were also tested at different particle loadings. It was found that dispersing nanoparticles results in higher burning rate by means of enhanced radiative heat absorption and thermal conductivity. An optimum particle loading was found for each particle type at which the maximum burning rate was achieved. It was observed that the burning rate again starts to reduce after this optimum point most likely due to the formation of large aggregates that reduce thermal conductivity and suppress the diffusion of species.

PUBLIC ABSTRACT

In spite of recent attention to renewable sources of energy, liquid hydrocarbon fuels are still the main source of energy for industrial and transportation systems. Manufactures and consumers are consistently looking for ways to optimize the efficiency of fuel combustion in terms of cost, emissions and consumer safety. Increasing burning speed of liquid fuels has been of special interest especially in aerial transportation sector. Burning rate dictates issues such as maximum combustor power, and can be used to improve either the size or power output of a combustor. In this regard, polymers are known to have higher burning rate than regular hydrocarbon fuels. Nanomaterials have also better thermal and optical properties compared to bulk materials and are known to improve heat transfer in liquids. In this thesis, trace amounts of a long-chain polymer as well as several types of carbon based nanomaterials with different morphologies are added to liquid fuel and combustion of liquid fuel droplets, as the main building block of a spray system, is examined experimentally. In general, both additives resulted in faster burning of liquid fuel which could be interpreted as higher energy in specific period of time or smaller engine size. It was also found that the shape and physical properties of nanomaterial additives could play an important role on the combustion behavior of liquid fuel.

TABLE OF CONTENTS

LIST OF TABLES

LIST OF FIGURES

1 INTRODUCTION

1.1 Background and Motivation

In spite of the recent attention to renewable and sustainable sources of energy such as wind, solar and biomass, fossil fuels are still the major source of energy in the world with 82% of world energy supply in 2011 [1]. The fraction in the US is quite similar and fossil fuels account for about 80% of energy supply. Petroleum, as a liquid fuel, is the main form of fossil fuel in the US by supplying 36% of the total energy and is followed by natural gas and coal with 27% and 18% energy supply respectively. While the main users of petroleum in the US are transportation and industrial sectors with 71% and 25%, the contribution of liquid fuel in transportation sector is more significant and 92% of energy in this sector is provided by liquid fuels [2]. However, transportation systems are not the only users of liquid fuel and many other combustor systems such as gas turbines, boilers, liquid fuel rocket engines as well as many industrial burners and furnaces use liquid fuel as the energy source. Ease of handling, storage and transportation, high energy content and very diverse range of applications are the main reasons that have made liquid fuels so popular.

For liquid fuel to burn and release its energy in any of the aforementioned applications, it should first go through a series of processes to convert to fuel vapor and be ready to mix with the oxidizer. This is obtained by atomizing liquid into very small droplet to increase fuel surface area exposed to hot gases and enhance gasification and mixing. Therefore, atomization is a crucial step in liquid fuel combustion and needs special attention in order to improve combustion characteristics. There have been numerous studies on both spray and droplet combustion to better understand design criteria of an efficient and stable combustor, to determine heat transfer rate and also to examine the formation of pollutant emissions.

During spray, both modes of heterogeneous (i.e. drop combustion either in groups or individually) and homogeneous (i.e. fuel drops of less than 10 microns) combustion occur. In the early twentieth century, the studies on spray combustion were focused on droplets size and velocity distribution. However, when it comes to combustion analysis,

complex and random nature of spray combustion imposes many difficulties. Normally a liquid spray consists of many small drops. So the simplest analysis is to consider the fuel spray as an aggregate of single droplets. With such assumption, one might estimate the combustion rate of spray as the sum of combustion rates of isolated droplets. However, an isolated droplet combustion does not fully represent drop combustion in the spray because of many phenomena available in spray and yet absent in isolated drop combustion [3]. In reality, droplets in fuel spray are very close to each other and may not be considered as isolated from each other. Interactions between droplets in spray is very complex and combined effect of many parameters such as turbulence, temperature, pressure, wall-droplet interaction, and acoustic. is involved. Nevertheless, spray experiments may only provide insight on global effects of droplet interactions and do not provide a controlled environment to study effect of specific parameters on combustion. On the other hand, isolated drop experiments could provide the opportunity to study the effect of each parameter separately. Furthermore, in certain situations the flow field is sufficiently simple that the combustion process of an isolated droplet could be considered for detailed theoretical and experimental studies. Therefore, sometimes it is useful to consider droplet combustion as a model scenario to provide insight on complex phenomena governing heterogeneous combustion [4].

In studying vaporization and combustion of isolated droplets, the effect of convection must be considered. However, because of significant complexities that presence of convection imposes on heat and mass transport phenomena, the models of droplet vaporization and combustion have been presented for spherically symmetric droplets. The "Spherical Symmetry" is a condition in which convective flows (natural and forced convection) are sufficiently reduced and droplet, flame and soot shell are all spherical and concentric. For the spherically symmetric configuration shown in Figure 1.1a, transport is only possible in radial direction. In the liquid phase only diffusion exists but in the gas phase transport consists of both diffusion and diffusion induced convection or Stefan flow. When either or both of natural and forced convection present, a non-radial relative velocity is formed between the droplet and gas phase. This relative velocity exerts a shear stress on the surface of droplet which results in circulation inside the droplet [4]. To account for convective effects, several experimental investigations have been conducted to postulate

empirical correlations [5]. One of the most widely used empirical equations is the one developed by Wise et al. [6]:

$$K_{Forced} = K\left(1 + 0.24Re^{1/2}Pr^{1/3}\right) \tag{1.1}$$

Where Re is Reynolds number and Pr, Prandtl number, is assumed to be unity. In this equation K is the burning rate defined under spherical symmetry assumption:

$$D_d^2 = -Kt + D_0^2 \tag{1.2}$$

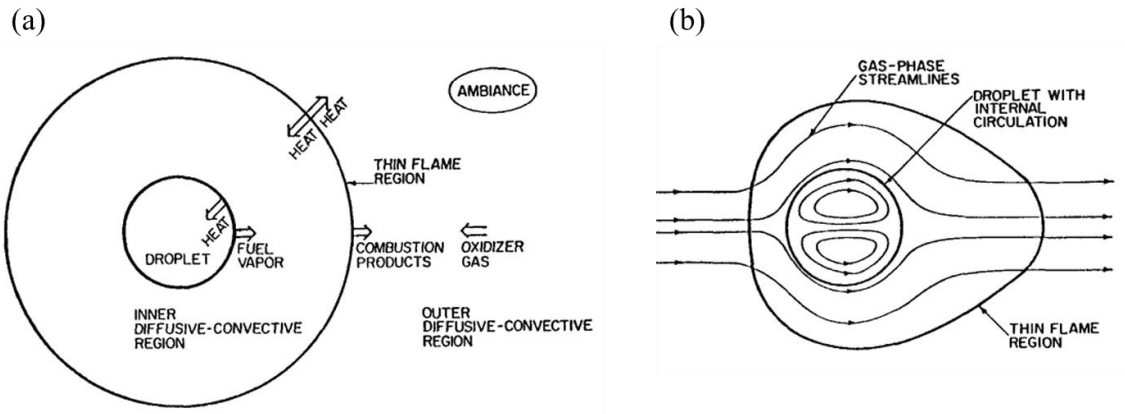

Figure 1.1 Schematic flow configuration of (a) spherically symmetric droplet combustion and (b) convective droplet combustion [4]

Equation 1.2 is known as D^2 law of combustion which states that the square of droplet diameter decreases linearly with time. In this equation D_d and D_0 are droplet instantaneous and initial diameters. Wise et al. also found that burning rate under conditions of natural convection is a function of Grashof Number, Gr. Such correlations could consistently be valid only when an accurate measurement of K is possible in the limit as $Re \to 0$ and $Gr \to 0$ [7] and this limit is obtained under zero gravity conditions.

Generally three main techniques have been used in experimental investigation of fuel droplet combustion: free drop, suspended drop and supporting drop method. The suspended and supported drop methods could also be used in microgravity test.

In a free drop technique, small droplets of the same size are generated in sequence and allowed to fall into a hot chamber or pass through a flat burner under gravitational force. The extent of vaporization and combustion processes are then recorded through high

speed imaging. This method is generally used to measure total burning rate and ignition delay of fuel droplets [8–11].

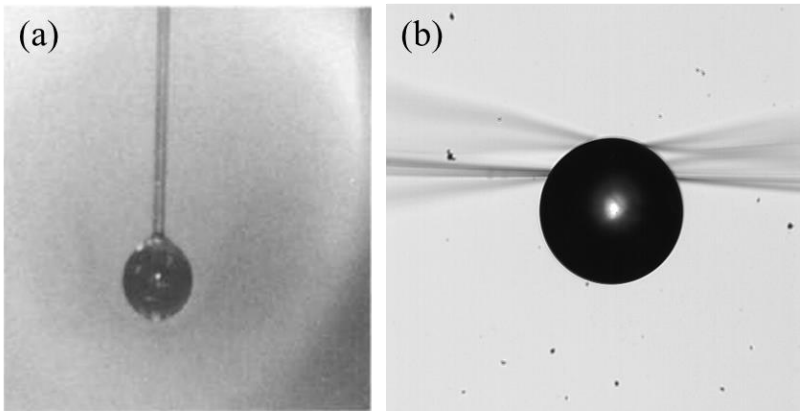

Figure 1.2 Anchoring droplet on fiber in two major experimental arrangements (a) suspended droplet technique [12] (b) supported droplet technique [13]

To remove the effect of natural and forced convection, Reynolds and Grashof Numbers should become zero or very infinitesimal:

$$Re = \frac{U_\infty D_d(t)}{\nu} \tag{1.3}$$

$$Gr = \frac{g\beta(T_s - T_\infty)D_d(t)^3}{\nu^2} \tag{1.4}$$

From equation 1.3 it is understood that if the motion of the droplet relative to its surrounding is controlled, Reynolds Number will become almost zero and consequently zero forced convection will be obtained. This is done by anchoring a droplet with a fiber through either the suspended or supported drop techniques (Figures 1.2a and b). In the suspended drop technique, a single droplet is suspended from a fiber made of a low conductivity material, such as quartz, ceramic or silicon carbide (SiC). The drop is then ignited and the extent of combustion is recorded for further analysis. This technique is also used in measurement of ignition delay when the suspending drop is exposed to hot stagnant environment for the auto-ignition to take place. Since the drop is suspended from a single fiber, not very thin fiber could be used. The fairly thick fiber (70-200 microns) used in this technique changes the shape of droplet from spherical to elliptical through high surface tension force. Therefore the fiber may influence combustion by altering droplet shape and flame structure. The large thickness could also influence burning rate through heat conduction and change soot propensity of fuel droplet. With the advancement of

technology very thin fibers (less than 20 microns) are now available. In the supported drop technique several fibers could be used in different arrangements to hold a single or even an array of droplets to study drop-drop interactions. The benefit of using very thin fiber is that effects of heat transfer and surface tension are minimized and more accurate burning rate can be measured.

If Grashof Number in suspended and supported drop techniques could be minimized, then the burning rate will be of a spherically symmetric drop. Based on equation 1.4, there are several ways that could yield a very small Gr; lower gravity, higher environment temperature and smaller droplets could reduce Gr. Also, $\nu = \frac{\mu}{\rho}$ and in ideal gas $\rho \propto p_\infty$, so $Gr \propto p_\infty^2$. Therefore, reducing environment pressure can also be considered as a way to reduce Gr and suppress natural convection. Among all of the methods, reducing gravity have been used frequently due to its simple concept. Microgravity on earth could be achieved through either dropping the experimental setup in a drop tower (or drop shaft) or by performing the test in a reduced gravity airplane. Drop tower is simply a very long vertical tube that could provide microgravity as low 10^{-6}g. The duration of microgravity interval is a function of tower height. For example the drop tower in NASA's Zero Gravity Facility is a 142 m long steel vacuum chamber which provides 5 seconds of microgravity [14]. On the other hand, reduced gravity airplanes could provide longer period of microgravity but need more operational logistics.

In application of liquid fuels and when it comes to utilizing it, the physico-chemical properties of the fuel have been altered to achieve better performance. These modifications target a wide range of properties such as viscosity, surface tension, vapor pressure, boiling point, and soot propensity and are meant to influence performance characteristics such as burning rate, pollutant emission, safety and engine efficiency. For many years and as long as requirements of engines and emission were not very strict, study of multicomponent fuel was not of any importance. However, with the current stringent environmental regulations and also engines' sensitivity to fuel composition, any change in fuel properties should be well examined and understood. Furthermore, a commercial liquid fuel is actually a blend of many different components that each behave differently compared to the blend. Even so, usually a mixture of a certain number of components, known as a surrogate, could

represent its properties. Since understanding kinetics governing combustion of a binary (two components) or multicomponent fuel has less complexity compared to a commercial fuel, it is normally useful to consider surrogates in order to clearly understand the influence of any modification or additive on fuel.

In the area of liquid fuel modification, reducing pollutant emission has always been one of the main motives that has driven research in the field. It has been known for a long time that injecting water or steam into an engine could reduce thermal NO formation, but due to technical complexity it was not always practical especially as a design modification for the existing engines and gas turbines. The idea of direct addition of water to fuel received attention in the 1970s [15]. It was found that that water addition could be very advantageous in reducing different types of pollutants; thermal NO as one of the major portions of NO_x is direct product of high flame temperature in an engine. Water addition could reduce flame temperature and reduce thermal NO emission accordingly. It also will increase OH radical production which are effective in oxidation of soot precursors. The difference in boiling temperature of water and base fuel will also result in heterogeneous nucleation and micro-explosion of liquid droplet. This micro-explosion atomizes the droplet into very smaller droplets that have shorter combustion time which is not long enough for pyrolytic reaction to proceed and form carbonaceous residues and particulate matter [15,16].

Oil in water emulsions have been also studied because of their fire resistant nature in the event of accidental fuel spill [17,18]. It is believed that presence of immiscible water in fuel droplet (e.g. diesel) prevents it from reaching its high boiling point and fuel vapor formation is suppressed. Therefore, even in presence of sufficiently intense ignition source, very little fuel vapor can be formed and the generated gas mixture will fall outside flammability limit (Figure 1.3)

Fire safety could also be attained through modifying fuel viscosity. Ameri et al. showed that adding long chain polymers to transportation fuel will induce non-Newtonian shear thickening behavior in the fuel [19]. The imparted non-Newtonian viscosity will change the behavior of fuel in the event of impacting a surface, like fuel spillage in a crash

scenario, and will suppress formation of mist and splatter which are more susceptible to combustion due their larger surface to volume ratio (Figure 1.4).

Figure 1.3 (left) Combustion of untreated liquid fuel (right) Combustion and extinction of emulsified fire-resistant fuel [20]

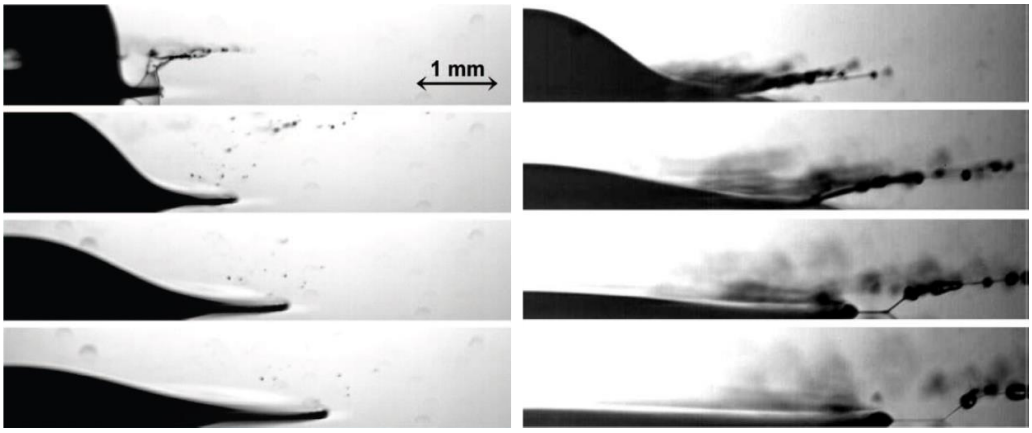

Figure 1.4 Spread test of liquid fuel droplet on a surface for (left) Jet-A fuel without additive (right) Jet-A fuel with polymeric additive [19]

Study of multicomponent fuel is not limited to only water-oil emulsions, surrogates or physico-chemically modified fuels. Utilization of coal in liquid form has always been one of engineers' dreams after invention of internal combustion engine. Coal as one of the most abundant and wide-spread resources of energy in the world has been one of the main energy sources for many years. However, its poor environmental credentials and also its solid state of matter has made limitation on its practical application. Coal liquefaction technologies are still very expensive and have their own environmental issue such a high CO_2 emission from gasification process or from heat and gas input to the reactors. The idea of crushing coal into micro meter sized particles and mixing it with oil in order to directly burn in industrial furnaces became attractive in 70s. However, agglomeration of coal particles and unstable physical state of mixture brought up some challenges that was hoped to be solved by scientific and technological advances in future years.

1.2 Objectives and Outline

The objective of this thesis is to examine combustion of liquid fuel droplets when mixed with polymeric additives or carbon nanoparticles. It was mentioned that polymer addition could have promising effects on improving fire safety of transportation fuel. However, the limited number of studies on polymer combustion are about combustion of solid polymers and the effect of polymer additives on the combustion of liquid droplet has not been investigated. Nano-sized carbon particles are also believed to enhance heat transfer and internal circulation in liquid droplets and could also be used to increase the energy content of low energy fuels such as ethanol. All experiment will be carried out using fiber supported technique and main combustion characteristics such as burning rate, burning time and flame shape will be examined. The morphology of soot residues along with qualitative soot emission will be also studied.

Chapter 2 presents a literature review of liquid droplet combustion including a history of droplet test and different experimental and measurement techniques used in this field. Main theoretical and numerical models and their assumptions will be also addresses briefly. In chapter 3, the experimental arrangement and procedures will be discussed in detail. Image processing and data analysis technique will be explained in this chapter. In chapter 4, combustion of diesel, jet fuel, decane, dodecane and hexadecane doped with

different percentages of a long chain polymers will be examined. Burning rate will be measured for each case and the result will be compared with pure fuel combustion. The morphology of soot particles and their size distribution will be discussed too. Chapter 5 will present experimental results on combustion of colloidal suspension of carbon-based nanoparticles in ethanol, diesel and jet fuel. The effects of nanoparticles size and morphology on the burning rate and combustion behavior will be investigated in this chpter. Finally chapter 6 will wrap up this thesis with conclusions and proposed future work.

2 LITERATURE REVIEW

2.1 Introduction

Our present understanding of droplet combustion is only as old as mid twentieth century. While our understanding of liquid fuel combustion before then was mainly based on low temperature evaporation of liquid droplets (mainly of water), the development of gas turbines, liquid fuel rockets and modern industrial furnaces pushed combustion scientist to reevaluate their understanding and start to develop new more realistic models. Early works of Godsave [21] and Spalding [22] and also those reviewed later by Williams [23] established the classical theory of droplet vaporization and combustion, also known as spherically symmetric diffusion controlled model of combustion of a droplet, which is illustrated in Figure 2.1.

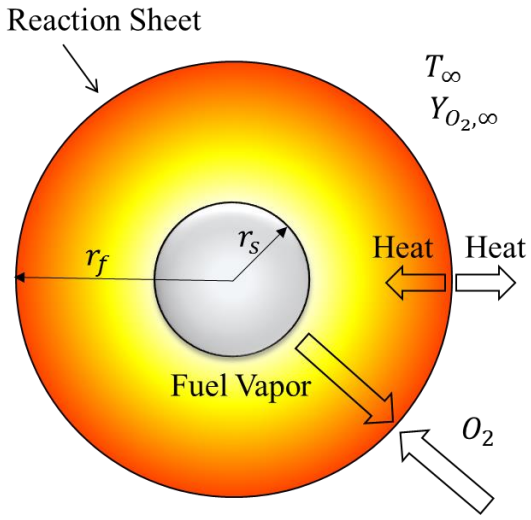

Figure 2.1 Schematic of idealized model of droplet burning

From the classical theory of droplet combustion, the rate of change of droplet surface area is:

$$\frac{dr_s^2}{dt} = \frac{2(\lambda/c_p)}{\rho_l}\ln(1 + B_{h,c}) \tag{2.1}$$

where λ, c_p and ρ_l are thermal conductivity, specific heat and density of fuel droplet. In equation (2.1), $B_{h,c}$ is the heat transfer number of combustion and is defined as:

$$B_{h,c} = \frac{c_p(T_\infty - T_s) + (\frac{Y_{O,\infty}}{\sigma_O})q_c}{q_v} \quad (2.2)$$

In above equation, q_v, q_c, $Y_{O,\infty}$ and σ_O are latent heat of vaporization, heat of combustion, mass fraction of oxidizer in ambient and stoichiometric mass ratio of oxidizer to fuel respectively. Defining the right hand side of equation (2.1) as droplet burning rate constant, K_c, will reduce this equation to the following equation (2.3):

$$r_s^2 = r_{s,0}^2 - K_c t \quad (2.3)$$

where $r_{s,0}$ is the initial droplet diameter. It should be noted that similar relations holds for droplet evaporation with a different constant of K_v and heat transfer number of vaporization, $B_{h,v}$. Equation (2.3) implies that the square of droplet diameter decreases linearly with time and therefor is called d^2-law of combustion. From experiments, it is found out that generally droplets of volatile hydrocarbon fuels burning in air at room temperature have burning rate constants in the range of 0.8 to 1.2 mm^2s^{-1}. Using pure oxygen as oxidizer, the burning rate almost doubles to the range of 1.8 to 2.3 mm^2s^{-1} [5]. In microgravity and due to lack of natural and forced convection effects, the burning rates will take smaller values [24]. These values also vary with the molecular weight and heavier hydrocarbons have smaller burning rate constants.

The accuracy of d^2-laws of combustion and evaporation for single component fuels has been examined by many experimental works and a summary of them have been listed in papers such as the work of Williams [23] and Faeth [25]. Along with experimentations, analytical and computational works have been also evolved in different areas of droplet combustion [26,27]. Since the present thesis is about combustion of polymer and nanoparticle in fuel, next sections will only focus on the phenomena associated more with multicomponent fuels.

2.2 Combustion of Multicomponent and Emulsified Fuel Droplets

In the early studies of droplet combustion, the effects of multicomponent were not considered and the studies were focused on pure fuel combustion. This was mainly because of commercial fuel blends were highly refined and produced to a very narrow specification range. Furthermore, requirements for engine efficiency and also emission regulations were

not very strict so it was not deemed necessary to study multicomponent effects. However, with more stringent design requirements for a higher efficiency, less fuel consumption and stricter emission regulations, it has become more important to consider multicomponent effects. To understand heterogeneous multicomponent fuel combustion, Law [28] proposes to consider three main factors: (1) the relative concentrations and volatility of components, (2) the miscibility of components (which affects the phase change and therefore the surface vapor pressure characteristics), and (3) the rate of mass diffusion, the rate of surface regression and the intensity of motion within droplet. The factors in (3) influence the rate at which the components are transported to the droplet surface where gasification takes place.

C.K. Law with a large body of work is undoubtedly of the pioneers in the area of multicomponent droplet combustion. In one of his early theoretical works on the vaporization of binary fuel, using frozen[1] combustion mode assumption he could justify some of the behaviors of multicomponent droplets [29]. He concluded that due to slow diffusion rate compared to the surface regression rate, the droplet vaporization consists of an initial transient regime followed by a diffusion limited, almost quasi steady regime. Once, due to surface regression, the droplet diameter becomes very small and comparable to characteristic diffusion length, the volatility takes over and a final volatility limited regime begins. Furthermore, he explained that the entrapment of the volatile components within the droplet may cause internal nucleation, either heterogeneous or homogeneous, to occur which itself can result in fragmentation of the droplet known as “micro-explosion”.

Lasheras et al. [30] explained micro-explosion and showed that under certain specific conditions of fuel composition and oxidizer, binary droplets can undergo disruptive burning as a result of homogeneous nucleation. For micro-explosion to occur for a binary droplet, interior droplet temperature should reach a value larger than the

[1] In combustion of multicomponent fuel droplets, the following two limiting behaviors may be reached [38]: in the fastest and intensely convective limit, strong internal circulation could provide rapid mixing and therefor the droplet interior could be approximated as uniform. This mode is called “distillation” mode. In contrast to distillation is “frozen” mode which is envisioned as the slowest with no internal circulation such that the droplet composition can be assumed to remain constant.

superheat limit of the mixture. During combustion of a multicomponent droplet, the more volatile component will preferentially evaporate in a thin layer near the surface of the droplet and so will control the surface temperature. Since the heat conduction inside the droplet is very fast, the droplet temperature also increases rapidly. At this point, if one of the components have a superheat limit large than that of the mixture, homogeneous nucleation within the droplet will occur. Therefore by controlling the concentration of different components we could induce micro-explosion as a means of secondary atomization and improve fuel/air mixing and consequently better utilization of combustion system.

Wang et al. considered mixtures consisting of an extremely heavy component or components with very different boiling points [31]. In general, a three-staged combustion with diffusion being the dominant liquid phase transport mechanism was observed: (1) an initial period of preferential gasification of the volatile component with a droplet temperature of relatively low, (2) a transition period during which the droplet temperature increases but the burning rate is extremely low and the flame size shrinks. This period is actually a heating zone to bring the temperature to a value close to the boiling point of less volatile component. (3) Finally, there is a quasi-steady period during which the droplet temperature is relatively high, the concentration within the droplet remains constant and the concentration at the droplet surface mostly consists of low volatile component. Figure 2.2 displays the experimental data for the droplet diameter change for two binary droplets consisting of different concentrations of heptane/hexadecane. The case with abundant amount of more volatile component, i.e. heptane, depicts the above mentioned three-staged combustion, however for the blend made with more of hexadecane the first and second periods merge and so the whole duration of combustion appears to made of only one zone.

Wang et al. also suggested that for multicomponent droplets, made of several hydrocarbon fuels, micro-explosion is not possible in atmospheric pressure [31] and super-atmospheric pressures are required. Mikami et al. [32] proposed that homogeneous nucleation within a binary fuel droplet is a stochastic process. Through developing a model they suggested that the occurrence of micro-explosion for larger droplets is relatively

deterministic while in smaller droplets, like those in a spray, this phenomenon is more stochastic as a result of nucleation time being comparable to or larger than droplet lifetime.

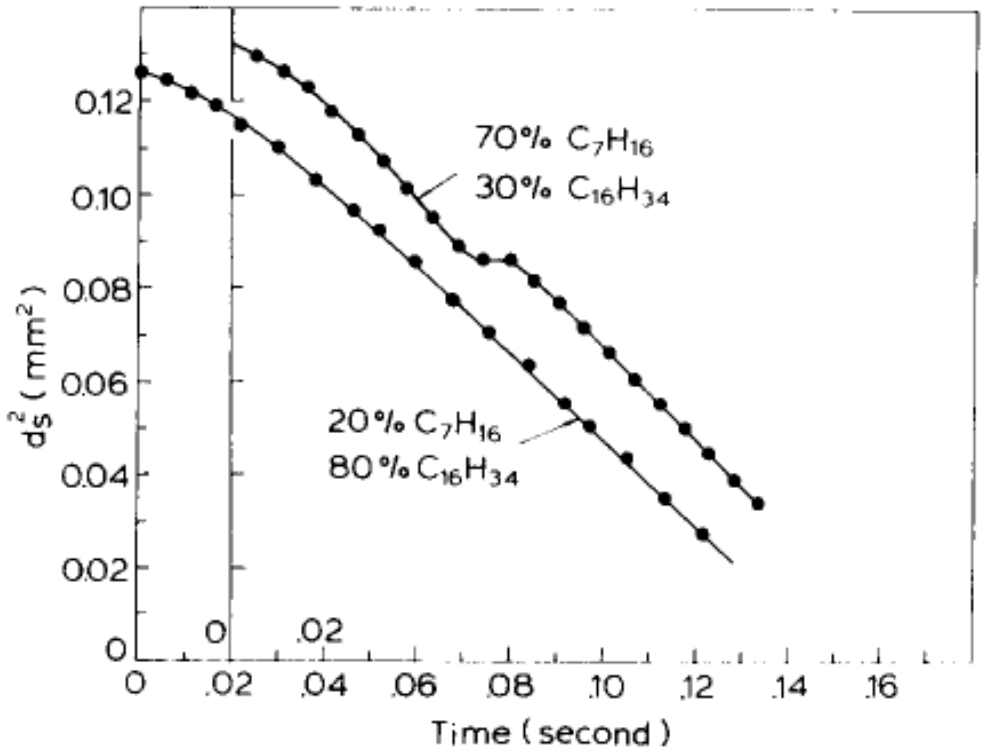

Figure 2.2 Evolution of d^2 with time for heptane/hexadecane droplets [31]

One of the other main classes of multicomponent fuels that have attracted many interests in past decades are water in oil (W/O) emulsions [15,16]. A number of potential benefits such as reduced formation of NO_x, soot [33,34]and carbonaceous residue [35–37] have been offered for W/O. These benefits actually arise from the effect of dilution in both gas and liquid phase reaction and also from the secondary atomization (micro-explosion). The early works in this area tried to focus on the mechanisms dominating combustion and hence uncover the combustion physics of W/O emulsions. According to Law, Lee and Srinivasan [38], the combustion characteristics of O/W emulsion droplets depend on the relative volatilities and concentrations of oil and water, the intensity of internal circulation, and the fact that oil and water do not mix. Through their experiments, they did not observe any internal bubbling under atmospheric pressure which made them proposes that it is internal circulation that inhibits internal bubbling. However, it has been observed that for n-paraffin at atmospheric pressure, microexplosion occurs starting with n-pentadecane [4] and n-hexadecane [39]. It is postulated that the microexplosion may occur for the base fuel

with boiling point higher than the superheat limit of water. In terms of combustion regimes, W/O emulsions follow similar rules as explained previously for multicomponent droplets. For example, Jackson et al. [40] studied combustion of emulsions of water in n-heptane and reported a staged combustion in which first heptane (as more volatile component) and then both heptane and water control the burning process.

Lasheras et al. [41] explained that internal bubbling owes its growth to inertial effects. In other words, it is pressure difference between the superheated vapor and the liquid and also the inertia imparted to the liquid by the motion of the bubble surface that are governing the growth rate. In more recent studies, Watanabe et al. examined microexplosion and puffing behavior of W/O droplets both experimentally [42] and numerically [43] to find any possible correlation between the mass of generated vapor and breakup time for microexplosion. However, they did not observe any strong correlation and verified the older understanding that the breakup time is closely related to the superheat temperature of the mixture.

Owens et al. examined addition of water to diesel fuel and reported no significant change in the power output and yet up to 30 percent less oxides of nitrogen emissions [44]. However, they reported 250 percent increase in unburned hydrocarbons which could give these water/fuel blend attractive fire resistance characteristics. Later, Wang and Law [45] and Weatherford et al. [17] also reported fire-resistant potentials in W/O emulsions. The fire-resistant nature is believed to be due to a lower temperature of W/O droplets (compared to neat fuel) which in turn results in weaker fuel vaporization and therefor the generated gas mixture will fall outside of flammability limit [18].

2.3 Droplet Ignition

To set the liquid fuel on fire and utilize its energy, an ignition is always the very first step. Different fuels have different ignition times which for normal alkanes increases with the number of carbon atoms in one molecule [11,46]. Increasing environment temperature, oxygen concentration and pressure showed also reduce ignition delay [11] of pure fuels. The effect of initial diameter on the ignition delay has been also investigated. Through a series of experiment in hot environments Saitoh et al. [47] found that at the vicinity of the ignition limit (a point below which droplet completely vaporizes and

ignition can no longer occur), ignition delay decreases as initial diameter increases. This happens because near the ignitable limit the local Damköhler number (the ratio of transport time to the chemical reaction time) is too small to produce ignition. In other word, the distance over which transport phenomena acts is so small and before chemical reaction kicks in the fuel vapor spreads out and ignition is not obtained. Both similar and opposite results were reported by Takei et al. [12]. They found out that the ignition delay increases as the initial droplet diameter increases for the case hexadecane. However, heptane showed a completely opposite trend and ignition delay decrease as the initial droplet diameter increased. This could also be explained by different volatilities of hexadecane and heptane: for droplets with larger initial diameter or less volatility, longer ignition time should be due to heating or vaporization because more time would be required to bring surface temperature to around the boiling point. For high latent heat fuels (less volatility), not much gasification takes place until surface temperature reaches to a value close to the boiling point but after that, vigorous gasification starts. For this case, reaction time could be ignored compared to the vaporization time. However, for more volatile fuels, such as heptane, larger droplet diameter means larger surface area that could provide more fuel vapor and hence the gaseous mixtures reaches its flammability limit in a shorter time.

The ignition of multicomponent droplets has also been the topic of much research. By developing a model, Bergeron et al. [48] showed that the ignition of binary droplets is controlled by the more volatile component. Experiments and numerical analysis have also suggested that increasing the concentration of more volatile component can significantly reduce the ignition delay [49,50]. For W/O emulsion, it was seen that ignition delay increases with the addition of water for both single droplets and droplet arrays [51]. An initial diameter at which ignition time is maximum was also observed for mixed fuels by Takei et al. [12]. For mixtures of heptane/hexadecane, this diameter increases with decreases of heptane (more volatile component) or ambient temperature. It was reported for water in decane droplets that when the droplet size is too small, a rapid increase in mass flux causes a delay of auto-ignition. In addition, opposite to pure fuels, increasing ambient temperature did not seem to have a significant effect on reducing ignition delay [52]. This is deemed to be due the simultaneous vaporization of both fuel and water at high temperatures.

2.4 Effect of Initial Droplet Diameter

There has been always a debate about the effect of droplet initial diameter. The dimension of droplet contributes in several non-dimensional number, such as Reynolds number, and could play as an important factor in determining the heat transfer and combustion regime. The larger initial diameter provides larger surface area and hence more radiative heat absorption. It was previously mentioned that the ignition time increases as the droplet diameter decreases at the region near the ignition limit [47]. However, more recent studies uncovered a completely opposite behavior; Segawa et al. invented a new method to accurately measure the ignition delay of fuel droplets experimentally [50]. In their experiments, filled a chamber with propane-air mixture and placed a single droplet on a support fiber in the middle of the chamber. Then the combustible mixture was ignited and the flame front propagated toward the droplet and ignited it. The ignition delay then was measured as the interval between the time it takes the flame front to pass the droplet and the time they saw the first visible flame. They found that the ignition delay of pure fuel droplets increases as the initial droplet diameter increased and the fuel volatility decreases. However, the influence of initial diameter was reported to decrease as the fuel volatility increases. More recent computational work of Awasthi et al. on combustion of heptane droplets in zero gravity also proposed that the ignition delay increases with droplet diameter [53].

Saitoh et al. reported that if the initial droplet diameter is less than 1 mm, the natural convection does not influence the peripheral distribution of mass burning rate drastically [47]. Hara et al. examined the effect of initial diameter on burning rate and concluded that the d^2-time linear relationship is established for the entire period of combustion if the droplet large; however, for small droplets, the value of burning rate constant was observed to start to fall and as a result extinction occurred [54]. Nakaya et al. measured burning rate of droplets in argon-rich and carbon dioxide-rich ambient under microgravity for droplet with initial diameters ranging from 0.41 to 0.82 mm [55]. They found that the instantaneous burning rate linearly decrease with the square of droplet diameter after the initial heating period. However, the apparent burning rate did not show to be dependent of the droplet diameter.

2.5 Polymer Combustion

Addition of polymers to oils has s history as long as droplet combustion. However, the intent of adding polymer was never regarding combustion characteristics but more focused on the drag reduction potentials. It was shown that adding trace amounts of soluble polymers (as low as 0.02 ppm) could result in turbulent drag reduction [56] and increase the capacity of oil pipelines [57]. Mist suppression of fluids of low shear viscosity can also be achieved by addition of low concentrations of long linear chain polymers. For example, it was shown that the addition of less than 100 ppm polyisobutylene to jet fuel can generate significant visible changes in mist formation and sometimes eliminate small droplets and cause filaments to form [19,58]. Chao et al. also showed that ignition suppression could be achieved with only 10 ppm of a polymeric additive [58].

Studies on polymer combustion are not as extensive as liquid droplet combustion because of more complicated nature of polymer combustion and also very fewer application (as fuel) compared to conventional hydrocarbon fuels. While combustion of liquid droplets occurs only in gas phase, chemical reactions in polymer combustion may also occur in condensed phase as well as at the solid-gas interface [59]. In order to understand these complexities, researchers have mainly focused on combustion of polymer sphere or particles [60–63]. They showed that polymer drops follow the traditional d^2-law of combustion and have higher burning rates compared to hydrocarbon oils. Since polymer spheres swell during combustion, Basavanahalli et al. [64] proposed a mass loss measurement technique, instead of conventional diameter measurements, and found that the ratio of flame diameter to droplet diameter (flame standoff ratio) holds a smaller value than that of hydrocarbon fuel droplets.

An increased demand for high performance and yet improved safety fuels for rocket engines in the last decade has driven new studies on combustion of gel fuels. Gels are liquids whose properties have been altered by the addition of certain gelling agents (gellants) and as a result their behavior resembles that of solids. Solomon et al. [65] burned a mixture of 30% organic gellant and 70% JP-8 (military grade jet fuel) on a support fiber and observed staged combustion. They explained the swelling as a result of formation of a non-permeable elastic layer around the droplet which reduces fuel evaporation and hence

solvent and fuel vapor bubbles start to form inside the droplet as shown in Figure 2.3. Mishra et al. [66] examined the effect of gallant concentration on combustion of JETA1 gel propellants and reported that both burning rate and flame standoff ratio decrease as the concentration of gallant agent increases. Phase separation, bubble nucleation and micro-explosion were also observed during combustion of gel fuel droplets. The effect of ambient pressure and oxygen concentration on burning rate and time of micro-explosion was also investigated by Liu et al. [67] and similar behaviors as those of multicomponent fuel droplets was observed.

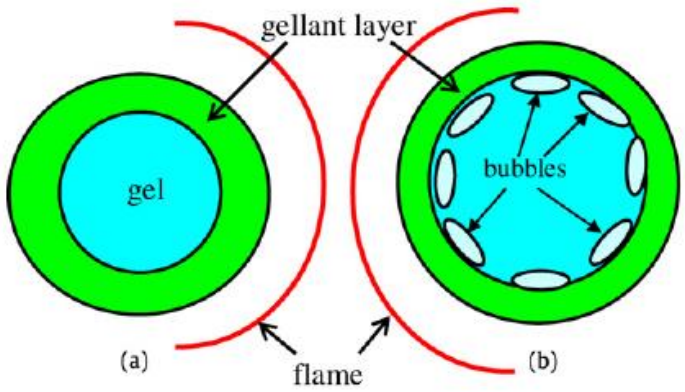

Figure 2.3 Formation of bubble inside a burning gel droplet [65]

While combustion of multicomponent fuel as well as polymer combustion have been studied for several years, there is not enough information available on a mixture of both. Combustion of gel fuel droplets also considers very high percentages of a gallant in a base fuel and no data is available on fuels with low percentages of a polymeric additive. In this regard, one of the main objectives of this thesis is to experimentally examine the effects of adding trace amounts of long chain polymer on combustion characteristics of hydrocarbon droplets.

2.6 Combustion of Fuel Droplets with Nanoparticles Additives

Addition of nano-sized particles to liquids in order to enhance heat transfer features is a new field of thermal-fluid sciences that has been under investigation only for the last three decades. This new type of fluid, known as nanofluid and typically categorized as suspensions of 1-100 nm nanoparticles in fluids, started to emerge in 80s. The work of Choi et al. [68] is probably one of the very first studies that proposed the concept of

nanofluids. They proposed that a new class of heat transfer fluids can be engineered by suspending metallic nanoparticles in conventional heat transfer fluids and exhibit higher thermal conductivity. This unique property, provides nanofluids with a great potential to be used in wide range of new industrial technologies such as cooling for micro- and nanoelectromechanical systems (MEMS and NEMS), power electronics, and light emitting diodes (LEDs) [69]. Several explanations have been proposed for enhanced heat conductivity of nanofluids: one of the theories proposes that it is because of nanoconvection caused by Brownian motion of nanoparticles in bulk liquid [70,71]. Another theory suggests that the layered structure plays as a thermal bridge between a solid nanoparticle and a bulk liquid [72]. There is also another theory in which the agglomeration of nanoparticles is considered as an important factor to enhance heat transfer [73].

Due to abundant sources of coal in the world and its inexpensive cost of extraction compared to other fuels, there has been always an interest to mix coal powder with water or liquid fuels and burn it directly in turbines or other internal combustion engines. There were also some efforts to produce stable coal-water or coal-oil slurries [4,74,75] but the agglomeration of particles turned out to be a limiting issue. New technologies leading production of nano-sized particles gave rise to nanofluid application and provided an opportunity to make new type of fuels by mixing energetic nanoparticles with conventional liquid fuels. Sabourin et al. [76] reported that addition of less than 1% functionalized graphene sheets (FGS) nano particles to nitromethane could significantly increase linear burning rate (175% increase) and reduce ignition delay. Aluminum and aluminum oxides nanoparticles have also been widely used as an energetic additive and have shown promising effects in terms of enhancing heat conductivity, increasing burning rate and reducing ignition delay [76–78]. Allen et al. used 2% (by weight) of 50 nm aluminum nano-particles in ethanol and JP-8 and reduced ignition delay by 32% and 50% respectively [79]. Gan et al. [80] showed that addition of nano aluminum particles might cause deviation from d^2-law of combustion in some circumstances and reduce burning rate. They explained that if the droplet lifetime is longer than the characteristic aggregation time, large aggregate are formed. These aggregates then will inhibit diffusion and so reduce the evaporation rate.

Given the above mentioned discussion on potentials of nanoparticles, as a fuel additives, to improve energy content and enhance burning rate and considering unique optical properties of carbon based nano particles [76,81,82], combustion of several hydrocarbon and alcohol based fuel doped with carbon particle will be examined in chapter 5.

3 EXPERIMENTAL CONFIGURATION

To be able to study combustion dynamics of liquid droplet and track its evolution in time, it is necessary to have the droplet fixed in space. Therefore, an experimental configuration similar to that used by Bae et al. [7] was designed and fabricated to perform droplet burning experiments. In this chapter, the main components of this configuration, including fiber support, ignition system, imaging tools, test procedure and data acquisition techniques will be explained.

3.1 Fiber Support System

To fix a liquid droplet in space, it should be mounted on a physical arrangement however the contact surface between the droplet and mounting arrangement should be as small as possible so a spherical shape is obtained and also heat transfer to and from the droplet is minimized. To achieve this objective, silicon-carbide (SiC) fibers were used. The fibers used in our experiment are 16-µm SiC fibers (NL-202 Nicalon™) purchased from COI Ceramics, Inc. The fiber initially comes as woven strands wrapped around a bobbin and single strands (16-µm) should be separated meticulously. Avedisian et al. [83] showed that for 13 $d_0/d_{fiber} > 13$ the fiber supported burning rates, measured over the linear portions of the droplet diameter evolution are close to the free droplet values. Given the initial droplet diameters of 500-1000 µm in this study, the 16-µm could satisfy this condition. Furthermore, the SiC fiber has thermal conductivities of 2.97 and 2.20 W/m.K at 25˚C and 500˚C respectively. Such low thermal conductivity combined with the very small cross section of the fiber will guarantee very minimal heat transfer from the droplet.

Figure 3.1 displays the top view of the experimental rig. The main components in this figure are the base plate, fiber support and ignition system. The base plate is a 0.5 inch aluminum plate that houses other components. This plate, which is shown in detail in Figure 3.2, could be adjusted to different elevations using optical rods. However, the setup was not bolted on the bread board because it is necessary to move it around for each test in order to achieve a focused image.

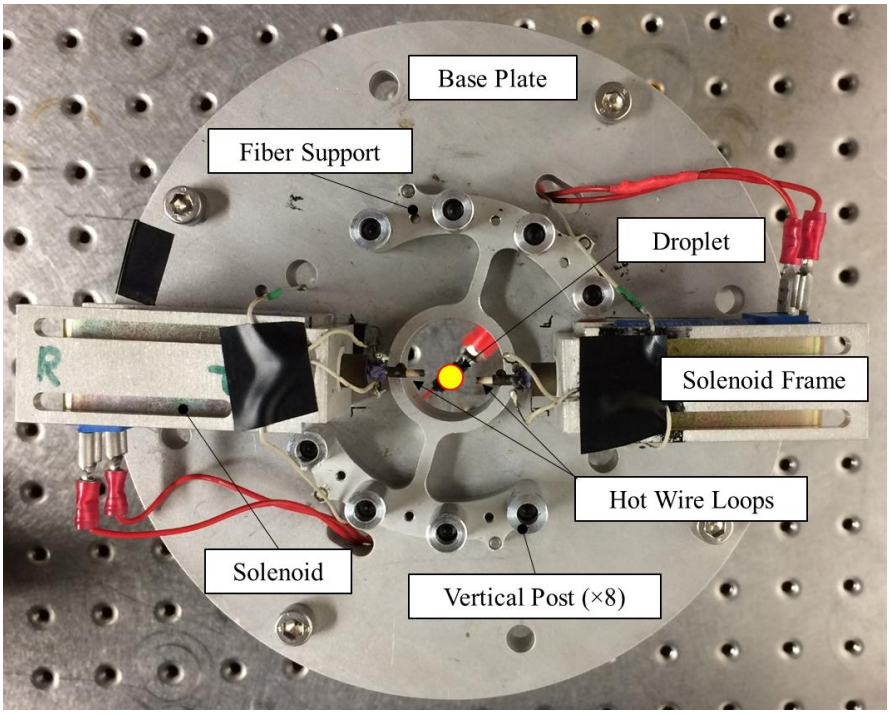

Figure 3.1 Top view of droplet combustion configuration (a side view is provided in Figure 3.12)

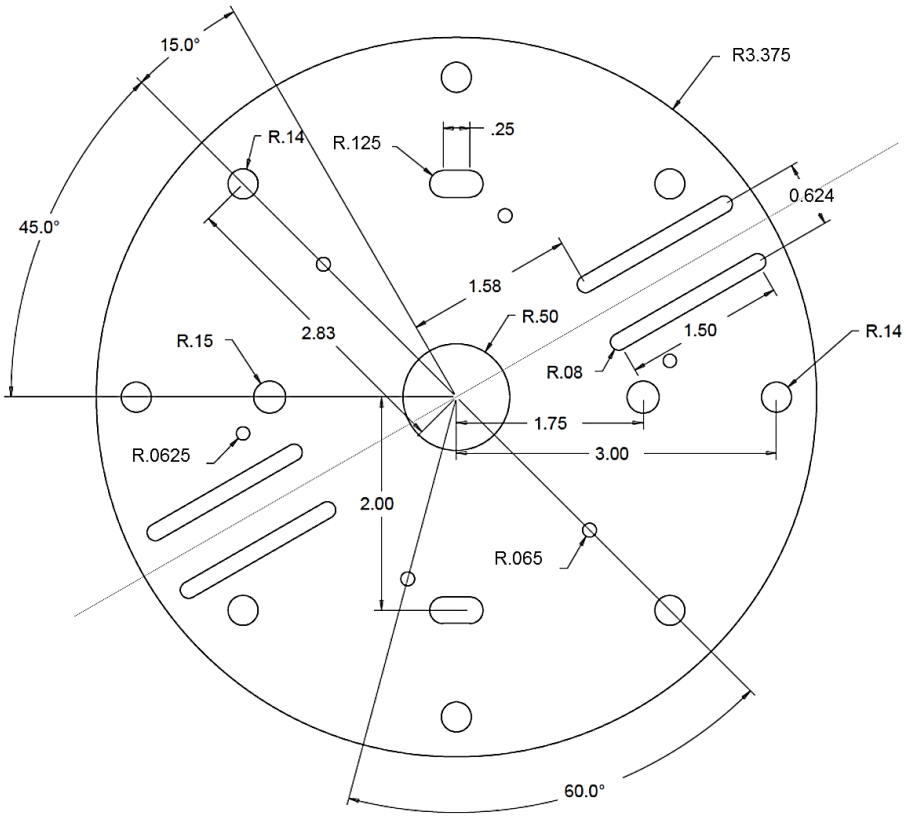

Figure 3.2 Schematic of base plate (see Figure 3.1); all dimensions are in inch and the thickness is 0.5 in

The fiber arrangement system consisted of a fiber support ring and eight vertical posts. The vertical posts were arranged in two curves, each including four posts along the curve in 15˚ increments. Several fiber configurations were considered but it was determined that an arrangement made with three fibers could provide enough surface tension to hold droplets of desired size. In this arrangement, as shown in Figure 3.3, three fibers are crossed by mounting them on the 0˚, 30˚ and 60˚ vertical posts. As mentioned before, due to their very small thickness, the fibers do not distort the droplet shape and a pure liquid fuel droplet takes a spherical shape during all of its burning period. The fibers interfere with the flame and a "glow" is observed at the location of flame. However it is believed that the fibers do not contribute to the heat transfer phenomena due to their low cross section and thermal conductivity. The glow on the fiber was also used as an indicator of ignition and extinction from which the burning time of each droplet was measured.

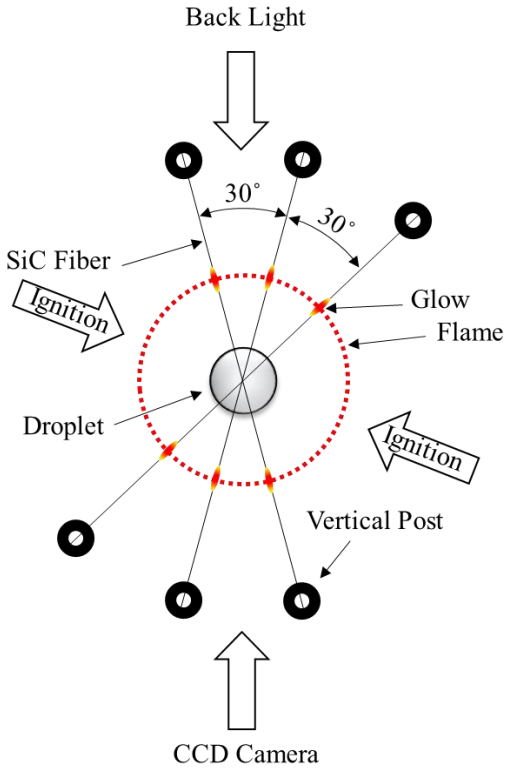

Figure 3.3 Experimental configuration: fiber arrangement on the fiber support ring

During several experiments it was realized that mounting fibers on the vertical posts is difficult due to limited space available on the base plate. Therefore a fiber support ring was designed and fabricated so that the fibers could be mounted off the main configuration

and then the fiber support ring is mounted on the base plate. As shown in Figure 3.4, there are seven threaded holes at each side support ring that give us the option to use different crossing fibers configurations.

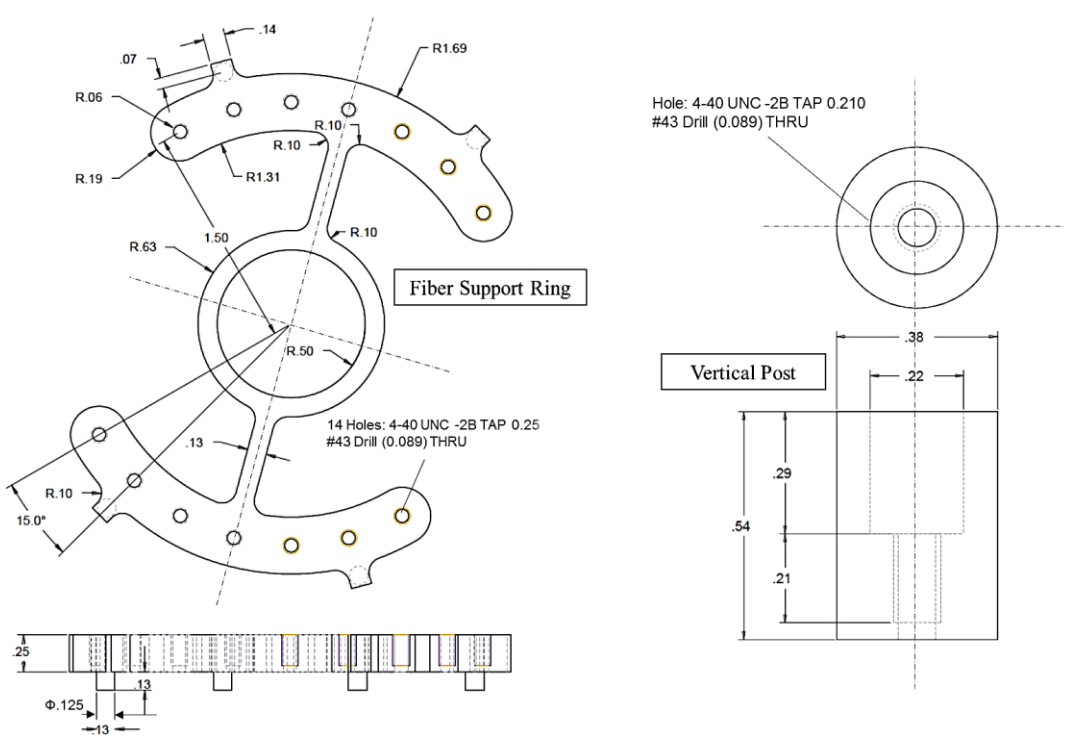

Figure 3.4 Schematics of (left) Fiber support ring and (right) vertical post (all dimensions are in inch)

Figure 3.5 Picture of fiber support ring with vertical posts

3.2 Ignition System

Ignition for liquid droplets was provided by means of hot wire. The mechanism by which hot wire provides ignition is to pass a pre-determined current through a resistance wire. For this purpose, Kenthal A-1, wire which is a high resistance chrome-aluminum-iron alloy, was chosen. In addition, wire resistance is inversely proportional to its cross sectional area. Therefore to get higher resistance and consequently higher amount of heat at certain current, a very thin 36-gauge wire (average diameter of 0.127 mm or 0.005 in) was chosen. Table 3-1 lists physical properties of the Kenthal wire used to make hot wire loops in the experiments.

Table 3-1 Properties of gauge 36 Kenthal A-1 wire [84]

Nominal Composition (%): Cr/Al/Fe	22 / 5.8 / balance
Diameter (mm)	0.127
Resistance at Room Temperature (Ω/m)	109.5
Melting Temperature (˚C)	1500
Maximum Operating Temperature (˚C/˚F)	1400
Density (g/cm3)	7.1
Thermal Conductivity at 50˚C (W/mK)	11
Specific Heat Capacity at Room Temperature (kJ/kgK)	0.460
Emissivity (oxidized condition)	0.7

For a droplet to ignite, there is a preheating period during which the droplet temperature increases to a value near the boiling temperature of liquid fuel. However, if not enough heat is available, the droplet will only vaporize and the ignition will never occur. To avoid this, either the hot wire loop should be placed very close to the droplet surface or the heating time should be increase. After passing current through the hot wire, the ending loop shape will expand toward the droplet and if it is very close to the surface it may contact the surface or destabilize the fiber on the fiber and cause it to fall off the fiber. Increasing the heating time will provide the ignition but the pre-ignition vaporization will also be high. Using two hot wires symmetrically at both sides of the droplet will provide more uniform heat distribution to the droplet and hence faster ignition. In addition,

it is desirable that the ignition source does not have any contact with the flame to prevent it from disturbing the flame and also playing as a heat sink. A retractable ignition system could move the ignition source away from the droplet right after ignition. The retraction mechanism, which will be explained later in this section, also has a benefit which could reduce the heating time even more than what we expect from two symmetric ignition sources: due to retraction of hot wires, the flow around the droplet is agitated and the resulting mixing augments heat transfer significantly and ignition takes place.

To obtain consistent ignition in all of the experiments, the amount of heat generated by the hot wires should be the same in all of the tests. Since the generated heat is a function of wire resistance, the length and the shape of the hot wire should be the same in all of the runs. Given the small size of the configuration, working with very small piece of wires is difficult. On the other hand, if the length of the Kenthal wire is too long, less heat compared to a shorter wire will be generated at a certain voltage. After several trial tests, it was determined that a 45 mm piece of Kenthal wire is a length that is long enough to provide the ease of manual work and at the same time short enough to generate the required heat to quickly ignite liquid droplets before pre-ignition heating results in mass loss and change in the initial droplet size and concentration. In addition, the voltage for ignition was set to 20 volts (1760 Out2 in Figure 3.13) for all experiments to assure same amount of heat of ignition.

To increase the surface area of the hot wires to which the droplet is exposed to, a loop shape was made by wrapping the Kenthal wire one turn around a 0.5 mm diameter drill bit. Then, the circular section of the hot wire was bent at 90˚ using a long nose plier. Figure 3.6 shows a hot wire loop inside a 10 mm ceramic insulator. The ceramic insulator is to prevent the Kenthal wire from contacting with the body of solenoid plunger and will be explained later in this chapter. The two hot wires were later placed in circuit (Figure 3.13) in a series connection. The reason for choosing a series connection over a parallel is to keep one of them in case the other one melted. In parallel connection, if one of the loops melts (which happens due to expansions and retraction in several runs) the other one will also melt due to the double amount of current. However, a series connection

will stop passing current if one of the hot wires breaks and therefore the other one will be saved and we will only need to replace the melted one.

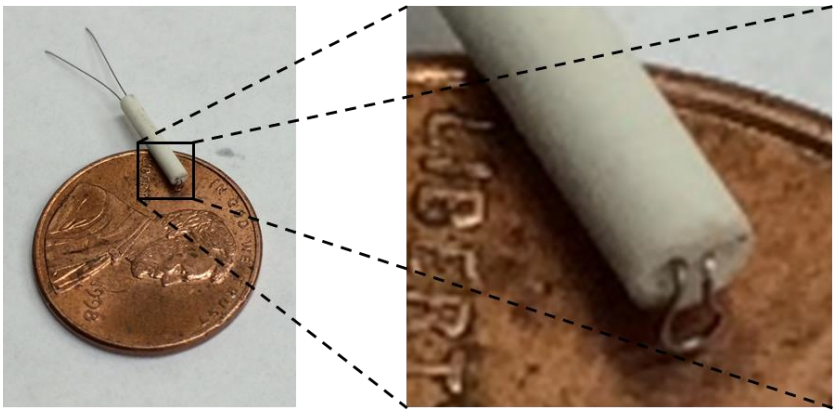

Figure 3.6 Experimental configuration: hot wire loop inside the ceramic insulator

3.3 Retraction System

In order to prevent any interference between the hot wires and flame around the droplet, the hot wires should be moved away from the droplet immediately after ignition. To reach this goal, two solenoids were used to retract hot wires after a certain amount of time. The solenoids used are two commercial solenoids (Deltrol Control D-22) with overall size of 1.130 (L) × 0.750 (W) × 0.750 (H) inches were used. The D-22 solenoid could run over a wide range of voltages (6 to 240 VAC and 6 to 110 VDC) and has power ratings of 4.2, 9.6 and 40 watt for continuous, intermittent and pulse duty cycles respectively. To successfully retract the hot wires, the solenoid plunger should be able to attach to the ignition system from one end and pull it back after the ignition took place. Therefore, a plunger was designed and fabricated from a ferromagnetic steel which is shown in Figures 3.7 and 3.8.

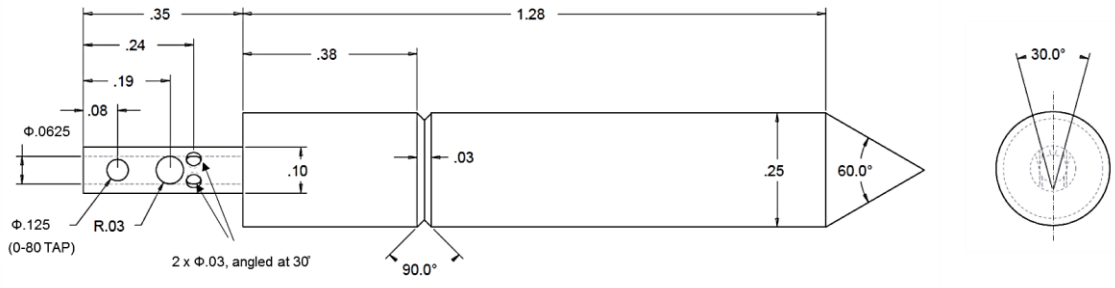

Figure 3.7 Experimental configuration: custom designed solenoid plunger

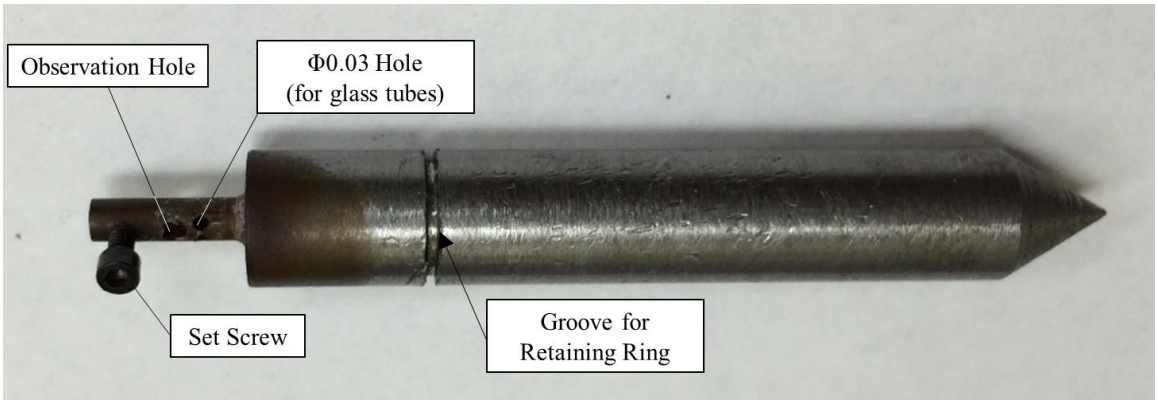

Figure 3.8 Picture of the fabricated plunger for solenoids

The hot wires cannot directly be attached to the plungers because the current passing through the hot wires will run through the plungers and a short circuit will occur. To avoid this, the hot wires should be first inserted into a two-hole thermocouple ceramic insulator (Omega Engineering model TRM-164116). For this purpose, the ceramic insulator was first cut into 10 mm (0.4 inch) pieces and then the hot wire loop was inserted through. The outside diameter of ceramic insulator is 1/16 inch which is equal to the 0.0625 inch inner diameter of the blind hole at one end of the plunger. To fit the insulator into the blind hole, the insulator should be ground with a sandpaper. However, it is easier and faster to ream the blind hole to a slightly larger diameter so that it could fit the insulator. Once the insulator and hot wire was fit into the plunger, a set screw (0-80 socket head cap screw) will be used to secure it in the hole. The two ends of hot wire leaving ceramic insulator should be then passed through the two angled 0.03 inch holes. Again, two 4 mm pieces of glass tubes, cut from 2 µL micropipettes (Drummond Scientific Company), were used to prevent Kenthal wires from contacting the body of plunger (Figure 3.9). To secure the glass tubes in the holes, small amount of oven-bake clay (Sculpey) was used around the glass tubes. To harden the clay, the plunger assembly was heated for 30 seconds by holding it very close to a 100 W halogen lamp.

To make sure that the location of each hot wire related to droplets does not change from experiment to experiment, a 0.31 inch long spring with wire and outside diameters of 0.025 and 0.375 inch respectively was used between the solenoid and a side-mount external retaining ring. When the solenoid is activated, the plunger will retract and the retaining ring will compressed the spring. After the complete burnout of a droplet, the solenoid will

be deactivated and the hot wire loops will be positioned back at their original location by the expansion of the spring and will be ready for a new round of experiments.

To accurately adjust the location solenoid, an aluminum frame was designed and fabricated as per the drawing shown in Figure 3.10. Small washers with the dimensions shown in Figure 3.11 were also made of Teflon PTFE tubes (OD: 3/8", ID: 1/4") to help plungers have a smooth motion.

Figure 3.9 Picture of the complete plunger assembly (with ignition system)

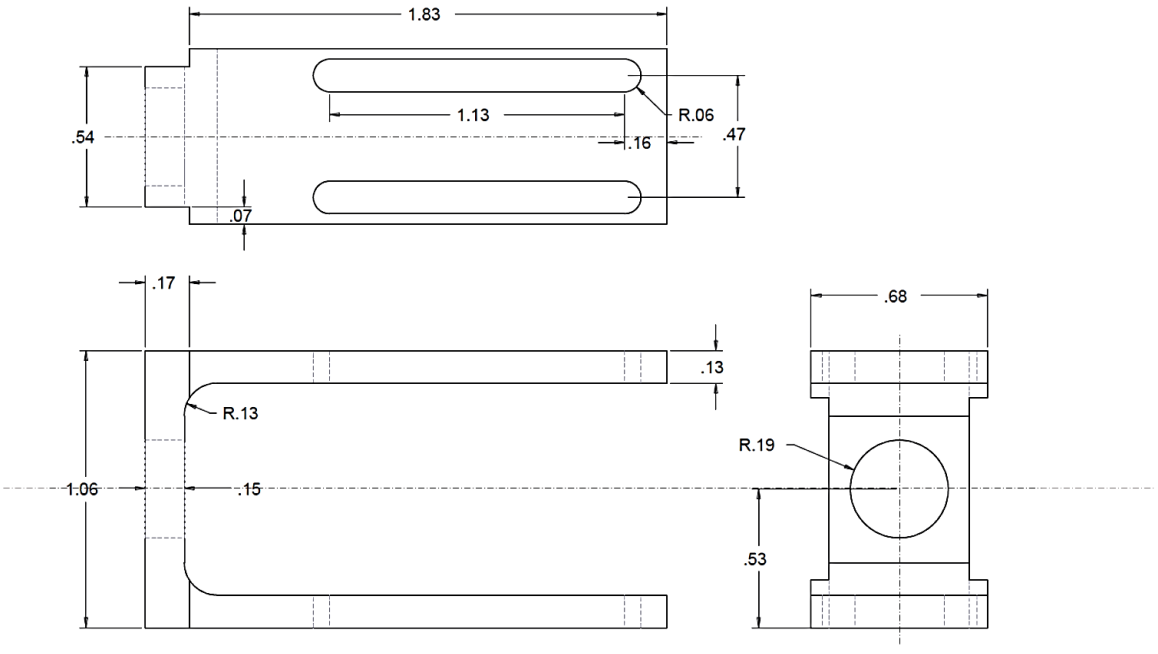

Figure 3.10 Schematic of the housing frame for solenoids

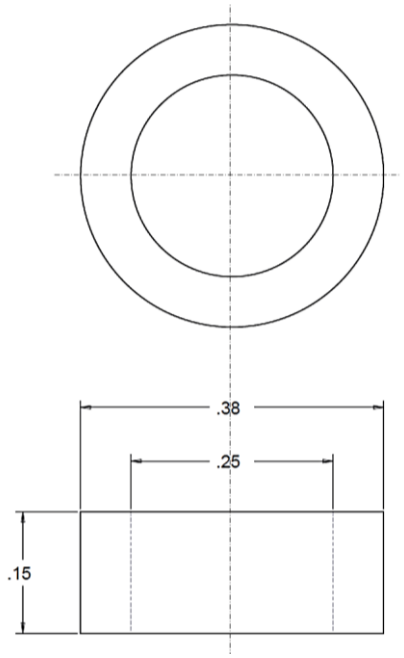

Figure 3.11 Schematic of the Teflon washer made out of Teflon PTFE tube

The retraction of the plunger results in a kick which transfers some vibrations to the fiber and could distort the droplet and flame shape and even cause it to fall off the fiber. To suppress the vibration, small pieces of 1/32" thick silicone rubber were placed between the solenoid and housing frame and also between the housing frame and base plate. These rubber plates also helped to adjust the height and position the hot wire loops at the right height. Finally, the power cables should be soldered to the Kenthal wires right where the leave the glass tubes. Due to the motion of plungers, the soldering are very likely to break after a few runs. To avoid this issue, a 28-gauge tangle-free and ultra-flexible wire used to power the hot wires. Figure 3.12 shows how the final ignition and retraction systems look.

3.4 Timing and Synchronization

The heating and burning of a droplet with an initial diameter in the range of 0.5-1.0 mm takes less than 2 seconds. Therefore it is crucial to control the timing of all major events. There are three events for the droplet combustion that need to be synchronized: triggering CCD camera, ignition (ON and OFF) and retraction (activation and deactivation). Normally the synchronization and triggering equipment is done by a using a delay generator but the DC power supply used to power ignition and solenoid cannot be triggered by a pulse train. Therefore a microcontroller board (Arduino UNO) was used to

control the timing of events. Figure 3.13 shows the diagram for the electric circuit used to control events. In this diagram, digital outputs 11 and 12 are used to send triggering pulses to hot wires and solenoids, respectively, while digital output 10 sends a TTL pulse train to the CCD camera via a BNC connector. The frequency of the pulse train should be equal to the imaging frequency set on the camera in order to obtain real time data.

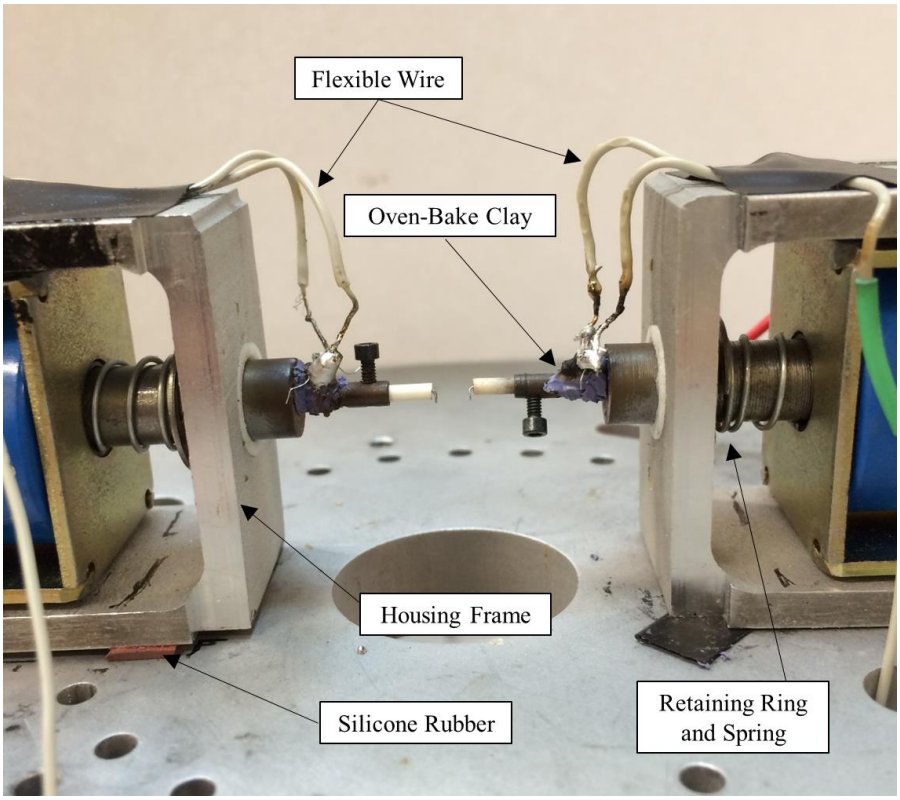

Figure 3.12 Final assembly of ignition and retraction systems on the base plate

Figure 3.14 shows the timing diagram of droplet combustion tests. As shown in this diagram, the CCD camera is the first thing which goes into operation. The camera will keep recording until its memory becomes full. For an image size of 1280×1024 and at 500 fps (frames per second) the camera will record for a duration of 4.2 seconds which is significantly longer than droplet burning period (less than 2 seconds). The next event is heating (hot wires) which starts after 2 frames from the droplet were captured. Either of these two frames could be used to measure the initial droplet diameter. The next event is retraction which is simultaneous with end of heating zone. Finally, once the droplet combustion is complete the plunger will be pushed back and the hot wires will be ready for another test.

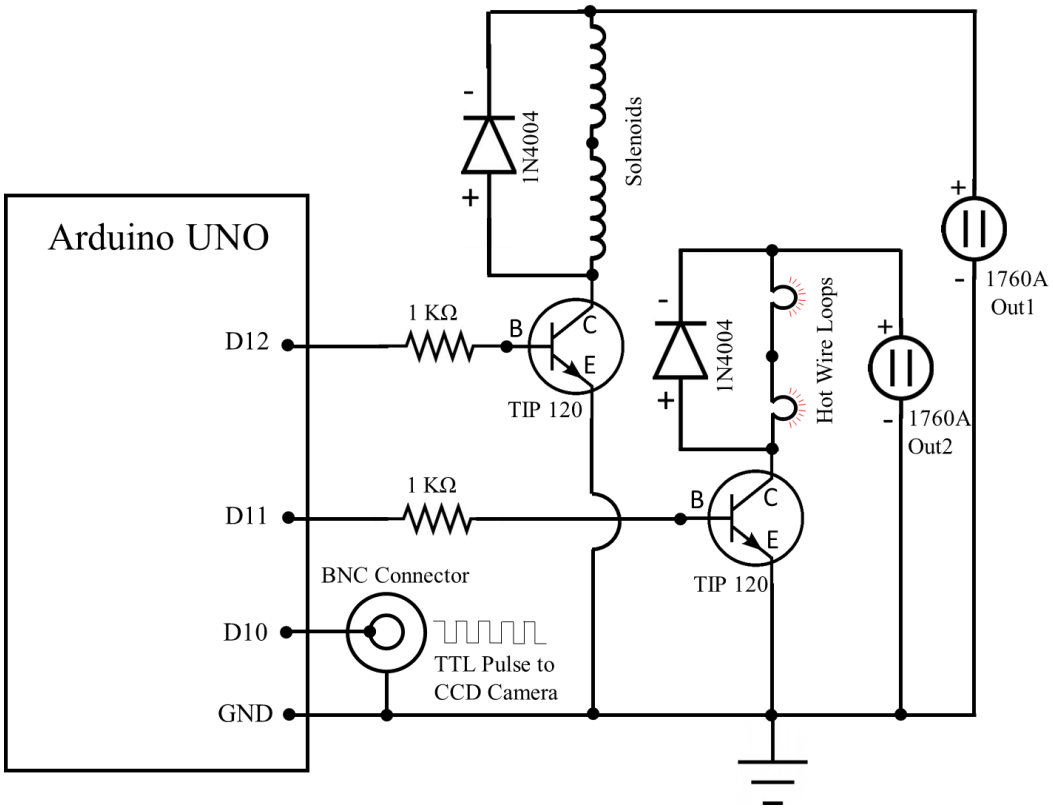

Figure 3.13 Electric circuit diagram of droplet combustion experiment

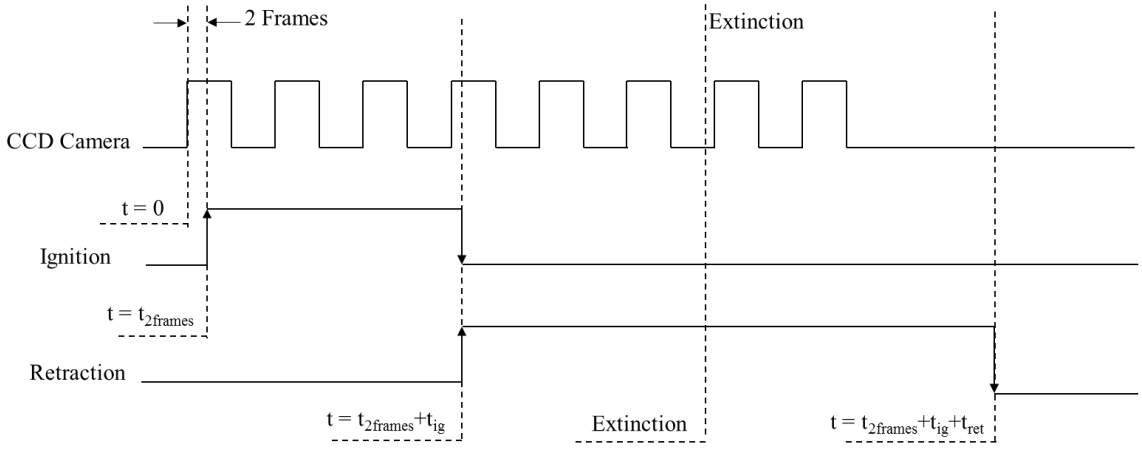

Figure 3.14 Timing diagram of droplet combustion test

3.5 Experimental Procedure and Data Acquisition

In spite of the very short duration of a droplet combustion experiments, which is typically less than two seconds, there are still several steps that need to be taken in order to achieve accurate and repeatable data. The following procedure outline explains all steps required in a droplet combustion experiment, however it is assumed that the fuel, fuel solution, nanofuel suspension has been already prepared according to the procedure explained in sections 4.2 and 5.2. Here is the step by step experimental procedure:

1. Prepare the cameras:
    a. Turn on the CCD camera (X-StreamVision XS-3) and remove the lens cap
    b. Change the image acquisition rate if required (i.e. 500 fps)
    c. Turn on the DSLR high speed camera (Casio EXILIM Pro EX-F1) and remove the lens cap
    d. Set the DSLR camera on high speed video recording by turning the knob to HS mode
    e. Change the video recording frame rate if required (i.e. 600 fps)
2. Set the events timing if required:
    a. Open the Solenoid.ino file prepared to program the Arduino (see APPENDIX)
    b. Make sure that the frequency of pulse train (variable “fr”) sending to BNC connector is equal to camera acquisition rate
    c. Change heating time (variable “tHeating”) if required. A heating time between 300 to 400 ms was used for different fuels in this thesis.
3. Turn on backlight
4. Turn on power supply and adjust the voltages:
    a. Output 1 should be set to maximum (around 25 volts) to provide quick plunger retraction.
    b. Output 2 should be set to 20 volts to make sure consistent ignition heat is generated in all experiment.
5. Load the microsyringe (Hamilton 1701SN) with fuel
6. Change the fibers

a. Remove the fiber support ring from the base plate
b. Replace old fibers with new set of fibers
c. Place the fiber support ring back onto the base plate

7. Deploy a droplet on the fibers cross using the microsyringe
8. Adjust the camera lens and distance between the experimental arrangement and the lens to obtain a focused and sharp image of the droplet (the camera should be on live mode to observe the droplet)
9. Set the camera on external triggering mode
10. Start recording on DSLR camera
11. Push the button on the Arduino to start the test
12. Stop recording on DSLR camera once the combustion is completed
13. Save the acquired images to computer
14. Calibrate the imaging area of interest by taking several focused and sharp images of an object with a known size (i.e. 1/32" bearing ball) located at the fibers cross. The setting on the camera should not change and must be similar to what was used in the experiment)
15. Return to step 6 for a new experiment
16. Turn off both cameras and put the caps back on the lenses
17. Turn off the backlight
18. Turn off the ignition and retraction power supply
19. Wash the microsyringe by first loading and unloading it with ethanol sand then distilled water for several times
20. Put all fuel containers in fire safe cabinet

It should be noted that the DSLR camera cannot be controlled by the Arduino and therefore is turned on and off manually in steps 10 and 12 respectively. However, the purpose of using this camera is to track the ignition and extinction times which could be measured by observing the glow on the fiber.

3.6 Summary

In this chapter the experimental arrangement and all of its subsystems were explained. Detail information of any single item and drawing of all parts were also presented. All the techniques used in assembling the parts was explained visually so that it could be easily duplicated. Then the timing of events and the electric circuit used to synchronize them was explained briefly and finally a detailed procedure for running an experiment was presented.

4 EXPERIMENTAL STUDY OF THE COMBUSTION OF HYDROCARBON DROPLETS WITH POLYMERIC ADDITIVES

In this chapter combustion of hydrocarbon fuel droplets with a combustible polymeric additive will be studied. After reviewing the experimental method, the effect of addition of a long chain polymers to transportation fuels (diesel and jet fuel) will be investigated. Then, three normal alkanes as the main components of the tested hydrocarbon fuel will be studied under the same conditions to better understand their combustion dynamics. The main focus in this study will be on calculating burning rate and understanding the phenomena observed during combustion of polymer added droplets. Finally, sample soot particles will be collected and their morphology will be studied using SEM microscopy.

4.1 Introduction

According to recent statistics released by National Transportation Safety Board (NTSB), 94% of transportation fatalities in 2011 are categorized as highway fatalities with two main sub-categories of passenger cars (35%) and light trucks and vans (27%) [85]. Having fire present in crash scenarios results in a several-fold increase in the number of injuries/fatalities, as crash fires account for 58% of the deaths in transportation accidents [86]. Recent studies on fire safety of transportation fuels proposed that adding long chain polymers to transportation fuel will induce non-Newtonian shear-thickening behavior in the fuel [19]. However, the end product of a transportation fuel is its combustion in engine and so the impact of any additive on the performance and emission characteristics of fuel needs to be investigated.

In terms of blending mixtures, adding polymer to a hydrocarbon fuel will change it to a binary or multicomponent fuel which have been studied for several years. Wang et al. studied behavior of fuel droplet composed of components with different volatility, boiling point and diffusion coefficients [31]. They showed that the combustion of binary droplets is initially controlled by the boiling point of more volatile component, but transitions to a process that is dominated by the less volatile component. To better understand the mechanisms of binary fuel combustion, Shaw et al. proposed a model to explain the effect

of impurities on evolution of binary miscible mixtures during combustion [87]. There is also a large body of research on combustion of water added hydrocarbons because of its promising effects on improving atomization and combustion performance[35,42,45,88–90]. Flammability mitigation and fire safety improvement [17,44] as well soot emission reduction [34] have been other motives to drive studies on water-containing diesel fuels.

In spite of similarities of water-hydrocarbon and hydrocarbon-hydrocarbon blends with polymer added fuels as a result of their binary natures, there are still major differences in combustion behaviors. While combustion of liquid droplets occurs only in the gas phase, chemical reactions in polymer combustion may also occur in the condensed phase as well as at the solid-gas interface [59]. In order to understand these complexities, researchers have mainly focused on the combustion of polymer spheres or particles [60,61]. They showed that polymer drops follow the traditional d^2-law of combustion and have higher burning rates compared to hydrocarbon oils. While combustion of multicomponent fuel as well as polymer combustion have been studied for several years, there is not enough information available on a mixture of both. In this regard, the main objective of this chapter is to experimentally examine the effects of adding long chain polymer on combustion characteristics of hydrocarbon droplets.

4.2 Experimental Design and Measurements

The focus of this chapter is to understand combustion behavior of transportation fuel when blended with a polymeric additive. For this purpose, Diesel and Jet fuels were selected as two of the main fuels in transportation industry. The diesel fuel used for this research is a commercial blend known as Diesel#2 and was purchased from one of Conoco's gas stations. The jet fuel in this study is Jet-A and was supplied from a municipal airport in Iowa City. However, since both of diesel and jet fuel are composed of many different constituents with different properties, it might be difficult to fully interpret the result. Therefore, n-decane (99+%) and n-dodecane (99%) as main components of jet fuel and n-hexadecane (99%) as the main component of diesel were purchased from Acros Organics and studied under same condition.

The polymer used to induce shear thickening effect in the work of David et al. [19] is Polybutadiene (PBD). Polybutadiene is a very long chain polymer formed from

polymerization of the monomer 1,3-butadiene ($H_2C = C = CH - CH_2$) and has a wide range of applications from making tires and plastics to golf balls and toys. PBD is also combustible and could be used as a fuel in various solid rocket boosters. In this study, a commercial grade Polybutadiene known as 140ND provided by Firestone Polymers was used. 140ND, which is elastic and has a solid form in room temperature, is shown in as shown in Figure 1.1. This polymer has number and weight average molecular weights of 110,000 and 230,000 gr/mole respectively (data provided by Firestone Polymers). The number average molecular weight (M_n) is the statistical average molecular weight of all the polymer chains while the weight average molecular weight (M_w) takes into account the molecular weight of a chain in determining contributions to the molecular weight average. The more massive the chain, the more the chain contributes to M_w.

Figure 4.1 Polybutadiene 140ND in room condition

Polymer-fuel solutions were prepared by blending PBD in each hydrocarbon at different concentrations (up to 3.0%, by weight) using a magnet stirrer. All of the solutions were prepared at the same stir speed and for 24 hours. To avoid evaporation and any change in the concentration of solutions, no heat was used and the solution containers were sealed by a rubber stopper during and after preparation. All of the experiments were conducted right after solution preparation to avoid any possible sedimentation or agglomeration of polymer strands.

The experimental apparatus was inspired by the work of Bae et al. [91]. A schematic of the fiber support arrangement is shown in Figure 4.2. The configuration consists of a base plate, a fiber mount to hold three 16-μm-diameter SiC fibers (NL-202 Nicalon™ fibers) and two other aluminum frames to hold the solenoids. All parts drawings and the assembly process have been explained in detail in chapter 3.

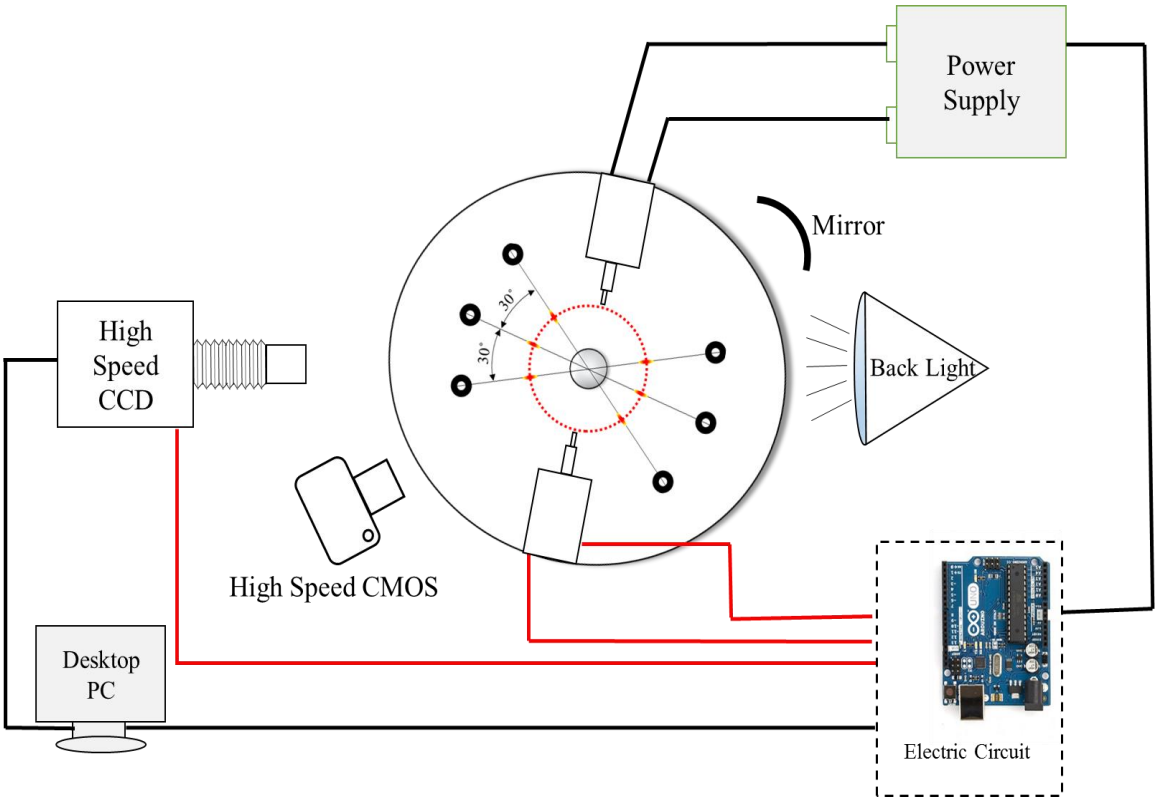

Figure 4.2 Schematic diagram of experimental arrangement

The ignition was provided by two symmetrical hot wire rings made of 36 gauge annealed Kenthal wire as explained in chapter 3. The rings were made by wrapping equal lengths of Kenthal wire around a 0.6 mm drill bit to make sure equal resistance and consequently heat will be generated in all cases so long as the voltage was kept constant. Different hydrocarbons used in this study have different thermal diffusions and so different heating times will be required for each case to generate ignition. This time was obtained through a trial and error process and is listed for each case in Table 4-1. It was also tried (visually) to keep the same distance between the rings for all. Two solenoids were used to retract the hot wires right after heating time ends to avoid any interaction with flame and droplet evolution due to excessive heat transfer effects. Normally the heating time shown in Table 4-1 is not enough to ignite either of the fuel types but this quick retraction of hot wires creates two vortices that improve convection around the droplet and ignite it right away. Due to the vibrations from solenoid retraction the droplet starts to bounce up and down which may generates some erroneous data for a very short time. The moment of this bouncing event has been marked as ignition in Figure 4.4. The SiC fiber were crossed at

an angle of 30˚ with each other making a total angle of 60˚. Small droplets with diameters in the range of 0.6 to 1.0 millimeter were generated using a 10-µl microsyringe with a 33 gauge needle (Hamilton 1701SN) and were deployed on the intersection of fibers.

Table 4-1 List of fuels with polymer concentration and heating time for each case

Hydrocarbon	PPD Concentration (wt%)	Heating Time (ms)
Jet-A	0 (pure fuel case)	400
	.5	400
	1	400
	2	400
	3	400
Diesel#2	0 (pure fuel case)	400
	.5	400
	1	400
	2	400
	3	400
n-Decane	0 (pure fuel case)	300
	0.1	300
	0.2	300
	0.4	300
	0.8	300
	1.6	300
n-Dodecane	0 (pure fuel case)	300
	0.1	350
	0.2	350
	0.4	350
	0.8	350
	1.6	400
n-Hexadecane	0 (pure fuel case)	400
	0.2	400
	0.4	400
	0.8	400
	1.6	400
	3.2	400

Two cameras were used at two different angles to record the droplet and flame behavior in time: a black and white CCD high speed camera (X-StreamVision XS-3) attached to an extension tube (Nikon PB-6 Bellows Focusing Attachment) and a 105 mm lens (Nikon AF Micro-Nikkor-F/2.8) to trace droplet evolution and a color CMOS camera (Casio EXILIM Pro EX-F1) to see the moment of ignition and flame changes during combustion. To obtain a larger image, a concave mirror (4.0 in diameter × 9.0 in focal length) was placed on the other side of the droplet, across from the color camera, and the camera was focused on the magnified image of the droplet in the mirror. The black and white droplet images were captures at 500 fps while the color camera recorded its video at 600 fps. Aligned with the CCD camera, a projector (Kodak Ektagraphic model AF-2) was placed to serve as backlight. The timing of all events (hot wires, solenoids and CCD camera) was controlled by a microcontroller board (Arduino Uno) with a temporal resolution of 1ms.

The backlit images were exported to an image processing software, Spotlight, developed by NASA [92]. Since the droplets' initial diameter were small enough, and also given the very low surface tension between the droplets and fibers, the droplets remained spherical throughout most of the combustion process. Therefore, the recorded area of droplet was assumed to be the area of a circle. The supporting fibers are also seen in the acquired images that must be eliminated to obtain only the image of the droplet. Therefore, the following image processing operations (also shown in Figure 4.3) are applied on the stack of images to remove the fiber and yield only the droplet:

1. Defining an area of interest (AOI): any image processing operation is performed on individual pixels or an array of them. Given the large number of pixels in each image and large number of images in each experiment (between 700 to 1200), the processing and analysis of images could be quite time consuming. To save the time, only the area of each image that covers the whole droplet is considered for further processing. Considering the limited motion of the droplet in space during combustion, a rectangular box similar to each frame around the droplet shown in Figure 4.3 could be considered as an AOI. If the droplet moves beyond the AOI boundaries, the process should be stopped manually and

restarted after adjusting/resizing the AOI to a new location. For more information, see reference [92].

2. Arithmetic operation: the backlit images from CCD camera are grayscale and therefore are composed of pixels with intensities between zero (black) and one (white). The aim of this operation is to increase the intensity of all pixels in a way that the pixels representing the fibers reach to a value equal to one or greater. While a adding a large value may result in losing some of the droplet pixels and fading them into the background, a very small value may as well not completely remove the fiber. In this research, and based on the intensity of the fibers pixels which are typically greater than 0.3, it was determined that adding a constant value of 0.7 to all pixels will result in the fiber to fade away in the white background and will only the droplet as shown in the second image (from the left) in Figure 4.3.

3. Contrast enhancement: the image of the droplet after the previous operation is dim and needs to be restored for further processing. Enhancing the contrast via a linear contrast stretch function will generate the center image in Figure 4.3.

4. Intensity inversion: this operation is required because in the last step we will need to count the number of white pixels in AOI and currently the interior of the droplet is mostly black. In this step, a threshold value of 0.5 with an inverse mode is defined; all pixels with an intensity equal or greater than this threshold will become zero (black) and the smaller intensities will turn to one (white).

5. Morphological operation: due to light refraction, especially for pure or polymer added fuel droplets, a bright area will be formed in the center of the droplet. This area, which will become black after all above operations, will need to be white in order to be counted as part of the droplet cross sectional area. The morphological operation will find all the black pixels within the droplet area and will change their intensity to one.

6. Counting the white pixels: now that the fibers as well as the effects of light refraction have been removed from the image, we have a white circle which

represents the cross section of a burning droplet. Through counting the number of white pixels we will be able to determine the instantaneous diameter of the droplet in pixels. The diameter in pixels could be later converted to millimeters through calibrating the AOI with an object with known size.

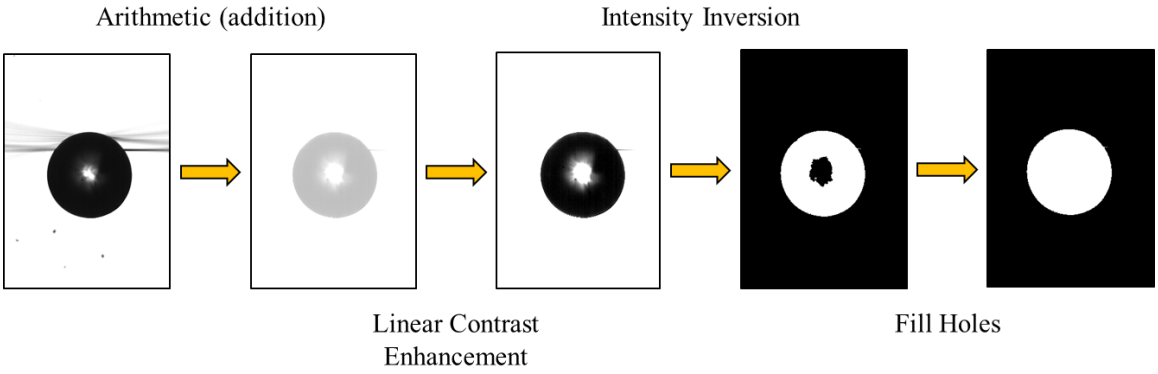

Figure 4.3 Image processing operations to measure the diameter of a burning droplet

Given that the circular cross section of a droplet is proportional to the square of the droplet diameter, the instantaneous droplet diameter in pixels was calculated by counting the number of pixels per circle for each frame in Spotlight. After calibrating each experiment with an object with known size, the diameters in pixels were converted to millimeter. The object used for calibration was a bearing ball with nominal size of 1/32" whose exact diameter were measured by a Scanning Electron Microscope (SEM). The cross section regression data were taken to diagrams similar to Figure 4.4 to compare with the d^2-law of combustion described through the following equation:

$$\left(\frac{D}{D_0}\right)^2 = 1 - K\left(\frac{t}{{D_0}^2}\right) \tag{4.1}$$

where D, D_0, t and K are droplet instantaneous diameter, droplet initial diameter, time and burning rate constant respectively. However, because of the binary nature of droplets and due to boiling and swelling phenomena, there were periods during which droplets took some irregular shapes. Figure 4.4 represents diameter evolution of a jet fuel droplet with 0.5% PBD concentration. After going through an initial thermal expansion, all of the polymer added cases follow the classical d^2-law in four distinguished regimes: three fairly straight segments (I, III and IV) representing steady droplet burning and a very unsteady transition zone (II) which comes with multiple droplet swelling and sputtering events.

Because of these strong swellings, the droplet undergoes severe volume changes and therefore the data in zone “II” are very scattered. Removing irregular shapes and fitting a first order line through the rest of the data in this zone yields a slope very close to the line fitted to the data before swelling begins. Nevertheless, due to the large differences in the values of intercepts, the data points in zone “II” were not considered in later calculations of apparent burning rate. Only for the sake of a cleaner representation, the data with a deviation of less than 10% from the linear regression obtained in zone “I” will be shown in next figures. These points have been marked with red circles in Figure 4.4.

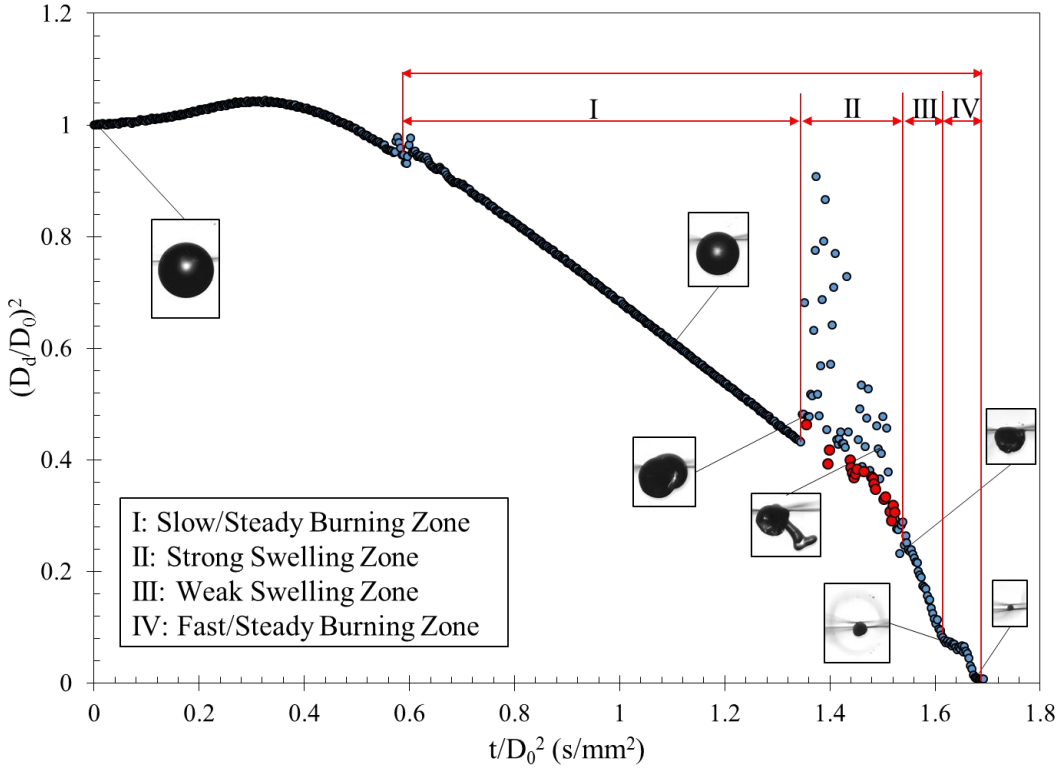

Figure 4.4 Evolution of droplet diameter square for a jet-A droplet with D_0 = 0.85mm and PBD concentration of 0.5%.Red marks are points with less than 10% deviation from linear regression in zone “I”

4.3 Combustion of Diesel and Jet Fuel with Polymeric Additive

In this section, the result of combustion of diesel and jet fuel droplets doped with different percentages of PBD are presented. The cases for which experiments were carried out are shown in Table 4-1. For each case, a minimum of five runs were carried out and the combustion process recorded using high speed photography for further analysis. However, because of to the droplet swelling and sputtering events it is possible that the

droplet goes out of focus or in rare cases loses significant amount of mass due to strong microexplosion. Hence, only three runs of each case that had highest quality of images were chosen for image analysis. The data in Figure 4.5, which are for five different runs of 1.0% PBD in jet fuel, clearly show the repeatability of the experiments and measurements. It is noteworthy that for each experiment the SiC fibers were replaced by a new set of fibers to avoid soot particles or other combustion residues from the previous experiment from interfering with the combustion of new droplet.

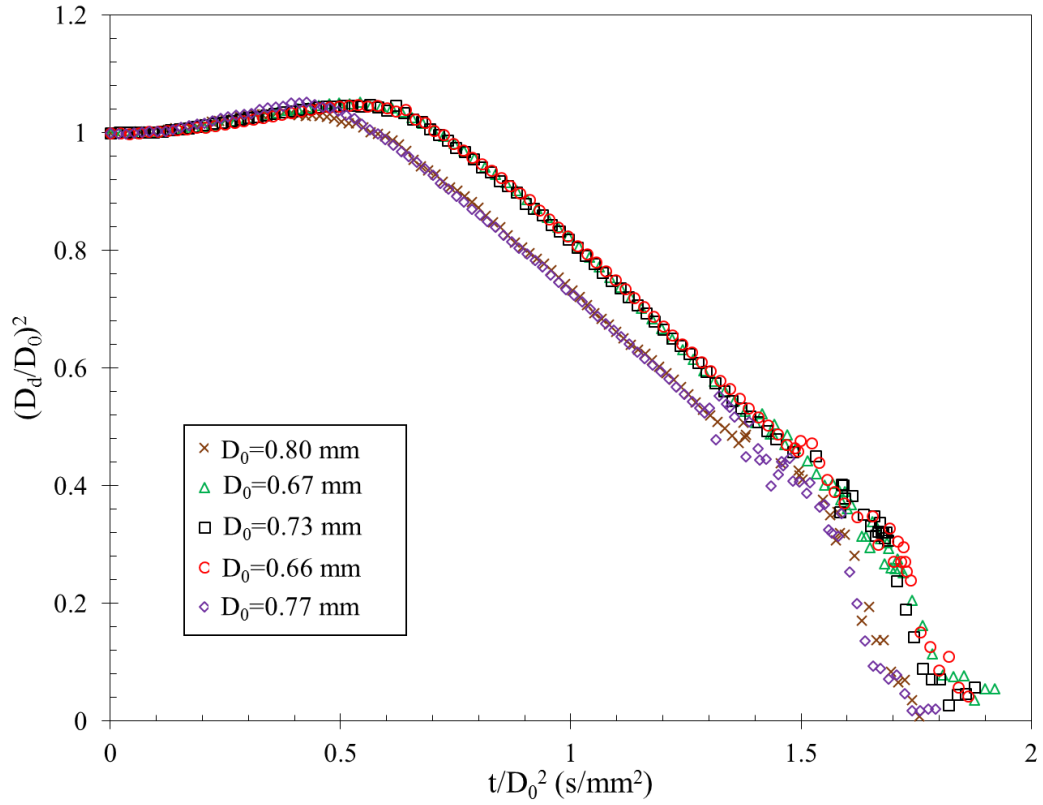

Figure 4.5 Evolution of diameter square for droplets of 1.0% PBD in jet fuel

After processing images of droplets in the Spotlight software, the instantaneous diameters were measured and the result graphed. The evolution of diameter square for jet fuel and diesel droplets doped with different percentages of PBD on d^2-law coordinate are shown in Figures 4.6 and 4.7, respectively. From the results shown in these figures, all of the cases, with or without added polymer, follow the classical d^2-law. In comparison with other binary fuels, polymer added fuel shows both similar and different behaviors during combustion; similar to binary fuel droplets composed of species with different volatilities, the higher volatile component (diesel and jet fuel in our study) starts to burn first. Wang et

al. studied combustion of binary fuel droplets in several cases including two-component mixtures with very different boiling points and two-component mixtures consisting of an extremely heavy component [31]. In both cases, the burning rate is initially controlled by the more volatile component. Once the concentration of volatile component at the droplet surface was sufficiently decreased, there is a transition to a phase which is dominated by the less volatile component. Similar to binary fuels, the droplet regression rate on d^2 coordinate shows distinguished regimes of combustion and transition between them, but the number of these regimes is more than two.

The changes in droplet surface area (or diameter square) shown in Figures 4.6 and 4.7 suggest different behaviors of jet fuel and diesel during heating and combustion processes. While jet fuel shows almost no dependence on polymer concentration in zone "I", diesel starts to burn slower as the concentration of polymer increases. Figures 4.8a and b show a closer view of initial preheating up to the ignition point for both jet fuel and diesel droplets respectively. By heating through hot wires a competition between thermal expansion, representing droplet heating, and droplet vaporization begins. Initially the rate of expansion is higher and therefore the droplet volume increases. But as the temperature increases inside the droplet, the vaporization rate increases and eventually it exceeds the expansion rate resulting in droplet shrinkage.

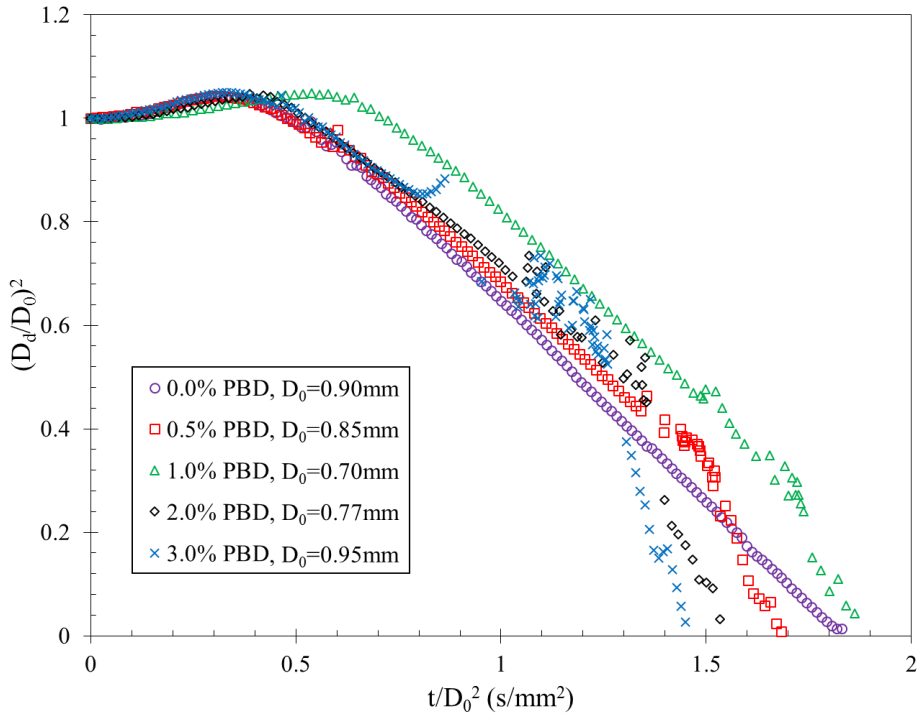

Figure 4.6 Evolution of diameter square for jet fuel droplets blended with different percentages of PBD

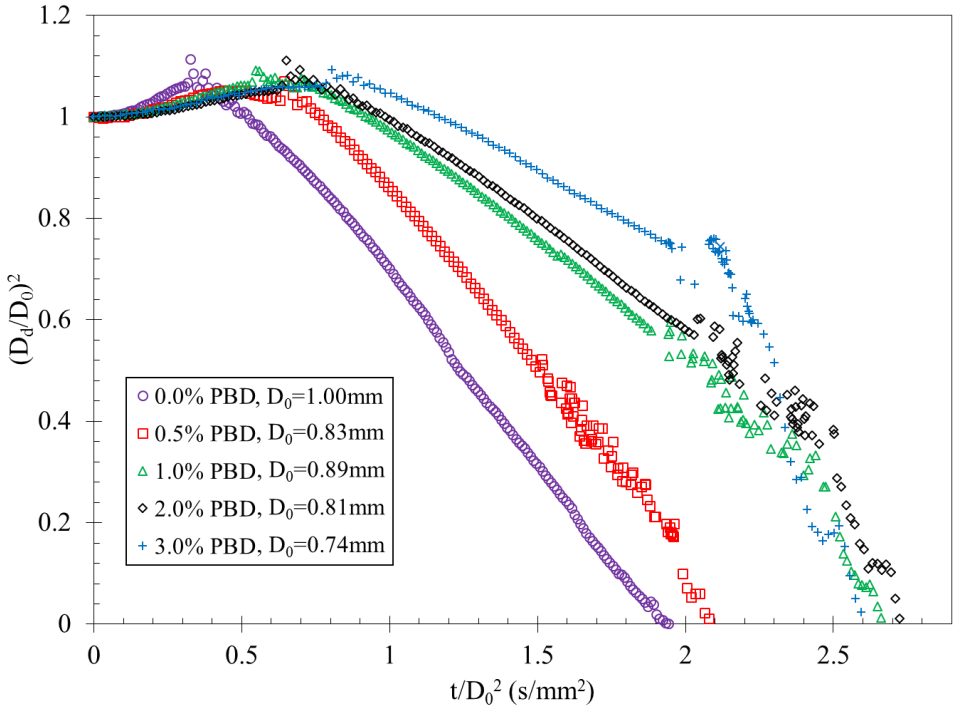

Figure 4.7 Evolution of diameter square for diesel droplets blended with different percentages of PBD

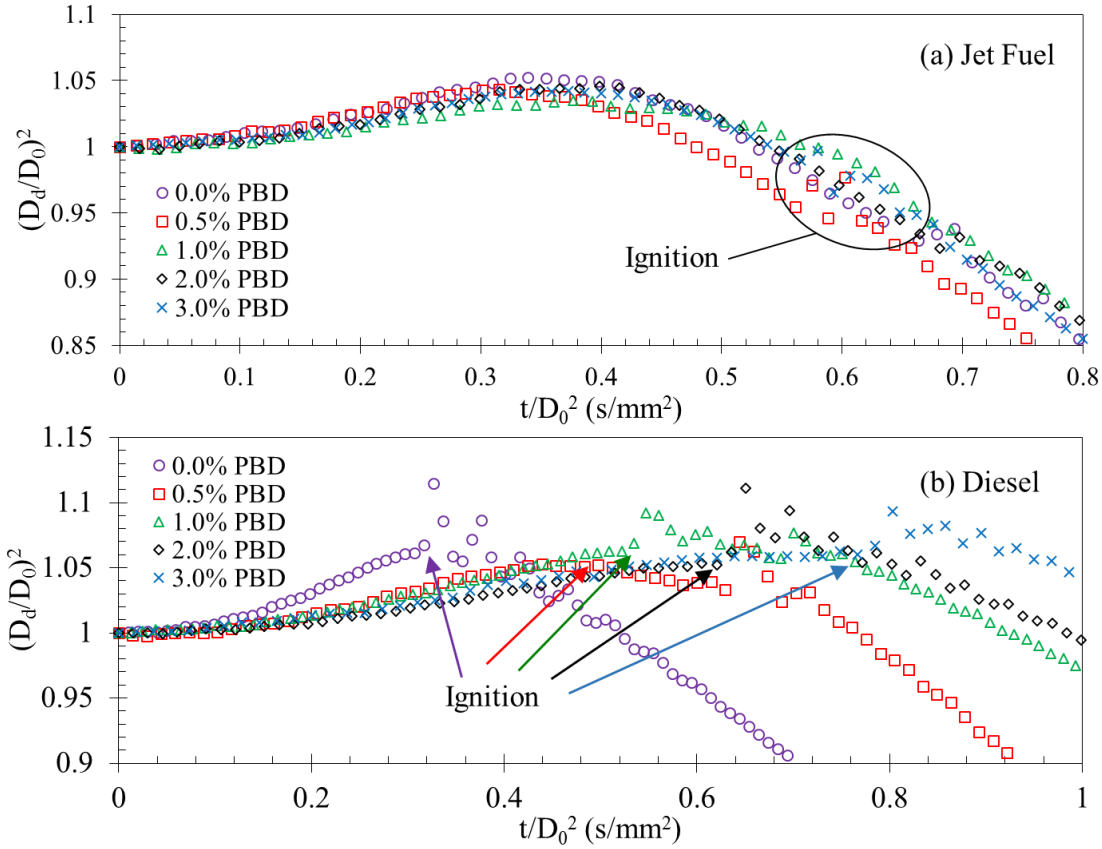

Figure 4.8 Evolution of diameter square for (a) jet-A and (b) diesel droplets in initial heating zone

For jet fuel it is observed that the addition of polymer has no effect on the preheating zone and ignition occurs in the downhill of the curve. However, polymer addition extends the diesel expansion period and ignition occurs right at the peak. In other word, polymer addition decreases the rate of vaporization and the volume continuously increases until the ignition results in strong heat transfer and mass loss. The same color arrows on Figure 4.8b point to the location of diesel droplets ignition at different PBD concentrations. The reduction of vaporization rate continues into the combustion zone and the diesel burning rate in zone "I" decreases as PBD concentration increases. Given the wide range of differences in the properties of diesel and jet fuel, it is difficult to establish a concrete explanation of such different behaviors. However, examining the combustion of main constituents of these fuels, i.e. decane and dodecane for jet fuel and hexadecane for diesel, under the same conditions, one might be able to better understand this different behavior. This will be done later in section 4.3.1 of the present chapter.

Polymer concentration has a significant effect on the onset and intensity of swelling zone. PBD, a soft plastic at room temperature, has an extremely higher molecular weight than those of diesel and jet fuel. It also has a much higher boiling point which gives it a less volatility and at the same time higher diffusion coefficient. Evaporation and combustion of the more volatile component results in a higher concentration of the less volatile component, i.e. polymer, near the droplet surface. The droplet surface tends to remain near the boiling temperature of the higher volatile component. But as the mass fraction of the polymer increases, the droplet surface temperature rises beyond the boiling temperature of fuel. For polymers, internal heating is followed by swelling and internal bubbling that causes sputtering of the polymer surface [60]. It appears that as the droplet temperature increases, polymer strands in the solution, especially those suspending in near the surface boundary layer, act as nucleation sites for the higher volatile component, as shown in Figure 4.9, and boiling starts within the droplet and close to the surface. Images *A1* to *A3* in Figure 4.10 show how a bubble is formed near the inner surface of droplet and grows until it bursts in image *A4* (also shown schematically in Figure 4.9). It should be mentioned that due to imparted non-Newtonian viscosity, micro-explosion as reported in water/oil emulsions [16] is not observed unless polymer concentration is relatively high like image *B4* in Fig. 5. Normally no micro-explosion was observed in low polymer cases and the very rare incidents of micro-explosion (such as *B1* in Figure 4.10) could be a result of impurities present in PBD. But regardless of polymer concentration, *B1* to *B4* in Figure 4.10 show that upon micro-explosion the droplet does not break into small splatters and viscosity helps it keep itself together by connecting ligaments stretched in different directions.

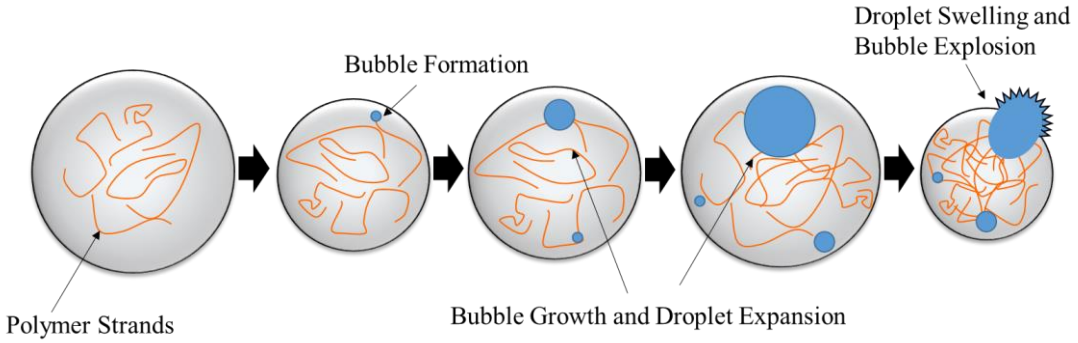

Figure 4.9 Bubble formation and growth inside a polymer added fuel droplet

The process of bubble formation and its following burst continues to occur strongly until a certain point that it transitions into a much less intense swelling zone. Figure 4.11 shows the ratio of droplet volume to its initial volume at the beginning and end of swelling regime (zone "II") and also at the end of weak swelling. According to this graph, the changes of both ratios at the beginning and end of the swelling zone are almost parallel and increase almost at the same rate. This offers that the same volumetric percentage of each droplet burns in zone "II" regardless of its initial PBD concentration. An analysis of our experimental result shows that (51±7)% of initial droplet volume burns under strong swelling condition in zone "II". In addition, the polymer content at the end of swelling zone could be approximated using the following equation:

$$PBD(wt\%) = PBD_0(wt\%) \times \frac{V_0}{V} \tag{4.2}$$

where V_0 and V are the droplet initial volume and volume at the end of zone "II" respectively. The following assumption have been considered to obtain equation (4.2):

- The effect of PBD density on the solution initial density is negligible due to its low concentration.
- Only the high volatile constituent, i.e. diesel or jet fuel, burns in zones "I" and "II".
- The density of liquid droplet does not change through combustion in zones "I" and "II".

Considering the above assumptions and using equation (4.2) it turns out that the concentration of PBD at the end of strong swelling zone is about (11.92±3.51)%. Once the concentration of diesel or jet fuel decreased enough, combustion transitions into the third zone in which liquid droplet still consists of mostly the base fuel but the polymer concentration has also increased several-fold. The very large polymer concentration in this zone (~12% for diesel as mentioned above) leads to very high viscosity so that the shear forces control bubbling and sputtering. Hence no strong swelling is observed in zone "III" and the droplet burns in an almost spherical shape at most times. The flame in this zone is very sooty which could be a direct result of high number of carbon atoms present in PBD. Images *C1* to *C4* in Figure 4.10 clearly show the soot shell formed around the droplet which is disturbed by plumes of hot gases leaving polymer surface.

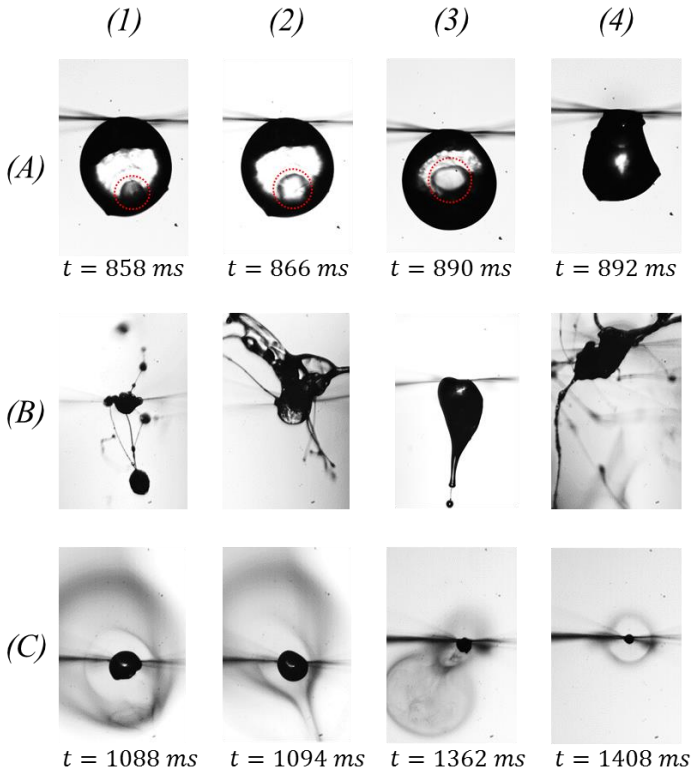

Figure 4.10 Swelling, sputtering and extinguishment of polymer added droplets (The time mentioned includes 400 ms heating time). A1-A4: 0.03PBD-0.97Diesel; B1: 0.005PBD-0.995Jet A, B2: 0.02PBD-0.98Jet A, B3: 0.01PBD-0.99Diesel, B4: 0.03PBD-0.97Diesel; C1-C4: 0.005PBD-0.995Diesel

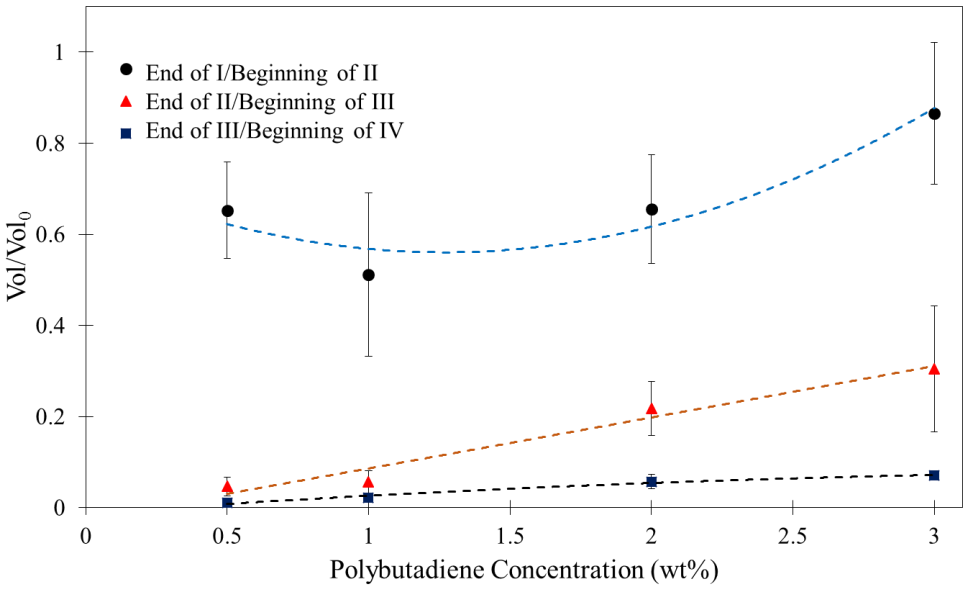

Figure 4.11 The ratio of diesel droplet volume to its initial volume at the beginning and end of strong swelling zone

Finally, combustion in zone “III” transitions to zone “IV” during which the droplet burns at a rate almost as fast as zone “III” but with virtually no swelling. The transition identified in the beginning of zone “IV” shown in Figure 4.4 is almost a flat line which correspond more to a heating process than a combustion one. The blue squares in Figure 4.11 show the ratio of droplet volume at the beginning of zone “IV” to its initial volume. Using equation (4.2) one more time, it turns out that concentration of PBD at the beginning of ending regime is (42.90±4.91)%. Comparing this concentration to the very low initial polymer concentration and given the fact that molecular weight of PBD is several orders of magnitude larger than that of diesel or jet fuel, it could be concluded that the combustion in zone “IV” is virtually polymer combustion. Therefore, the transition at the beginning of zone “IV” could be considered as the transition from combustion of high volatility component, i.e. diesel or jet fuel, to the combustion of low volatility part. In other word, in the history of droplet diameter of binary fuels in [31], the two main observed zones are equivalent to zones (“I+II+III”) and “IV” in our study and the flat transition between the two main sections corresponds to preheating of polymer. All polymer added droplets burn to completion and eventually extinguish in a flash. The yellow light, which simply represents a more sooty flame, could be because of impurities in the polymer. This could also be the result of residual char combustion that occurs in some char-forming polymers [93].

Figure 4.12 shows the variations of burning rate and the effect of adding polymer to jet fuel and diesel. It was previously mentioned that the droplets burn with almost same rate in the first two zones. The burning rate at the final stage is also very close to that of zone III. Therefore, two apparent burning rates defined as K_I and K_{III} (for zones “I” and “III” respectively) should suffice to distinguish between burning rates dominating each zone. As shown in this figure, the current levels of PBD in our base fuels result in a reduction in burning rates of zones I and II. However, the burning rate reduction in diesel is more consistent than in jet fuel where the reduction is more evident at PBD concentrations larger than 1%. This burning rate, represented as K_I in Figure 4.12, corresponds to the more volatile component, i.e. jet fuel and diesel and its reduction will be discussed in sections 4.3.1 and 4.3.2. On the other hand, blending more polymer in base fuel impacts the burning rate in the fast combustion zone differently and increase burning

rate to values even more than that of pure fuel. Higher values of K_{III} could be because of improved heat conductivity as the concentration of polymer increases. It could also be explained by flame standoff ratio (the ratio of flame diameter to droplet diameter) which is typically higher for polymers and makes the flame stand much closer to the polymer droplet than hydrocarbon fuels [94]. This proximity of flame front to the droplet surface increases burning rate especially in zone "IV" where combustion is controlled by thermophysical properties of PBD.

To see the combined effect of K_I and K_{III}, the burning time of jet fuel and diesel droplets were extracted from the captured images and presented in Figures 4.13. In this diagrams, τ_b/D_0^2 is burning time normalized by the square of initial diameter to cancel the effect of different initial diameters. The data in Figure 4.13 shows that adding trace amounts of PBD will decrease the total burning time of both diesel and jet fuel as a direct consequence of enhanced burning rate in the final stages of combustion.

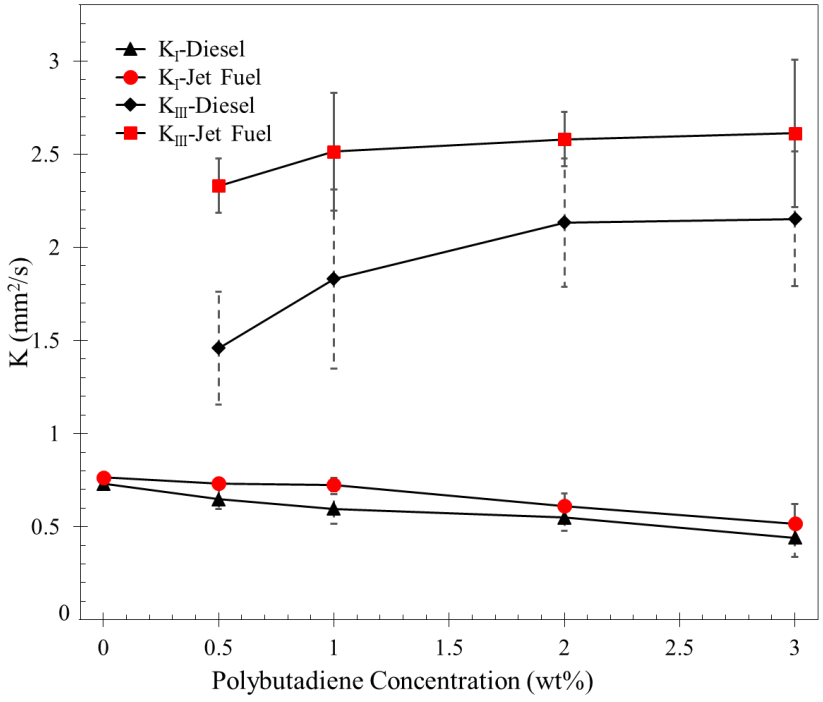

Figure 4.12 Apparent burning rates as a function of PBD concentration for jet fuel and diesel droplets. Each data point represent an average of at least three experiments. The error bars show the standard deviation

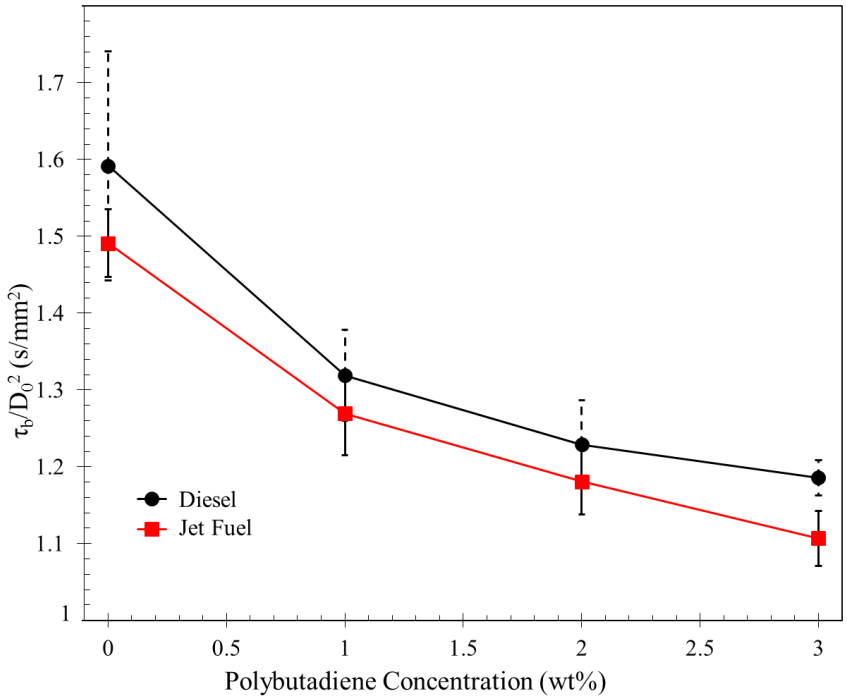

Figure 4.13 Variation of droplet burning time with PBD concentration for jet fuel and diesel droplets. Each data point represent an average of at least three experiments. The error bars show the standard deviation

4.3.1 Combustion of Decane, Dodecane and Hexadecane with Polymeric Additive

The combustion of diesel and jet fuel with a polymeric additive was examined in detail in section 4.3. Both fuels showed similar regimes and followed same patterns in all combustion zones with only a difference in the initial burning rate as polymer concentration increases. Since both diesel and jet fuel are blends of many components, it is almost impossible to identify the characteristic or component responsible for the observed behavior. To better understand what causes this difference, it is necessary to study simpler fuels that resemble our transportation fuels of study. For this purpose, n-decane and n-dodecane as main constituents of jet fuel and n-hexadecane as the main component of diesel were chosen.

The changes in the droplet diameter square and the effect of adding polymer to decane, dodecane and hexadecane have been shown in Figures 4.14, 4.15 and 4.16, respectively. These graphs propose that the combustion of polymer added alkanes consists of similar zones observed for transportation fuel in Figure 4.4.

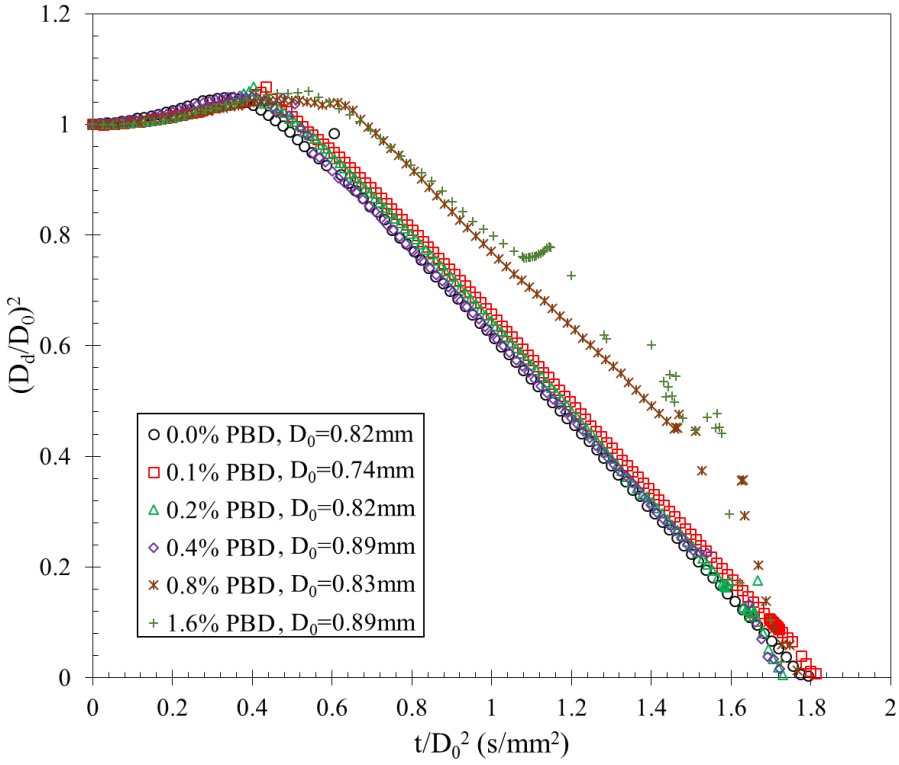

Figure 4.14 Evolution of d^2 for n-decane droplets blended with different percentages of PBD

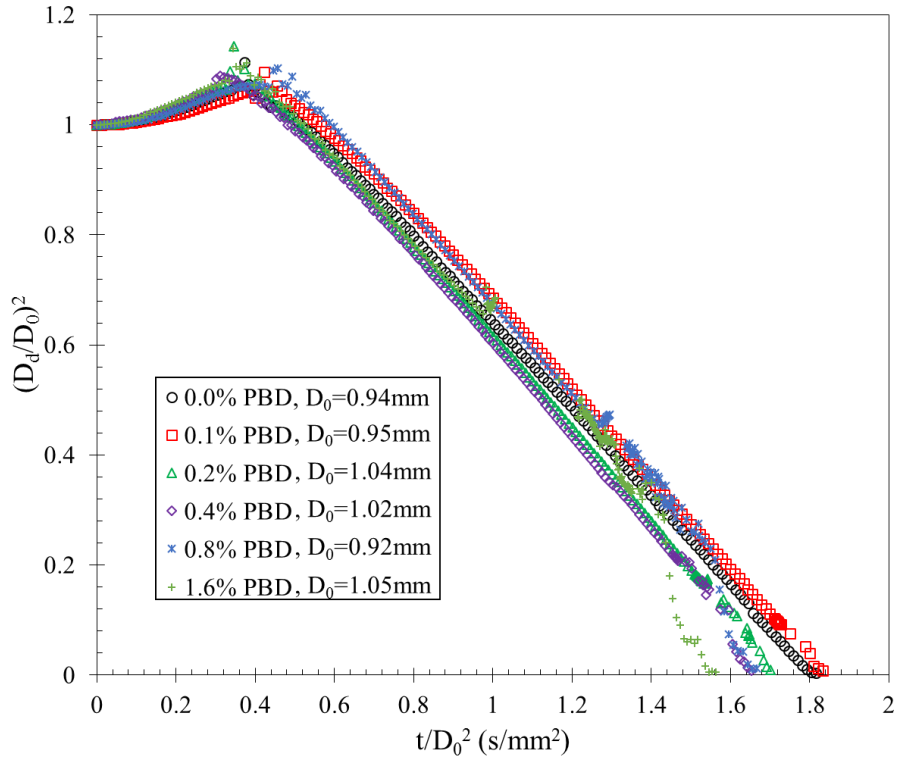

Figure 4.15 Evolution of d^2 for n-dodecane droplets blended with different percentages of PBD

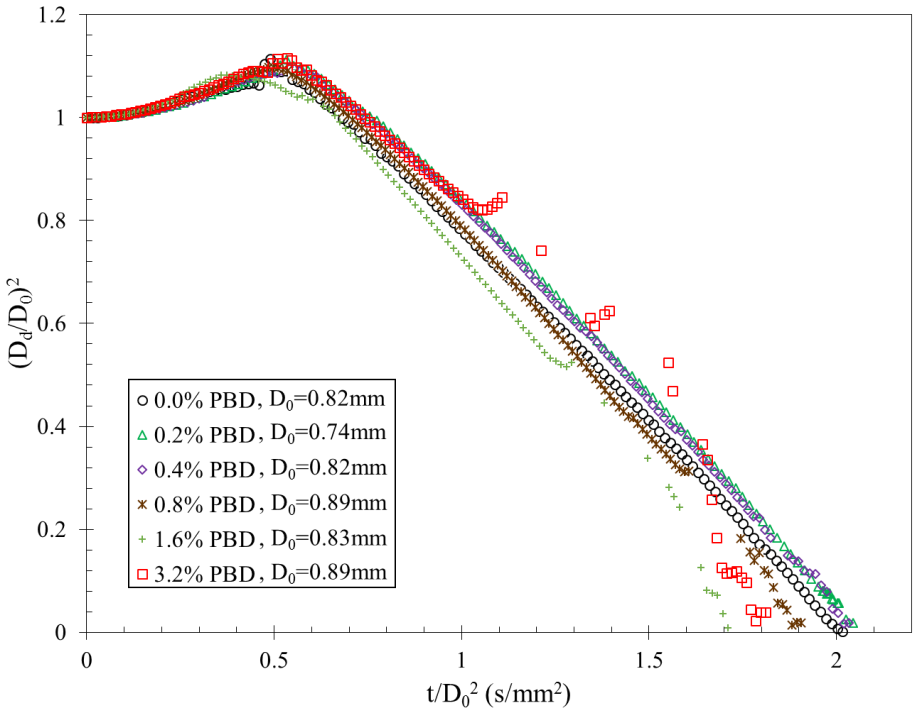

Figure 4.16 Evolution of d^2 for n-hexadecane droplets blended with different percentages of PBD

The similar combustion regimes seen in both alkanes and commercial transportation fuels could be simply explained by the binary nature of polymer added fuel which was already explained in section 4.3: in the first regime, higher volatility component, i.e. alkanes, dominates until the droplet surface regresses to a point where polymer strands, which now exist at higher concentration, are very close to surface. This polymer strands act as nucleation sites for higher volatile component and bubbling is observed locally on the droplet surface. Combustion in this regime is accompanied with strong swelling and sputtering but micro-explosion is not normally seen due to higher viscosity. Later when polymer concentration increases enough, strong swelling stops due to very high viscosity of droplet. Once the droplet runs out of alkane component, droplet combustion transitions to its final stage which is polymer combustion. The transition from alkane to polymer combustion passed through a short heating period which is required to increase the droplet surface temperature to the boiling point of polymer. Finally the droplet extinguishes in a flash which is a characteristic of very sooty combustion of polymers. Figure 4.17 shows several still images of a dodecane droplet with a 0.4% concentration of PBD. The gas pockets formed inside of droplets and their plume that are accompanied by an abrupt

increase in flame length can be observed in this figure. It could be also observed in Figure 4.17 that the droplet extinguishes in a flash at t = 1716 ms.

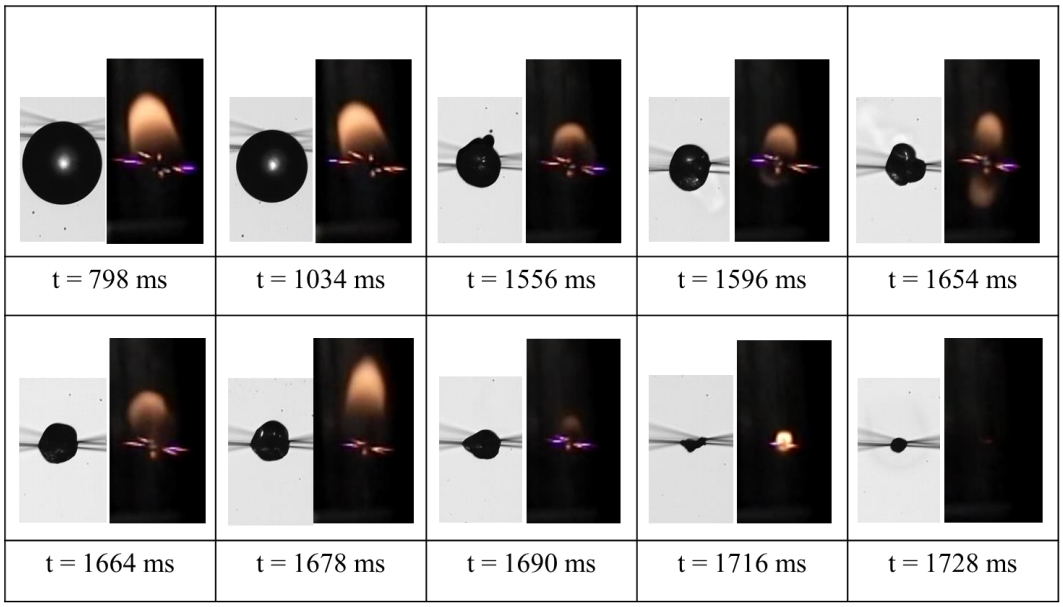

Figure 4.17 Change of droplet and its flame for a 0.4%PBD-dodecane solution (The time mentioned here includes 350 ms heating time)

Figure 4.18 represents the burning rates of decane, dodecane and hexadecane as a function of PBD concentration. From this figure it could be concluded that polymer addition has virtually no effect on the burning rate in the initial stage of combustion, i.e. K_I. In other word, alkanes show same behavior as jet fuel and different from diesel in zone I. This suggests that the different behavior of diesel in zone "I" should be a result of other components and additives. Burning rate in the slow swelling region, i.e. K_{III}, shows the same behavior as what was observed in both diesel and jet fuel. As it was explained before, the higher burning rate in this zone is because of improved heat transfer in the droplet. All of the three alkanes have ascending profiles for K_{III}, however in moving from lighter hydrocarbons to heavier ones the effect of polymer additive becomes more significant and K_{III} of hexadecane experiences higher rise compared to decane and dodecane as polymer concentration increases.

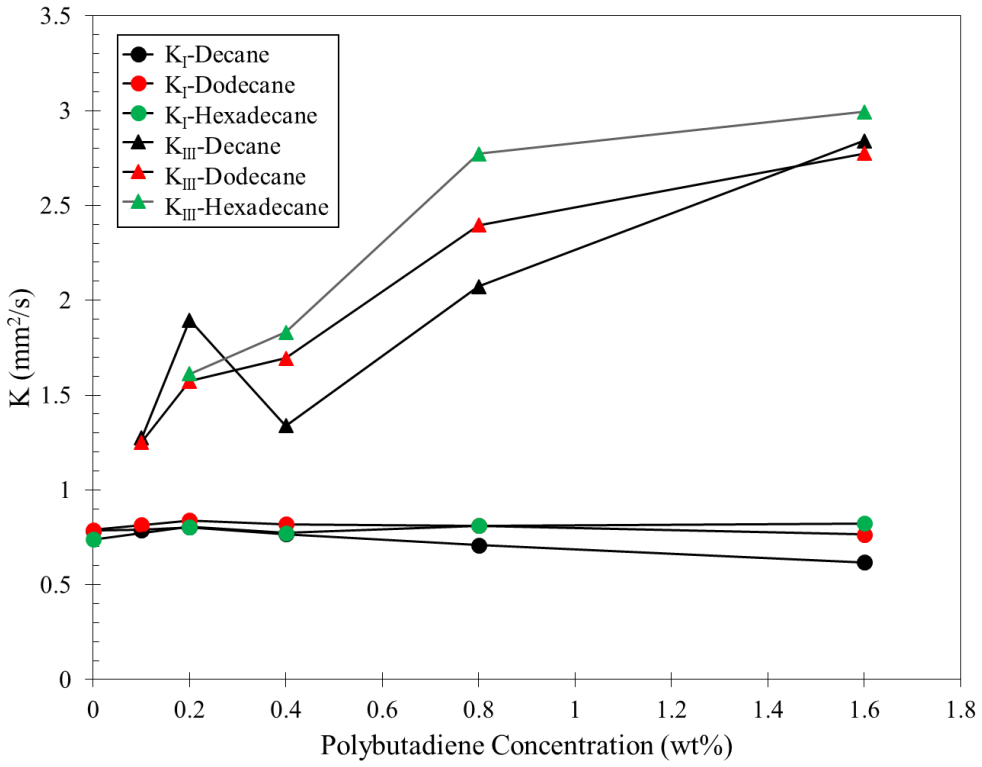

Figure 4.18 Changes of apparent burning rates of decane, dodecane and hexadecane droplets with PBD concentration

The burning time of droplets as a function of PBD concentration is also graphed in Figures 4.19a, b and c. It is seen that the total burning rate for all three alkanes decreases as polymer content increases. However, polymer addition seems to be more effective in terms of shortening combustion time as base fuels changes from C_{10} to C_{16} which should be due to more increased burning rate for hexadecane in zone "III" compared to the other two alkanes.

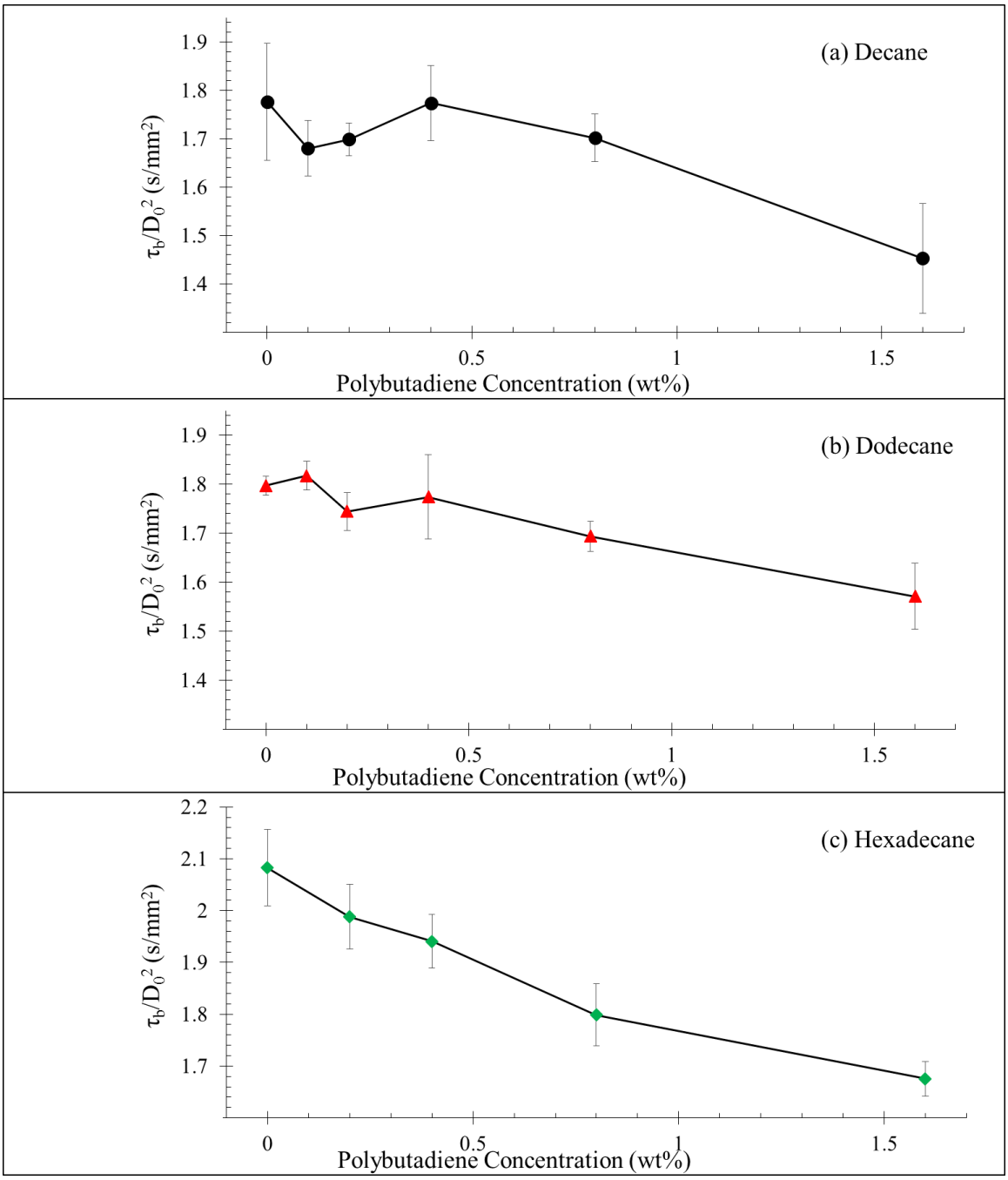

Figure 4.19 Droplet burning time as a function of PBD concentration for (a) decane, (b) dodecane and (c) hexadecane droplets. Each data point represent an average of at least three experiments. The error bars show the standard deviation

4.3.2 Viscosity and Surface Tension of Polymer Added Fuel

It was observed in Figures 4.4 and 4.6 that polymer addition results in a slightly different behavior in combustion of diesel and jet fuel in Zone "I". While the slope of diesel diagram in zone 'I' decreases as the polymer concentration increases, jet fuel shows a

weaker dependence on polymer addition. The effect of main constituents of each fuel (decane and dodecane for jet fuel and hexadecane for diesel) were investigated in section 4.3.1 by burning decane, dodecane and hexadecane droplets doped with trace amounts of PBD. However, as displayed in Figure 4.18, polymer addition did not significantly impact the burning rate in Zone "I". The other parameters that are deemed to have resulted in such different behaviors are surface tension and/or viscosity of the fuel-polymer solutions. Increased surface tension could suppress diffusion of mass from liquid to gas phase at the droplet surface. Viscosity could also suppress the diffusion of high volatile component to the surface. To better understand these mechanisms, both surface tension and viscosity of polymer solutions were measured using Langmuir-Wilhelmy balance (Minitrough System 4, KSV NIMA, Finland) and Torque Viscometer (Brookfield, series "DV-II + Pro") respectively.

To measure the surface tension, diesel-polymer and jet fuel-polymer solutions were prepared at PBD concentrations of 0.5%, 1.0%, 1.5%, 2.0%, 2.5% and 3.0%. All of the tensiometry measurements were performed using plate No. 3 (platinum Wilhelmy plate, perimeter = 39.24 mm, width = 19.62 mm, height = 10 mm). To make sure that the tensiometer is calibrated, its accuracy was first examined by measuring surface tension of both water and ethanol. The reference numbers for the surface tension of water and ethanol at room temperature (20˚C) are 72.75 mN/m [95] and 22.31 mN/m [96] that are very close to our measurements of 72.20 mN/m and 22.43 mN/m. After the accuracy of the tensiometer was verified, the surface tension of each solution was measured three times. The measured surface tensions displayed in Figure 4.22 suggests that adding polymer has almost no effect on the surface tension of fuel solution.

Similar polymer in fuel concentration as used in tensiometry were also considered for viscometry. A Brookfield torque viscometer was used to measure the viscosity of the polymer solutions. All measurements were carried out in a cylindrical container inside a cooling jacket with the cooling water was set temperature set to 25˚C. A torque viscometer measures the torque required to rotate a spindle submerged in a liquid at a certain angular and then calculated the viscosity from the measured torque. In order to have the viscometer yield the most accurate calculation and based on the viscosities of pure jet fuel and diesel,

Spindle No. 18 along with the “RV” setting of the viscometer was used (as per the tables provided in the Viscometer user manual) for all measurements. Before any measurement, the calibration and alignment of the viscometer was examined using a standard viscosity liquid at 25˚C. To count for the effect of non-Newtonian viscosity, all of the solutions were tested at four angular velocities of 6, 12, 30 and 60 rpm. The measured viscosities at these velocities have been shown in Figures 4.20 and 4.21.

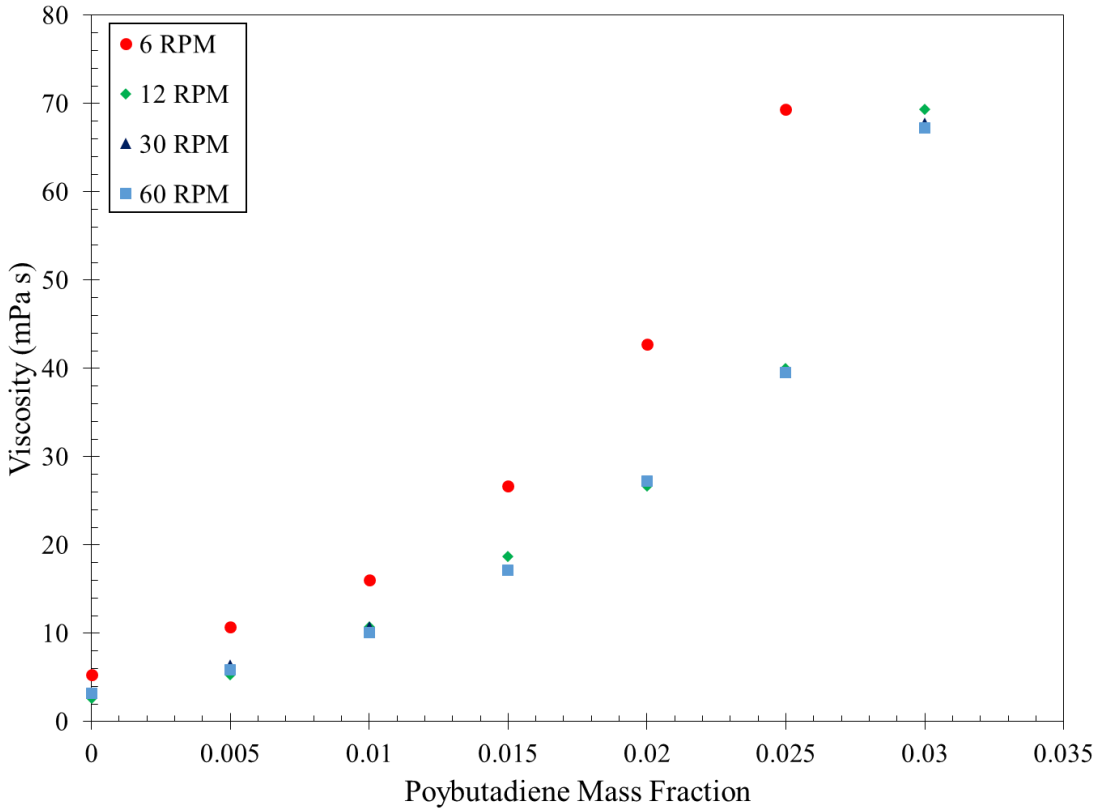

Figure 4.20 Viscosity of diesel as a function of PBD mass fraction

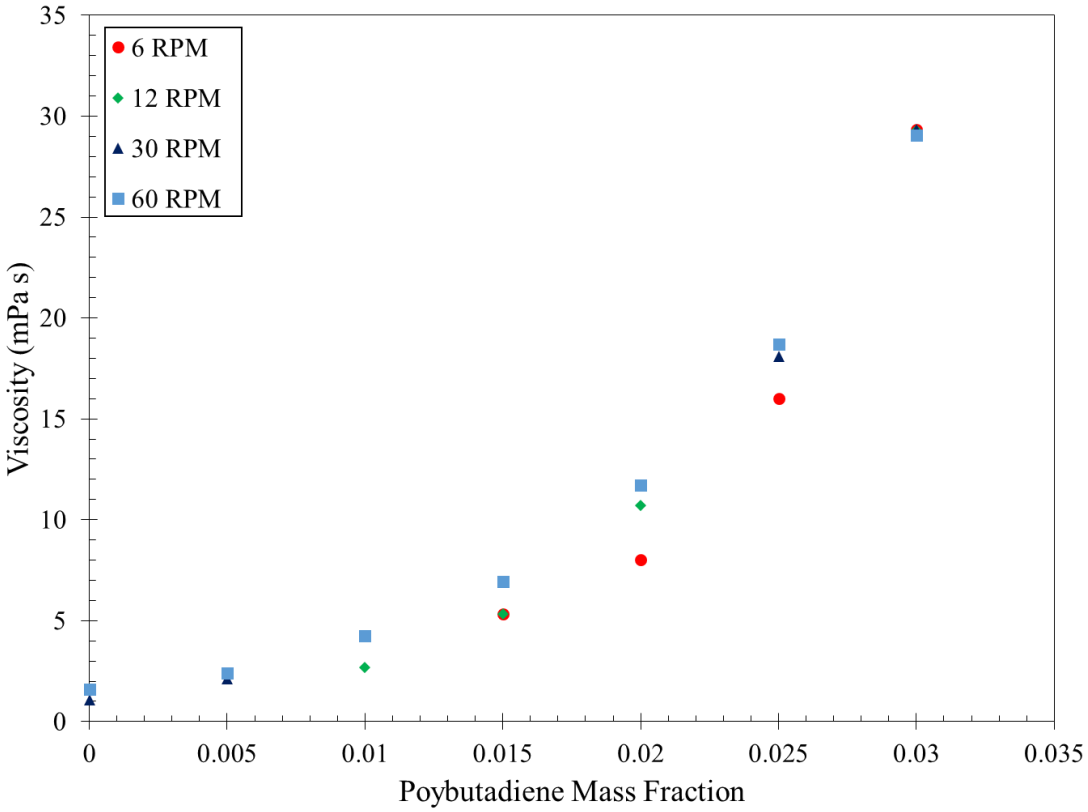

Figure 4.21 Viscosity of jet fuel as a function of PBD mass fraction

The average of all measurements at these four speeds was considered as the viscosity of each solution and plotted in Figure 4.23 to show the variation of viscosity as a function of polymer concentration. The small error bars suggest no non-Newtonian viscosity effect in the regimes that measurements were performed. However, the viscosity of solutions changed drastically with polymer addition. Figure 4.23 clearly displays that the viscosity of both diesel and jet fuel solutions increase exponentially with the following exponential regression:

$$\mu = \mu_0 e^{\theta X} \tag{4.3}$$

where μ_0, and X are viscosity of pure fuel and mass fraction of PBD respectively. The coefficient θ was found from experimental data to be close to 100 for both diesel and jet fuel, therefore it is only the higher μ_0 value in diesel (3.2 compared to 1.3 mPa.s in jet fuel) that results in a larger viscosity difference especially as polymer concentration increases. Thus, it could be deduced that viscosity is the only parameter suppressing transport of volatile species to the droplet surface and reducing burning rate in zone 'I'.

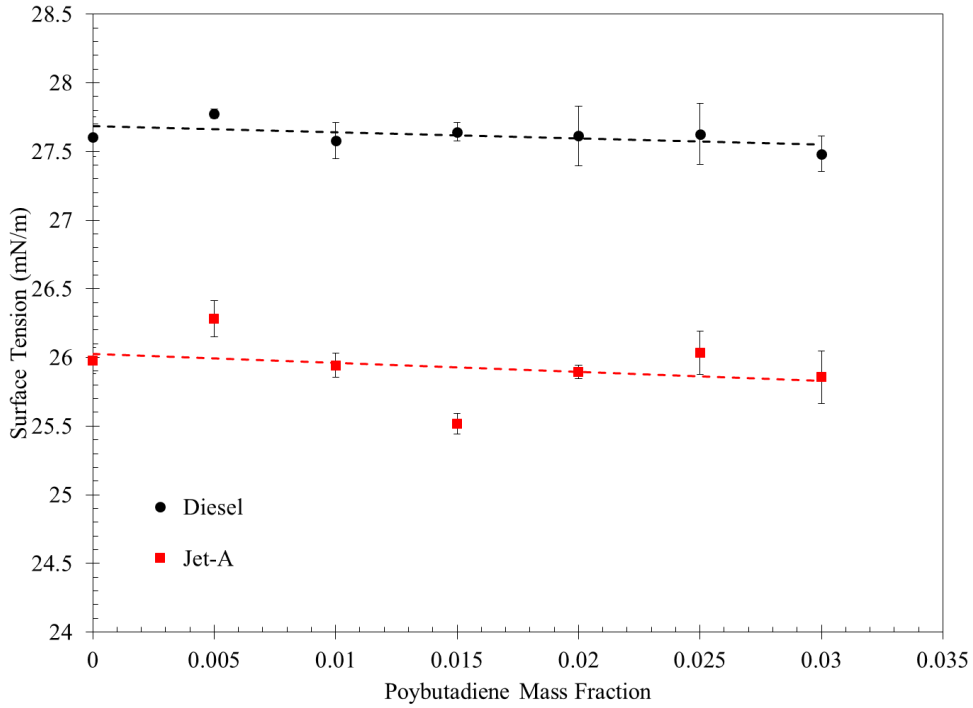

Figure 4.22 Surface tension as a function of PBD mass fraction for polymer in fuel solutions

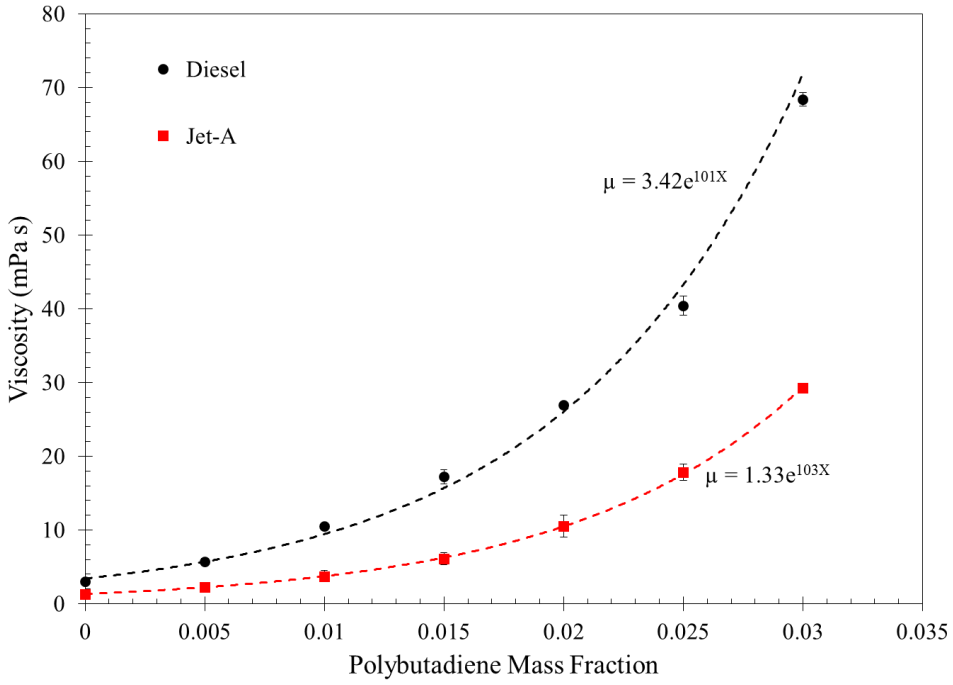

Figure 4.23 Viscosity of polymer added fuel as a function of PBD mass fraction. The error bars are standard deviation for measurements at 6, 12, 30 and 60 rpm

4.4 Soot Emission/Formation in Polymer Added Fuel

Pollutant emission is one of the main challenges in applications of fossil fuels. Therefore, studying combustion behavior of a modified or new fuel without examining its pollution emission seems absurd. Soot is one of the main pollutants formed due to incomplete combustion of hydrocarbons and is known as to be the second most important human cause of global warming [97]. In general, any additive that could change the thermofluid properties liquid droplet might influence its soot formation as well [91]. One possible mechanism is that the liquid motion within the droplet will influence transport of species to the surface. The transport properties are determined by the liquid viscosity and surface tension so if the thermofluid properties such as viscosity and surface tension could be modified then the sooting propensity might change. However, the polymer used in our case is combustible and emits large amounts of soot as it burns. It was already found in our observations of flames that the droplet combustion extinguishes in a flash which is a sign of a very sooty combustion. Yet, that happens at the end of combustion and time evolution of soot emission as droplet burns should also be considered. In this section, only the morphology of soot aggregates is studied to understand any effect of polymer addition on the shape and size of soot particles. The study of temporal emission of soot is proposed as future work within the scope of this thesis and will be completed later.

The SEM analysis of soot was performed in Central Microscopy Research Facility (CMRF) at the University of Iowa and using a Hitachi S-4800 Scanning Electron Microscope. To prepare samples, first conductive carbon tape (provided by CMRF) was cut into 7 mm pieces and attached onto a 0.5 inch aluminum stub (provided by CMRF). Then the fibers were removed from the fiber stand by cutting them using a scissors pair. Finally, the part of the fiber which hosted the soot particles (intersection of fibers) was placed on the carbon tape and the rest of it extending beyond the tape was trimmed using a razor blade.

SEM images of soot residues remained on the fiber after combustion of diesel droplets are shown in Figure 4.24. A comparison between Figures 4.24a and c shows that addition of polymer makes the soot aggregates stick to each other and results in formation of larger aggregates. Figure 4.25 displays similar images for decane which shows similar

behavior of larger aggregate formation at higher polymer content. However, polymer addition does not seem to have any effect on the size of individual soot particles. Generally the individual soot particle diameters are less than 60 nm with, with the largest diameters associated with heavily sooting fuels [98]. Analysis of SEM images in Adobe Photoshop and Spotlight showed that the size distribution of individual soot particles are 37±6 nm, 47±7 nm and 40±7 nm for 0.4%, 0.8% and 1.6% of PBD in decane respectively. These sizes are in agreement with the findings of Köylü et al. [98] and also offer that polymer addition has virtually no effect on the size of soot particles.

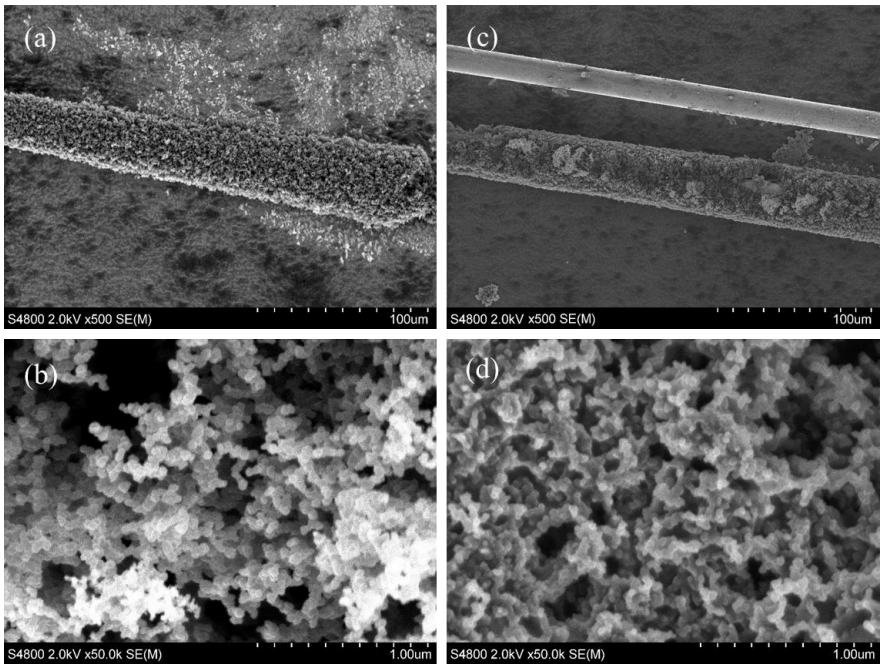

Figure 4.24 SEM images of soot aggregates remained on SiC fiber for (a, b) pure diesel and (c, d) 0.03PBD-0.97Diesel blend

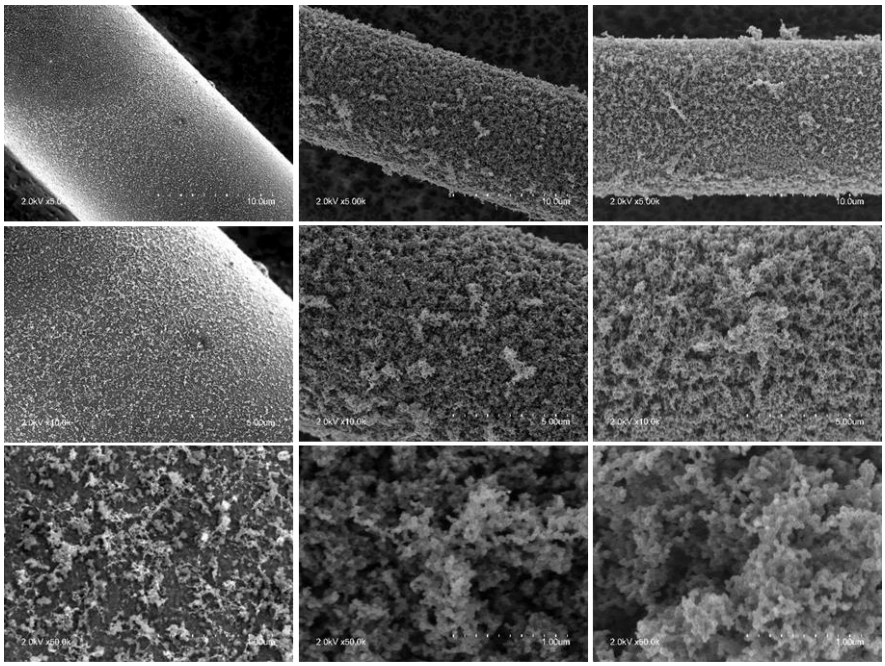

0.2% PBD 0.4% PBD 0.8% PBD

Figure 4.25 SEM images of soot aggregates remaining on SiC fiber after combustion of dodecane droplets at polymer concentrations of 0.2%, .4% and 0.8%

4.5 Conclusion and Summary

Combustion of droplets of hydrocarbon fuels, both commercial and normal alkanes, was studied experimentally to understand the effect polymer addition and the findings were disseminated through several presentations [99,100] and publications [13,100]. Polybutadiene, as a long chain polymer, was blended at different percentages in diesel, jet fuel, n-decane, n-dodecane and n-hexadecane. Liquid droplets with diameters mostly less than 1 mm were deployed on supporting fibers and ignited using hot wires. The heating and combustion process was captured by two high speed cameras and the images were analyzed to obtain burning rate. Overall, polymer added hydrocarbon shows the same behaviors as binary fuels in a way that first the high volatile component, i.e. hydrocarbon fuel, burns and then the combustion of droplet transitions through a very short heating period into polymer combustion. However, three distinguished zones were identified in the combustion of higher volatile component: an initial stage with a burning rate equal to that of pure fuel, a strong swelling and sputtering zone and a weak swelling regime. It is understood that the combustion of the high volatile component dominates initially and the burning rate is closer to that of pure fuel which slightly decreases as the polymer

concentration and consequently viscosity increases. As the combustion progresses and droplet surface regresses, polymers become closer to the surface and act as nucleation sites. As a result, the initial combustion zone is always followed by a strong swelling zone. The viscosity of droplet increases as the hydrocarbon fuel burns until a point that the swelling is controlled by the shear forces. This is the beginning of third zone and the final stage of high volatile combustion.

The morphology of soot aggregates remaining on the support fiber was also studied using Scanning Electron Microscope. It was seen that polymer addition results in formation of larger aggregates but has virtually no influence of the size distribution of individual soot particles.

5 EXPERIMENTAL STUDY OF THE COMBUSTION OF NANOFUEL-TYPE DROPLETS

In this chapter combustion of colloidal droplets, prepared by suspending energetic nanoparticles, into fuels will be studied. It is already known that addition of nanoparticles to liquid will enhance heat transfer but their effect on vaporization and combustion is not well understood. Several different energetic nanoparticles will be considered to be dispersed in a liquid fuel. Isolated droplets will be burned and combustion dynamics will be studied through high speed photography.

5.1 Introduction

Nanofluids-type fuels are a special type of nanofluids (explained in section 2.6) that have received great attention in recent years. In this type of fuel, nano-sized energetic materials and nanocatalysts are added to traditional fuel in order to improve their ignition and combustion properties. Previous studies have shown that addition of energetic nanomaterials such as aluminum and boron, and nanocatalysts such as cerium oxide could improve fuel performance by shortening ignition delay [79] and increasing energy release [78], burning rate [77,101] and ignition probability [102]. However, there are still challenges such as particle agglomeration and potential emission of metal oxides that may limit the application of nanofluids fuels and need to be investigated.

Studies on the addition of carbon particles to conventional liquid fuels started before the concept of nanofluids was proposed for the first time. The idea first became so attractive because it would enable the direct substitution of oil by coal as an energy source. Miyasaka et al. examined combustion of carbon in oil (COM) mixtures in furnace environment [75]. They found it very likely that agglomerates form during the burning of COM, implying that coal burns in the form of agglomerates instead of individual particles. It was also concluded that it is unnecessary to finely crush coal unless it could be reduced to micron-size. Later, Liu et al. examined the combustion of coal-water slurry (CWS) droplets and identified several stages of CWS combustion [74]. However, production of nano-sized carbon particle became possible with the advancement of technology and carbon-based nanomaterials were suggested as fuel additive in developing nanofluids fuels.

Sabourin et al. examined the effects of both metallic and non-metallic additives on nitromethane combustion and discovered that the burning rate may become more than double with low concentrations of functionalized graphene sheets [76]. Unique thermal and optical properties of carbon nanoparticles makes them particularly popular with low energy content fuels. Ethanol, which is itself used as a fuel additive, has lower energy content than conventional transportation fuels. Thus, addition of carbon based nanoparticles to ethanol could boost its energy content and at the same time provide other improvements in combustion behavior (such as burning rate increase and ignition delay decrease) of fuel blends.

5.2 Experimental Design and Measurements

The methodology used in conducting experiments and data analysis was explained in section 4.2. However, in contrast to the modified fuels used in chapter 4 which were mostly solutions, in this chapter we will be using colloidal dispersions, i.e. suspension, which have a different preparation process. To prepare the suspensions, ethanol and carbon nanoparticles (CNP) were used as the continuous and dispersed phase, respectively. The ethanol used as base fuel was pure anhydrous (200 proof purchased from Decon Labs, Inc.) and the nanoparticles were 100 nm (average) activated carbon (Nanostructured and Amorphous Materials, Inc., Product ID 1211NH) whose analysis is listed in Table 5-1. Figure 5.1 also shows an SEM image of these nanoparticles.

Table 5-1 Specifications of Nano Activated Carbon
(Average Particle Size: 100 nm)
Data provided by Nanostructure and Amorphous Materials, Inc.

pH (of the water in contact with particles)	9.8
Water (%)	1.06
Ash (%)	5.8
Carbon (%)	88.1
Apparent Density (g/ml)	0.37
Specific Surface Area (m^2/g)	~162

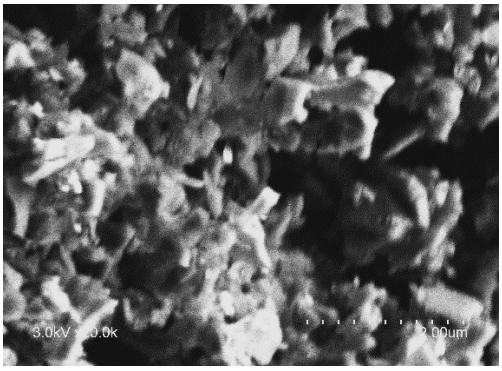

Figure 5.1 SEM image of activated carbon (CNP)

Preparing a homogeneous and stable suspension is a key step in performing any experiment with nanofluids. Many studies have shown that the combined effect of sonication and adding surfactant can suppress the coagulation of nanoparticles. Through sonication process, the sound waves that propagate in the suspension and result in alternating high-pressure and low-pressure cycles at 20 kHz frequency. These pressure cycles then apply mechanical stress to the attracting forces between the individual particles and thus reduce agglomeration by separating them from one another [103]. The particles were mixed with liquid fuels first by stirring them with a magnetic stirrer. Then an ultrasonic disruptor (Biologics 3000MP) was used to prepare the colloidal dispersion and avoid agglomeration. All of the suspensions prepared for droplet combustion in this work were prepared in a 25 ml glass Erlenmeyer flask and using a 3/16” probe (for sonication) in small volumes between 15 and 20 ml. Given the high volatility of ethanol and the great amount of heat generated during sonication, the sonication was performed in an ice bath to maintain a constant temperature and constant concentration of CNP in ethanol. The sonicator was set to work for 5 minutes, generating pulses of 4 seconds long and 4 seconds apart to avoid generating too much heat. A summary of the setting required to prepare particle-fuel suspension studied in this chapter has been listed in Table 5-2. The sonication power in this table is the percentage of maximum amplitude that could be applied by the tip of the probe. Given that the energy of a sound wave is proportional to the square of its amplitude, 30% of maximum amplitude listed in Table 5-2 is actually translated as only 9% of the maximum power (300 Watts). This energy is transferred to the suspension from the tip of the probe and therefore it becomes very important when a small size probe is used due to the fact high energy at a small surface area will generate a lot of heat.

Table 5-2 The sonication setting for different particle in fuel suspensions (CNP: Carbon Nanoparticle; MWNT: Multi-Walled Carbon Nanotube; GNP: Graphene Nanoplates; MWNT-OH: OH functionalized Multi-Walled Nanotube)

Base Fuel	Particle	Surfactant (1.5% wt)	Sonication Time (min)	Sonication Power (%)	On-Off Cycle (sec-sec)
Ethanol	CNP	-	5	30	4-4
Diesel	CNP	Span 80	5	30	4-4
Jet fuel	CNP	Span 80	5	30	4-4
Jet fuel	MWNT	Span 80	20	30	4-4
Jet fuel	GNP	-	5	30	4-4
Jet fuel	MWNT-OH	Span 80	20	30	4-4

Five CNP concentrations (by weight) of 0.1%, 0.5%; 1.0%, 1.5% and 2.0% in ethanol were prepared using the same protocol. While pure ethanol is a clear colorless liquid, the suspensions at all concentrations were found to be completely black. The suspension quality was then evaluated by carefully observing the nanofluids fuel in a test tube at different times to check for particle to agglomerate and settlement at the bottom of the tube. The suspension prepared by this protocol proved to be visually stable for at least 24 hours which is in agreement with observations in [82]. Given the long time stability of CNP-ethanol suspensions, no surfactant was used. All of the experiments were also performed within a short period of time after preparing the suspension. Figure 5.2 displays the stability of one of the suspensions in the first three hours after preparation.

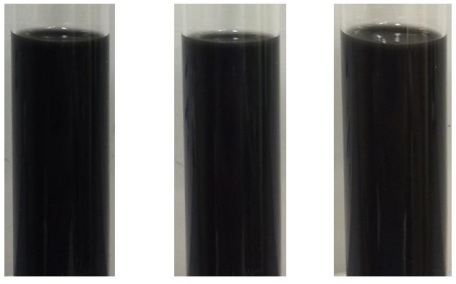

t = 0 t = 1 hr t = 3 hr

Figure 5.2 Stability of 0.1% CNP-Ethanol suspension in different times

5.3 Combustion of CNP-Ethanol Suspensions

In this section, the result of droplet combustion of CNP-ethanol suspensions are presented. Five suspensions with CNP mass concentrations of 0.1%, 0.5%, 1.0%, 1.5%, and 2.0% were prepared as per protocol explained in section 5.2. Several runs were carried out for each case and the SiC fibers were replaced with a new set of fibers before each run. The fibers are also suspected of providing a base for particles to accelerate their agglomeration. To examine this effect, a single SiC fiber was soaked in a 0.1%CNP-Ethanol suspension for one minute and then removed slowly. The sample fiber was then taken to SEM microscopy and investigate the agglomeration of nanoparticles on fibers. In SEM images, like those in Figure 5.3, only few particles were located on the fiber and hence it effect of fiber, if any, cannot be significant.

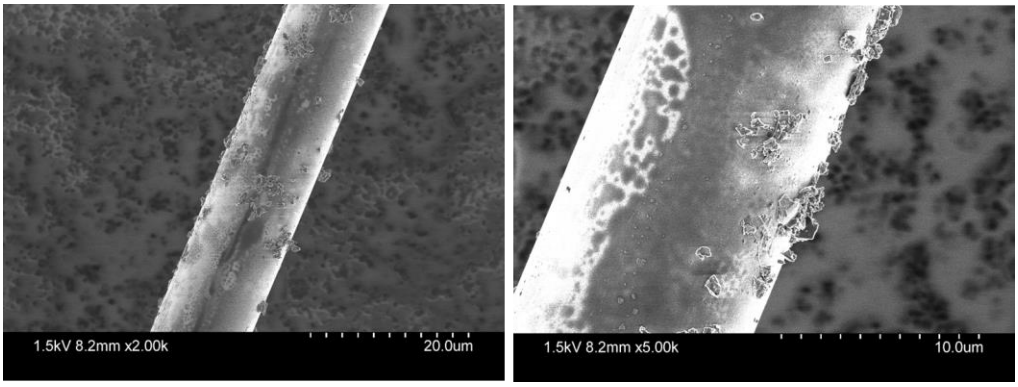

Figure 5.3 SEM images of a SiC fiber soaked in 0.1%CNP-Ethanol suspension. The small particles on the surface of the fiber are CNPs

The heating time for ignition was set to 300 ms for all of the cases. The whole duration of heating and combustion was recorded using two high speed cameras and the images and videos were used to obtain data such as burning rate, ignition and extinction time. It should be noted that ethanol does not produce a sooty flame and in contrast to hydrocarbon fuels is almost invisible to naked eye (Figure 5.4). However, the SiC fibers glow in presence of fire and therefor the moments of ignition and extinction could be tracked by the fiber glow.

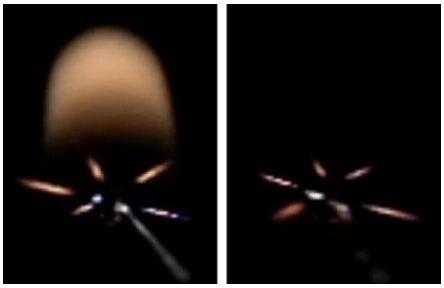

Figure 5.4 Combustion of (left) hexadecane and (right) ethanol on SiC fiber

Figure 5.5 represents the general behavior of a CNP-ethanol droplet during combustion and shows the droplet square diameter follows the traditional d^2-law of combustion. There is a heating zone before ignition that in contrast to hydrocarbon fuel does not come with an increase in droplet diameter. A comparison between the boiling points of hydrocarbon fuels tested in chapter 4 and ethanol could explain why we do not see expansion due to heating in ethanol. For the ignition to occur, the droplet surface temperature should be at its boiling point temperature. Therefore, for a sufficiently high boiling point fuel (such as decane, dodecane and hexadecane with boiling points of 447.2, 489.2 and 560.2 K respectively) the significant amount of thermal expansion of the liquid during this period could cause the droplet to exceed its initial size. On the other hand, ethanol has a boiling point of 351.5 K and needs significantly less heat to reach its boiling point, thus the initial expansion is not observed.

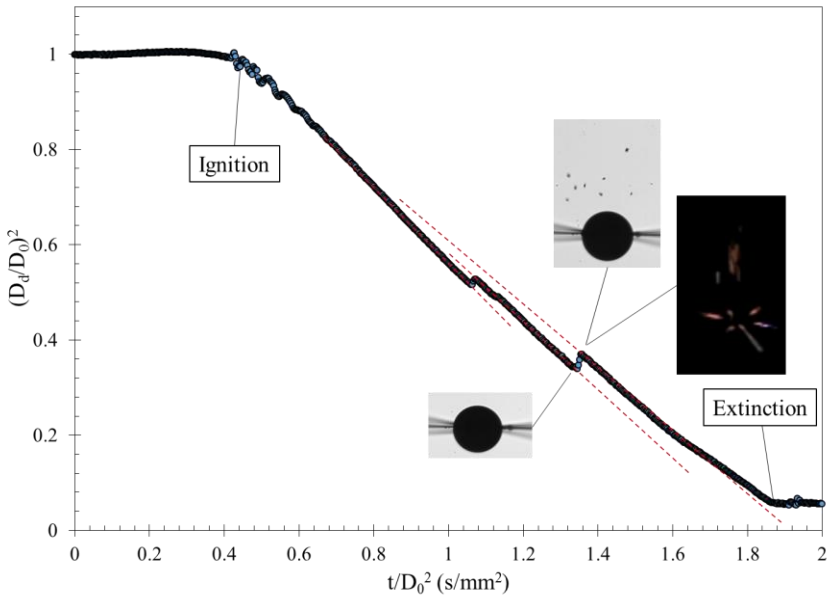

Figure 5.5 Evolution of droplet diameter square for an ethanol droplet with D_0 = 0.79 mm and CNP concentration of 1.0%. Red dashed lines represent the linear regression fit to each segment of the graph

After heating and ignition, a pure ethanol droplet has a steady combustion up to a point marked as "Extinction" in Figure 5.5. The mechanism of extinction is due to water buildup at the droplet surface and will be explained at the end of this section. For CNP-ethanol droplets, just moments before droplet extinction, several sparkles are observed moving up into the combustion gases. These sparkles are carbon particles that burn due to their closeness to the droplet surface at the moment of extinction. For higher CNP in ethanol concentrations (typically 1.0% and above), right after extinction the carbon agglomerate on the fiber turns a glowing red, which is a sign of char combustion. Figure 5.6 shows the moments of extinction and char combustion in a 2.0% CNP in ethanol droplet and how CNP agglomerate starts burning after ethanol flame completely extinguishes.

The data in Figure 5.5 also shows several jumps in the droplet D^2 reduction. These jumps, which correspond to a bulge in the droplet volume, are not seen in pure ethanol combustion (see Figure 5.8) and are due to the heterogeneous nucleation on the nanoparticles close to the surface. It was seen through many experimental runs that higher concentrations of CNP result in more frequent bulges. Each bulging event ends with a puffing event through which gases trapped inside the droplet leave the droplet and carry nanoparticles to the flame surrounding the droplet. The inner image in Figure 5.5 also

shows several sparkles that are nanoparticles leaving the surface of the droplet and burning in the invisible flame.

t = 508 ms t = 1084 ms (Extinction) t = 1278 ms (Char Combustion)

Figure 5.6 Flame extinction and char combustion in a 2.0%CNP-ethanol droplet (D_0 = 0.74 mm). For more clarity, the location of droplet and char have been marked with a red circle in their related images

The time dependent burning rates of CNP-ethanol droplets in Figure 5.7 show two zones of sharp increase and decrease in burning rate which are associated with ignition and extinction respectively. It is also seen that the burning rate between ignition and extinction has a slight gradual reduction. Looking at Figure 5.5 shows similar behavior and the slopes of linear segments, which represent burning rate, decrease as the droplet approaches the end of its lifetime. Therefore, a separate burning rate constant was measured for each section of the curves in Figure 5.8 and an effective burning rate was calculated using the following equation;

$$K_{eff} = \frac{\sum_{i=1}^{n} K_i.\Delta t_i}{\sum_{i=1}^{n} \Delta t_i} \quad (5.1)$$

where n is number of segments and Δt_i is the time interval over which K_i is measured.

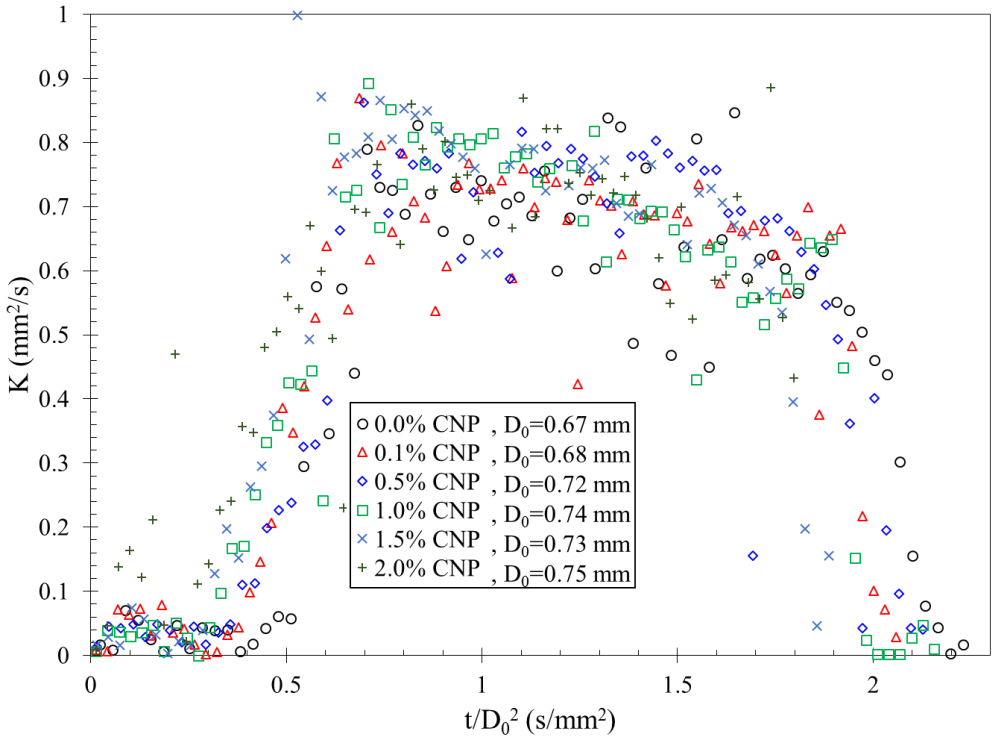

Figure 5.7 Instantaneous burning rate for ethanol droplets doped with different percentages of CNP

Figure 5.9 shows variation of effective burning rate for ethanol droplets at different concentrations of nanoparticles. In spite of the sharper decrease in the instantaneous burning rate of higher CNP content droplets, it is observed that increasing nanoparticle content increases the burning rate. This could be because of improved convective heat transfer inside of the droplet as a direct result of particle motion. In addition, nanoparticles improve radiation absorption and consequently more heat transfer from the flame to the droplet during droplet combustion.

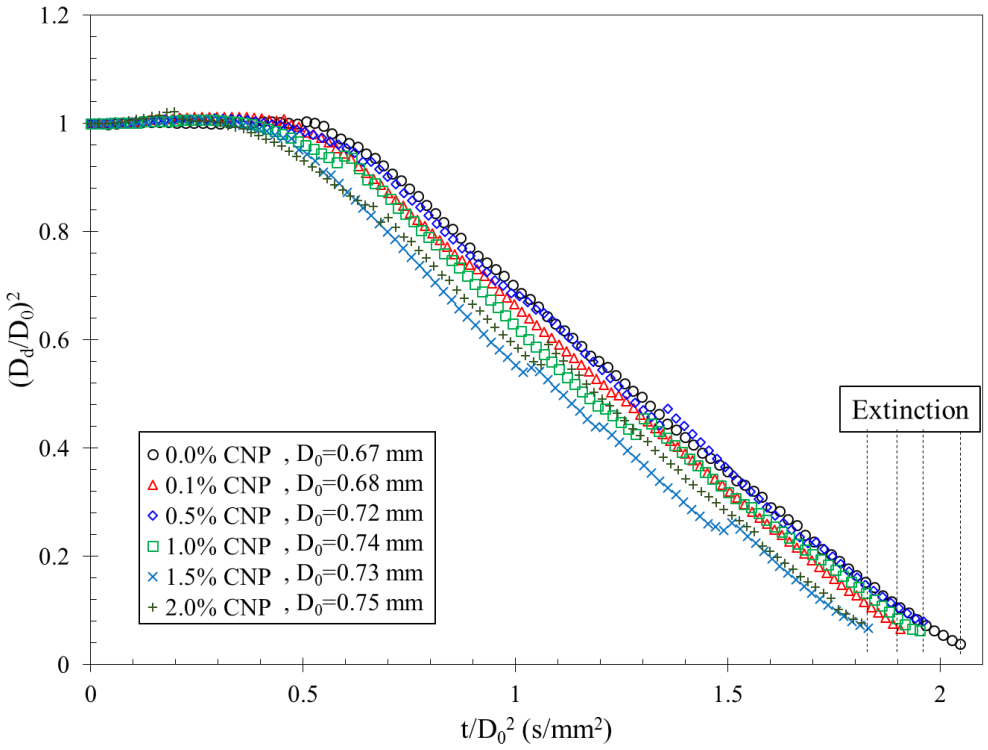

Figure 5.8 Evolution of d^2 for ethanol droplets doped with different percentages of CNP

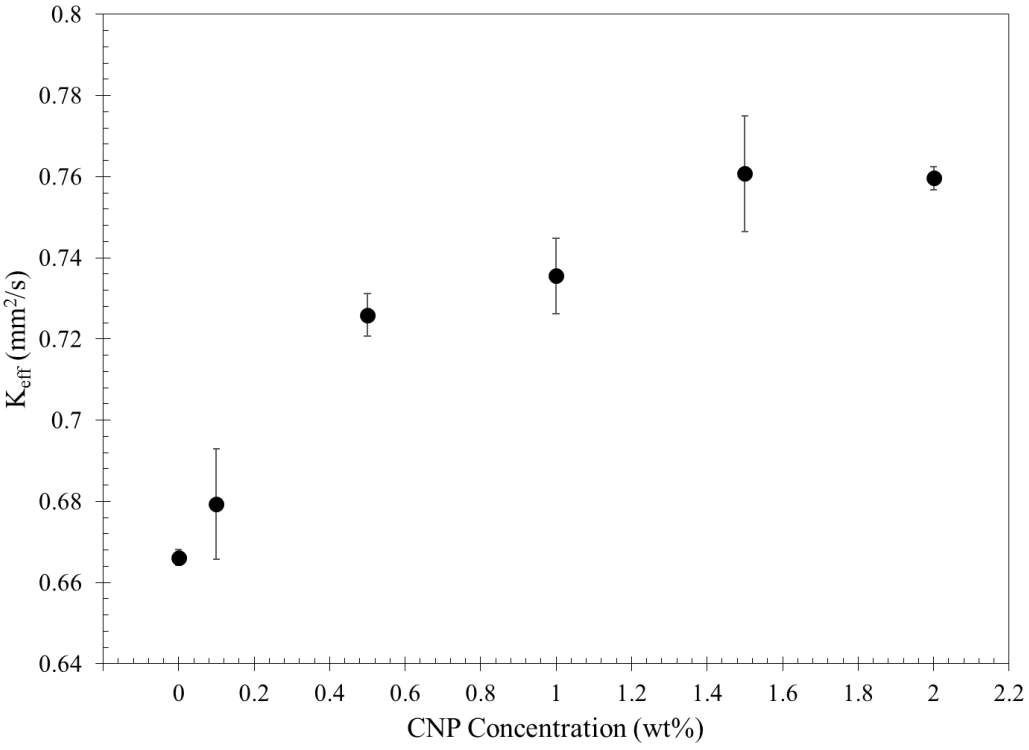

Figure 5.9 Effective burning rates as a function of CNP concentration within ethanol droplets

Figure 5.5 shows that there is an extinction limit for ethanol droplets and they do not burn to completion. Lee et al. showed that alcohol droplets freely absorb water from their environment during combustion [8]. This water, which could be from ambient gas or the water generated at the droplet flame, builds up in the surface layer of the droplet and could eventually extinguish the droplet flame. To investigate the effect of carbon nanoparticle addition on droplet extinction, the droplet diameter at the moment when the SiC fibers stop glowing was measured. Figure 5.10 shows the ratio of droplet extinction volume to its initial volume. The black points in this graph are based on the data originally obtained from images of droplet at the moment of extinction which shows almost no effect in droplet extinction volume and consequently diameter. However, as it is shown in Figure 5.10, the initial CNP volume in the droplets also increases and since the droplet contains almost all of its initial CNP content at the moment of extinction the actual ethanol volume should be decreasing as CNP content increases. On the other hand, the concentration of nanoparticles at the extinction is substantially higher and therefore the ethanol volume should be corrected by subtracting CNP volume from the original extinction diameter. It should be noted that part of CNP may burn during droplet combustion and therefore its volume at extinction may be less than what is shown in Figure 5.10 by the red triangles.

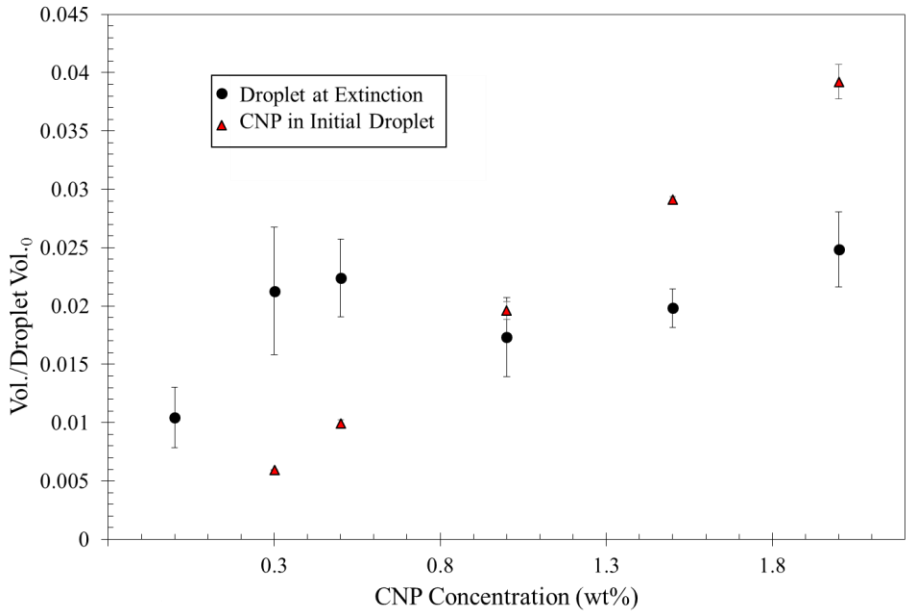

Figure 5.10 Droplet extinction size as a function of CNP loading within ethanol droplets

The SEM images of combustion residues remained on SiC fibers are shown in Figure 5.11. Ethanol droplets ignited at 1 atm will burn without sooting [104] and hence only unburned nanoparticles and ash, as presented in Table 5-1, is expected to be observed in these images. A Comparison between the morphology of the residues in this figure and the morphology of CNP in Figure 5.1 suggests that nanoparticle agglomerate does not burn when the concentration of nanoparticles in less than 1.0%. On the other hand, the morphology of the residues after the combustion of 1.0% CNP in ethanol is completely different and more like honeycomb. This honeycomb morphology is the ash remained after the char combustion which was previously discussed in this section. Given the extinction of ethanol flame at very small droplet sizes, it could be concluded that the particle concentration should be high enough (more than 1.0% in the case of CNP) so that the flame approaches the agglomerate before it completely extinguishes and hence the char combustion begins.

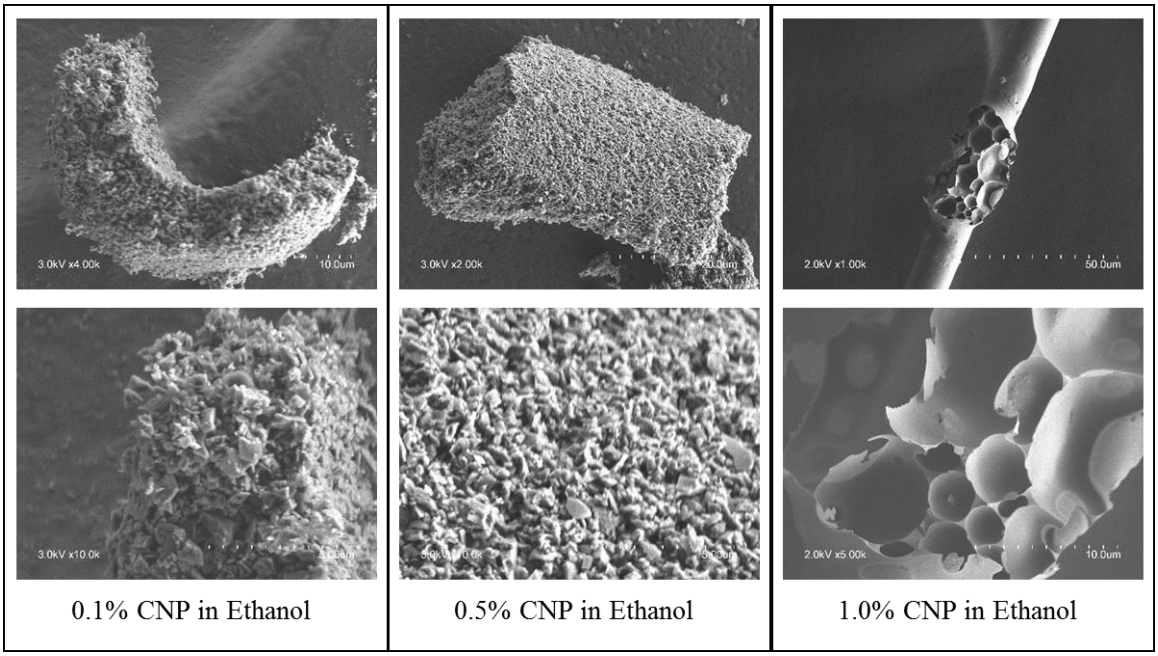

Figure 5.11 SEM images of combustion residues of ethanol-CNP droplets

5.4 Combustion of Carbon Based Nanoparticles in Hydrocarbon Fuels

It is now understood that carbon based nanomaterials have better thermal and optical propertied and could be considered as effective and yet safe fuel additives

[76,81,82]. However, these nanomaterials come in wide range of sizes and morphologies that may result in different combustion behavior. In this regard, the effects of size and morphology of carbon nanomaterials on combustion behavior of hydrocarbon droplets will be examined in this section. In the first part, combustion of CNP-jet fuel and CNP-diesel droplets will investigated. Then three different carbon based nanomaterial, Multi-Walled Carbon Nanotube (Short MWNT, Nanostructured and Amorphous Materials, Inc., Product ID 1235YJS), OH functionalized Multi-Walled Carbon Nanotube (Short MWNT-OH, Nanostructured and Amorphous Materials, Inc., Product ID 1248YJF) and Graphene Nanoplates (GNP, Strem Chemicals, Catalog No. 06-0210), will be suspended in jet fuel at different concentrations to examine the effects of nanoparticle morphology on the combustion of droplets.

5.4.1 Combustion of CNP in Jet Fuel and Diesel

Both of the CNP-jet fuel and CNP-diesel suspensions were prepared as per protocol explained in section 5.2. However, using sonication technique is not enough to produce stable suspensions and the CNP particles start to agglomerate immediately after the sonication stops. Adding a surfactant to the fuel can improve the dispersion properties and long-term stability of the nanofluids by changing the surface properties of the suspended particles with a chemical agent. Through this mechanism, it overcomes the van der Waals forces between particles that lead to agglomeration. In the current study and to reduce particle agglomeration, Span 80 (Sorbitan Monooleate, $C_{24}H_{44}O_6$) was added to the base fuel at a mass concentration of 1.5% and stirred on a magnetic stirrer for 30 minutes. Then the nanoparticles were added and the sonication was performed using the setting listed in Table 5-2.

Colloidal suspensions of CNP in both jet fuel and diesel were prepared at CNP loadings of up to 3.0% and droplet combustion experiments were performed at least three times for each concentration. The evolution of diameter square for jet fuel and diesel droplets doped with CNP on d^2-law coordinate are shown in Figures 5.12 and 5.13, respectively. In general, all of the cases seem to follow the d^2-law of combustion. Regardless of particle loading, several disruptions are seen during combustion. This is because of presence of solid particle and aggregates near the droplet surface which act as

nucleation sites and result in weak microexplosions. Furthermore, the different combustion behavior of jet fuel and diesel, as observed in polymeric solutions in chapter 4, is not observed anymore. This suggests that the effect of adding nanoparticles on the suspension viscosity is insignificant. Other studies have also shown that surface tension and viscosity of colloids does not experience a significant change at the particle loadings studied in the current research [77,105,106]. Similar to ethanol suspensions, the base fuel burns first and preferentially and the main part of CNPs agglomerate at the center of droplet and burn (in the form of char combustion) once the base fuel is mostly depleted. However, in contrast to ethanol, jet fuel and diesel droplets do not extinguish at small diameters and therefore char combustion occurs at all concentrations. Different sonication times (5, 10, 20, 30 and 40 minutes) as well both continuous and pulsatile sonication at both 1.5% and 3.0% surfactant were tried with MWNT and MWNT-OH. No difference was observed in the quality of suspensions prepared using 20, 30 and 40 minutes. Furthermore, increasing surfactant to 3.0% did not result in any stability enhancement. It was also observed that the suspension prepared using continuous sonication form agglomerate sooner than the one prepared using pulsatile sonication. Therefore 20 minutes pulsatile sonication as listed in Table 5-2 was found as the optimum setting.

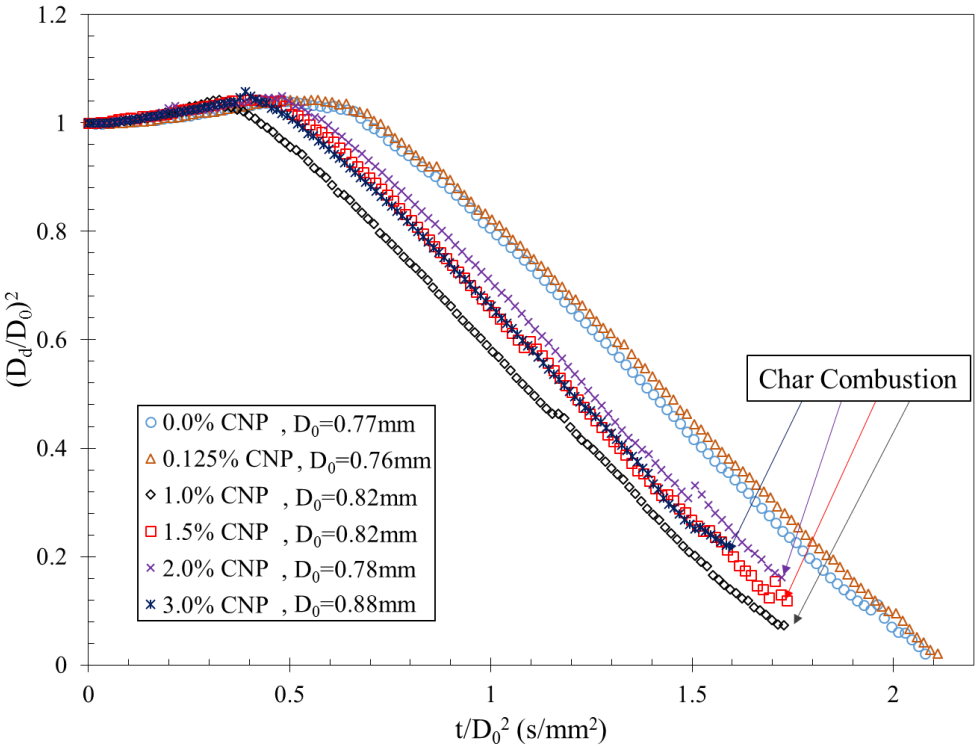

Figure 5.12 Evolution of d^2 for colloidal suspensions of jet fuel and CNP

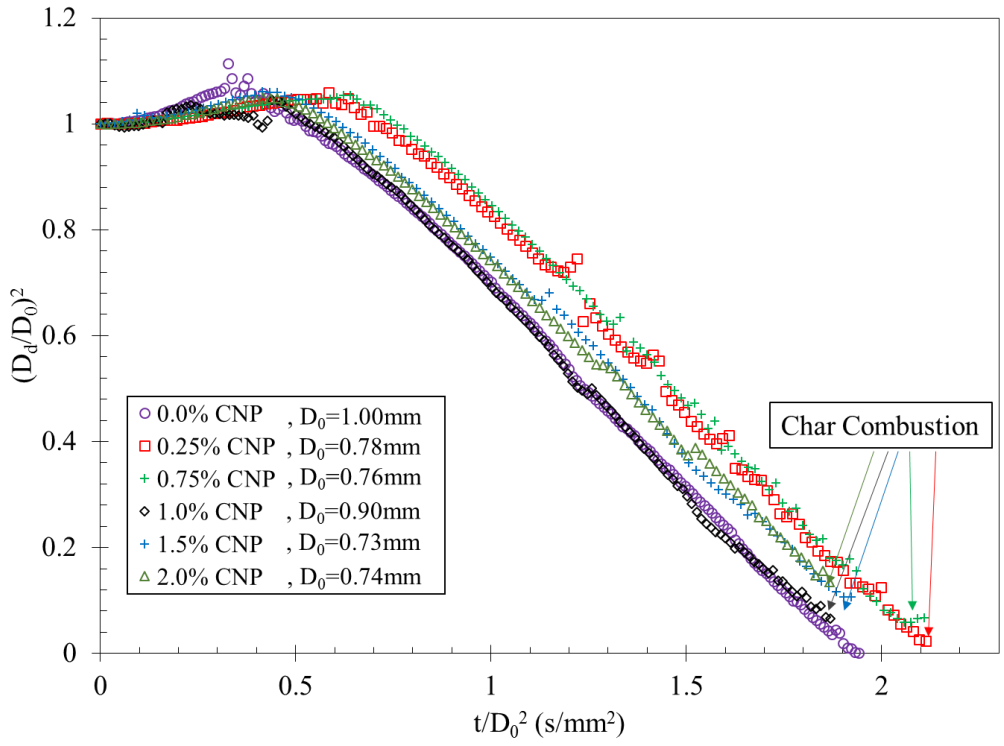

Figure 5.13 Evolution of d^2 for colloidal suspensions of diesel and CNP

Figure 5.14 displays several snapshots of 3.0% CNP in jet fuel. It is seen that CNP particle leaving the droplet form sparkles and burn in the flame. It is also clear in Figure 5.14c that once the base fuel was almost depleted and flame extinguished, the CNP aggregates start to burn as displayed in Figure 5.14d. Similar phenomena are also observed during combustion of CNP-diesel colloidal suspensions.

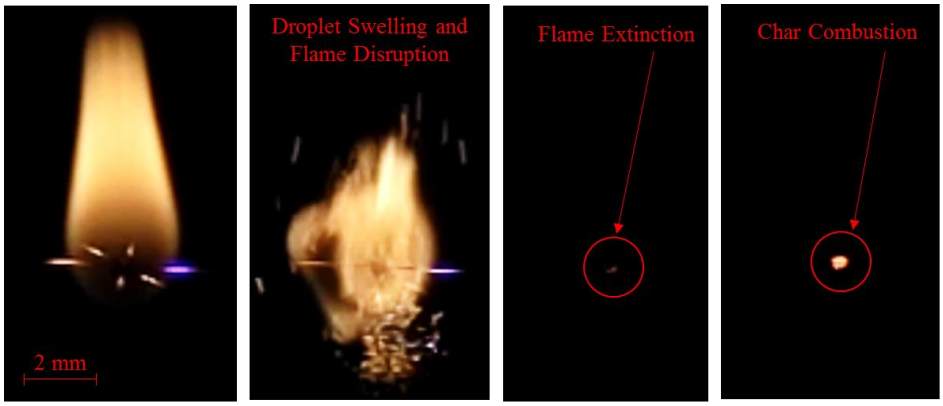

Figure 5.14 Burning sequence of a 3.0% CNP in jet fuel droplet (D_0 = 0.88 mm)

The slope of diagrams in Figures 5.12 and 5.13, which represent the burning rate, are very similar. Therefore, the apparent burning rate is calculated by averaging burning rates of at least three cases for each CNP loading. The variation of the average burning rate is shown in Figures 5.15 and 5.16 for jet fuel and diesel, respectively. It is understood from these figures that adding CNP could increase burning rate up to around 7% in both jet fuel and diesel at CNP loadings of 1.5% and 1.0%, respectively. However, adding more particles beyond these two concentration results in a drop in burning rates. It was previously mentioned that colloidal suspensions of carbon nanoparticles have a much lower transmittance compared to pure liquid fuels [82] which helps them use more of the absorbed radiation energy to heat up the droplet and enhance its evaporation. Increased thermal conductivity could be another mechanism responsible for the increased burning rate. However, according to Eastman et al. [107], the largest increases in thermal conductivity have been observed in nanofluids with little or no particle agglomeration. The formation of larger aggregates at higher CNP loadings could limit the extent of increase in thermal conductivity or even reduce it and hence be responsible for the reduction in the burning rates.

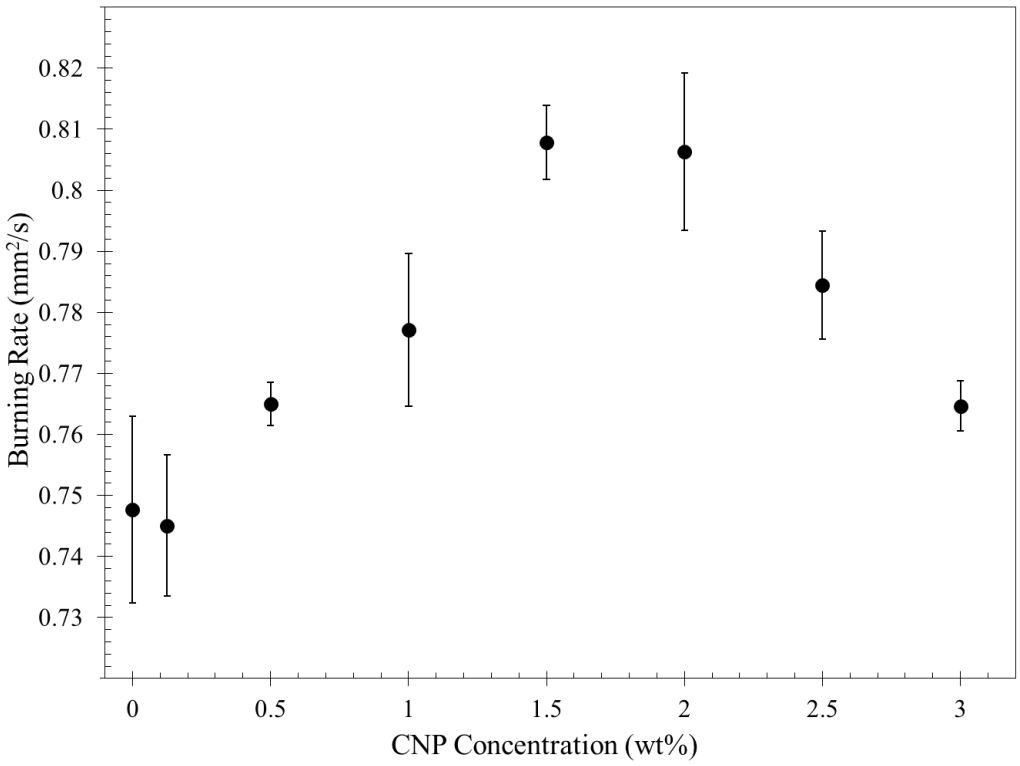

Figure 5.15 Burning rate as a function of CNP concentration within jet fuel droplets

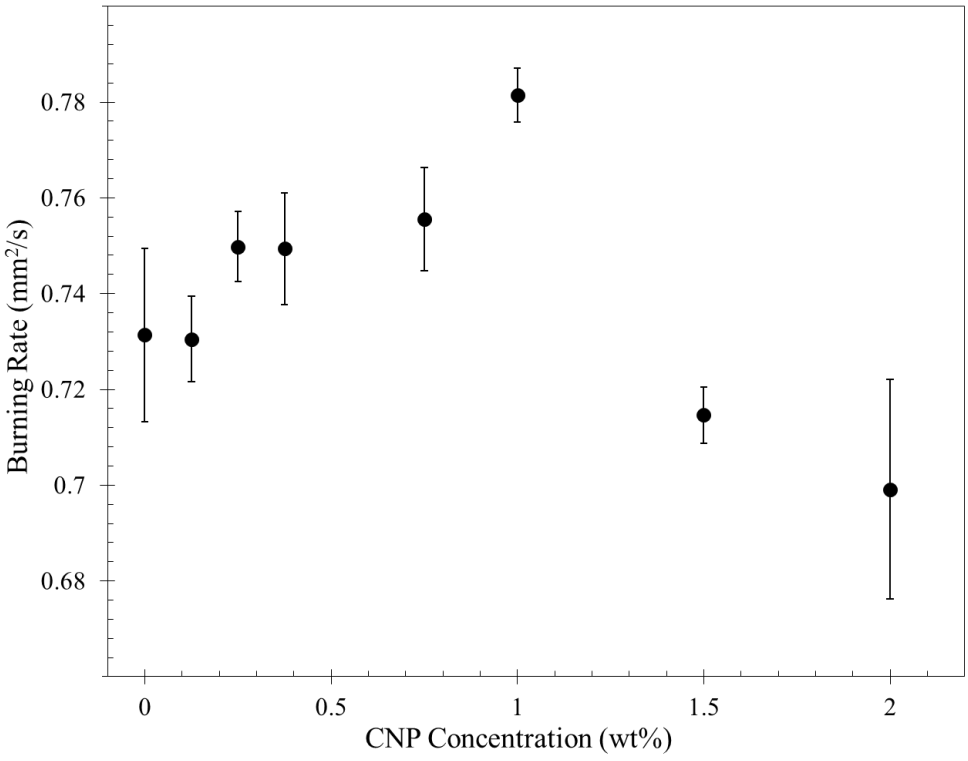

Figure 5.16 Burning rate a function of CNP concentration within diesel droplets

5.4.2 Combustion of MWNT and GNP in Jet Fuel

It was shown in section 5.4.1 that addition of CNP to both jet fuel and diesel could increase their burning rates at certain particle loadings. The reason for such increase was deemed to be the improved optical properties and thermal conductivity of colloidal suspensions. Particle morphology has been reported to influence both optical transmittance [82] and thermal conductivity [107]. Therefore, the aim of the work explained in this section is to investigate the effects of particle morphology on the burning rate of liquid fuels. For this purpose, Multi-Walled Carbon Nanotube (MWNT) and Graphene Nanoplates (GNP) were chosen to be suspended in jet fuel and studied experimentally under droplet combustion condition. OH-Functionalized nanoparticles have been also reported to increase the burning rate presumably due to increase reaction rate or heat transfer [76]. Thus, OH functionalized MWNTs (MWNT-OH) were also considered for this study.

The SEM images in Figure 5.17 show the morphology of both MWNT and GNP. MWNTs are tubes with inside diameter of 3-5 nm, outside diameter of 8-15 nm, length of 0.5-2 μm and Specific Surface Area (SSA) of greater than 233 m^2/g. MWNTs-OH are MWNTs having hydroxyl groups (–OH) attached at a mass concentration of 3.52%-3.89%. On the other hand, GNPs are platelets with average width of 5 μm, thickness of 6-8 nm and SSA of 120-150 m^2/g. Colloidal suspensions of these three nanoparticles in jet fuel were prepared as per protocol explained in section 5.2 and the setting listed in Table 5-2. It is worth mentioning that due to their tubular structures, both of MWNT and MWNT-OH tend to entangle with one another to form agglomerates and thus need longer sonication time.

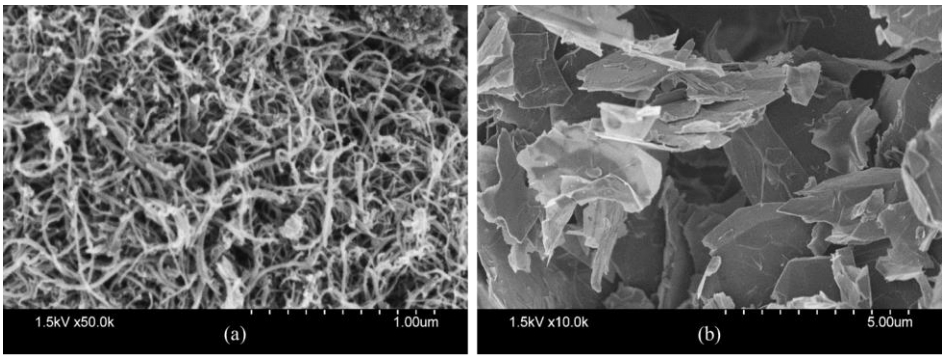

Figure 5.17 SEM images of (a) MWNTs/MWNTs-OH and (b) GNPs

Figures 5.18 and 5.19 shows the evolution of droplet diameter square for several droplets of MWNT and GNP in jet fuel. Again, and similar to colloidal suspensions of CNP studied in section 5.4.1, all of the cases seem to follow the d^2-law of combustion. Regardless of particle type, several disruptions are seen during combustion. As previously explained, this is because of presence of solid particle and aggregates near the droplet surface which act as nucleation sites and result in weak microexplosions. Figure 5.19 displays stronger and more frequent disruptions for GNP suspensions. It was also seen through the flame observations that GNPs do not burn and therefore remain as unburned agglomerates on the fiber after the droplet burnout. On the other hand, CNPs and MWNTs/MWNTs-OH burn as they leave the droplet surface through droplet swellings and flame disruption. However, the main portions of CNPs and MWNTs seems to burn after the droplet burnout and in the form of char combustion. Therefore, char combustion as shown in Figure 5.14d is only observed at the end of CNP and MWNTs\MWNTs-OH colloidal suspensions and GNP does not burn either in the flame or in the form of char.

To better understand the effect of nanomaterials morphology on burning rate, apparent burning rates for different concentrations of MWNT/MWNT-OH and GNP in jet fuel have been presented in Figures 5.2 and 5.21, respectively. In terms of effect of hydroxyl group in MWNT-OH, the data in Figure 5.20 do not show any significant difference. Even though functionalized nanotubes seem to have a slightly higher burning rates, especially at their optimum concentration, yet a decisive conclusion cannot be made due to the large uncertainties. In general, and considering CNP data presented in section 5.4.1, it could be concluded that addition of small amounts of all three types of nanomaterial results in an increase in droplet burning rate. However, the extent of this increases is significantly different for CNP, MWNT and GNP. For each particle type, an optimum concentration was found at which the maximum burning rate was achieved. It was observed that adding more particle after this point results in a reduction in burning rate possibly due to the formation of large aggregates.

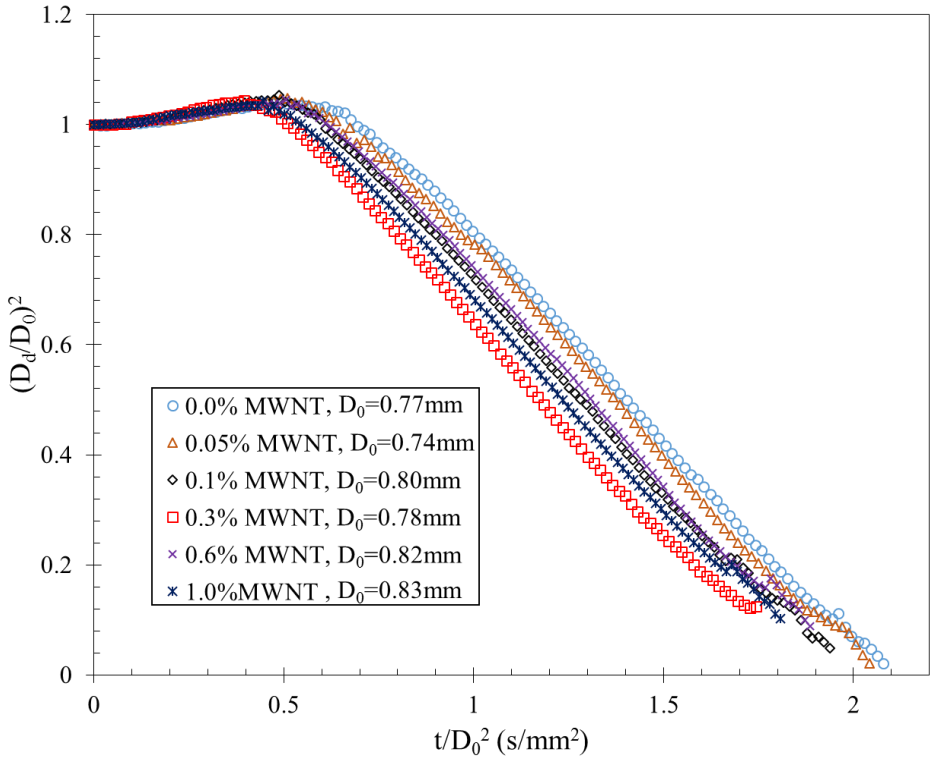

Figure 5.18 Evolution of d^2 for colloidal suspensions of jet fuel and MWNT

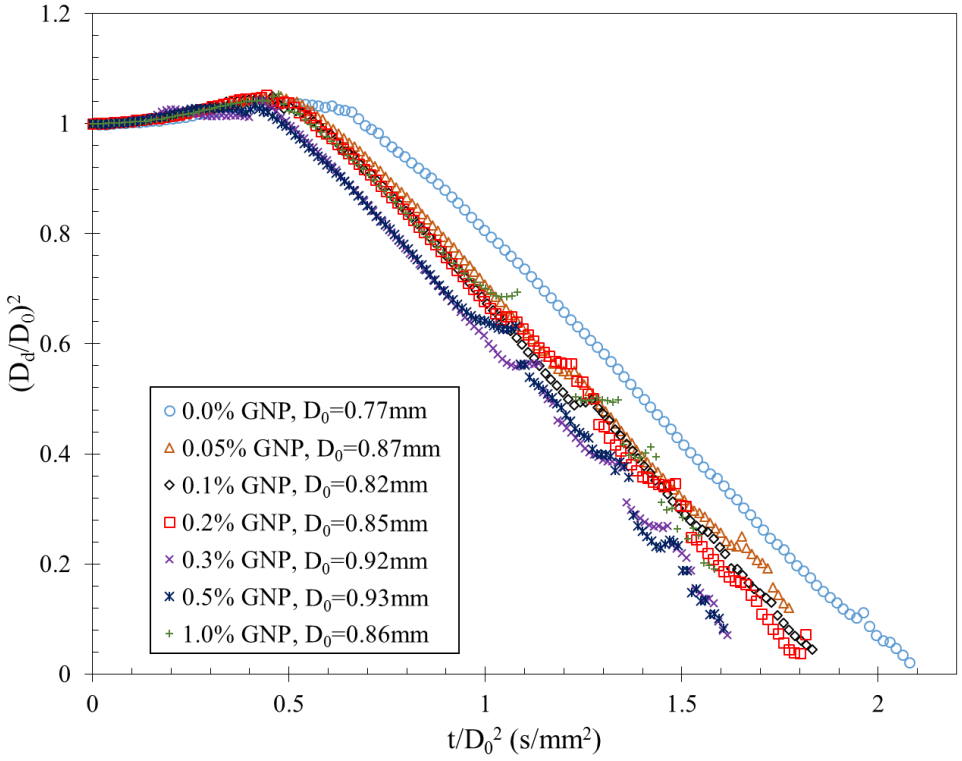

Figure 5.19 Evolution of d^2 for colloidal suspensions of jet fuel and GNP

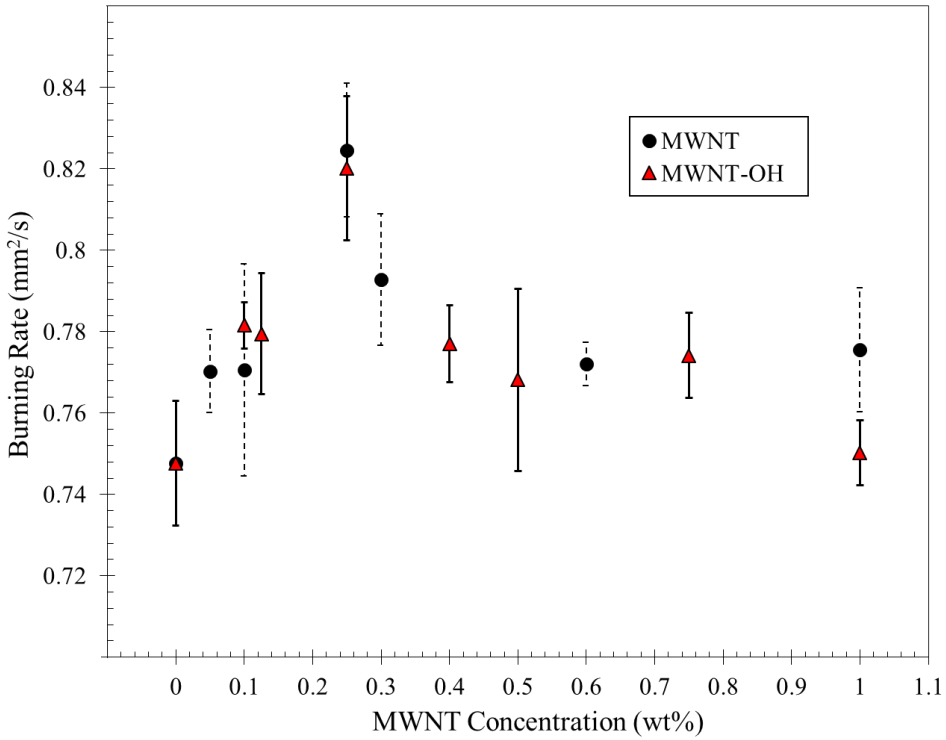

Figure 5.20 Burning rate a function of MWNT and MWNT-OH concentration within jet fuel droplets

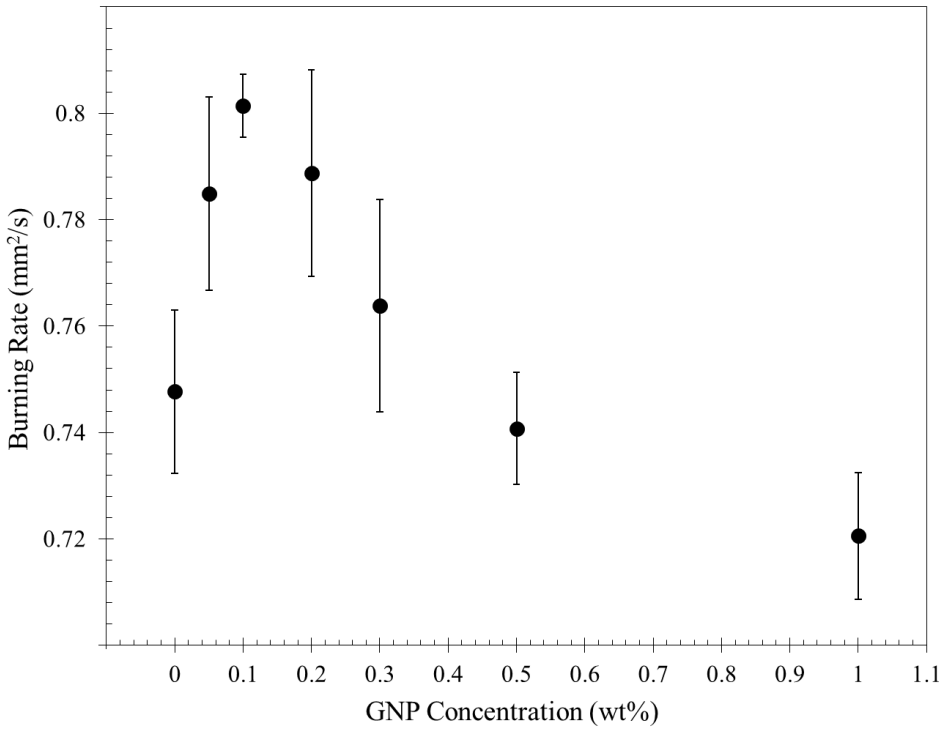

Figure 5.21 Burning rate a function of GNP concentration within jet fuel droplets

A summary of optimum particle loading and its corresponding burning rate increase (compared to pure fuel) for each particle has been presented in Figure 5.22. Comparing the performance of nanoparticles, MWNT provides its maximum burning rate at a much lower loading compared to CNP. Several properties could be responsible for such a better performance: compared to CNP, MWNT has higher specific surface area which could result in a higher thermal conductivity. Furthermore, the thermal conductivity of carbon nanotubes is known to be similar to the in-plane conductivity of graphite [107]. Other studies have shown that the thermal conductivity of carbon nanotubes can approach [108] or even exceed [109] that of natural diamond, which itself is known as the best thermal conductor in room temperature. However, the high surface area and string-shape morphology of MWNTs makes them more susceptible to wrap around each other and from an agglomerate faster than CNP colloids. That is probably why the burning rate starts to decrease in MWNT colloids at loadings beyond 0.25%, while in CNP colloids the burning rate increases continuously up to 1.5% particle loading.

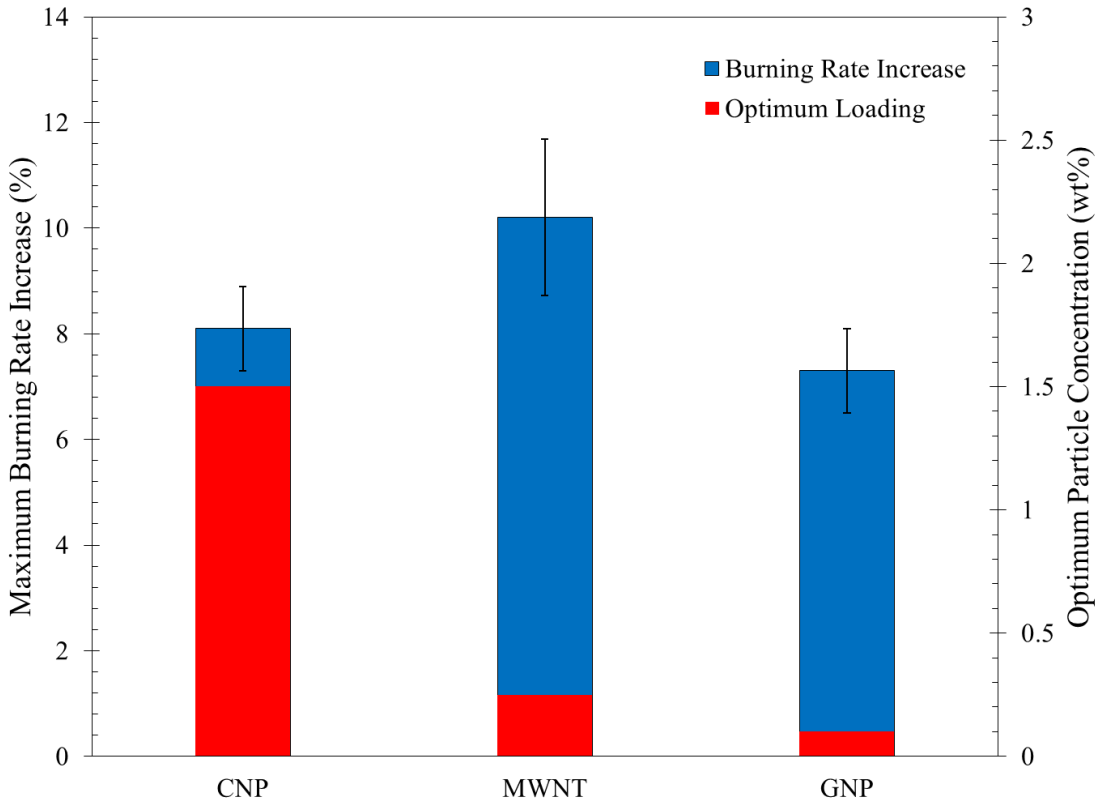

Figure 5.22 Bar graph showing the optimum particle loading and its corresponding burning rate increase for each particle

In spite of having the lowest surface area, GNP shows a good performance in terms of increasing burning rate at a low particle loading. Like other carbon-based materials, graphene sheets that form nanoplates are thermally conductive. However, the platelet morphology provides lower thermal contact resistance at lower loading levels, resulting in higher thermal conductivity versus other carbon particle and fibers. Nonetheless, the fact that these platelets do not burn remains to be a serious issue in their application as a fuel additive.

The clustering of particles within a colloidal suspension and formation of aggregates has also been reported as one of the factors influencing thermal conductivity of colloids [107,110]. According to Eastman et al. [107], the clustering of particles would create paths of lower thermal resistance and consequently increase thermal conductivity. Part of the volume of each cluster consists of thin liquid layers filling the space between the particles that allow for rapid heat flow among particles. Figure 5.23 illustrates the effects of clustering by showing the excess thermal conductivity k enhancement as a function of packing fraction of the clusters Φ. The packing fraction is defined as the ratio of the volume of the solid particles in the cluster to the total effective volume of the cluster (volume from which other cluster are excluded and can be much larger than the physical volume of the particles).

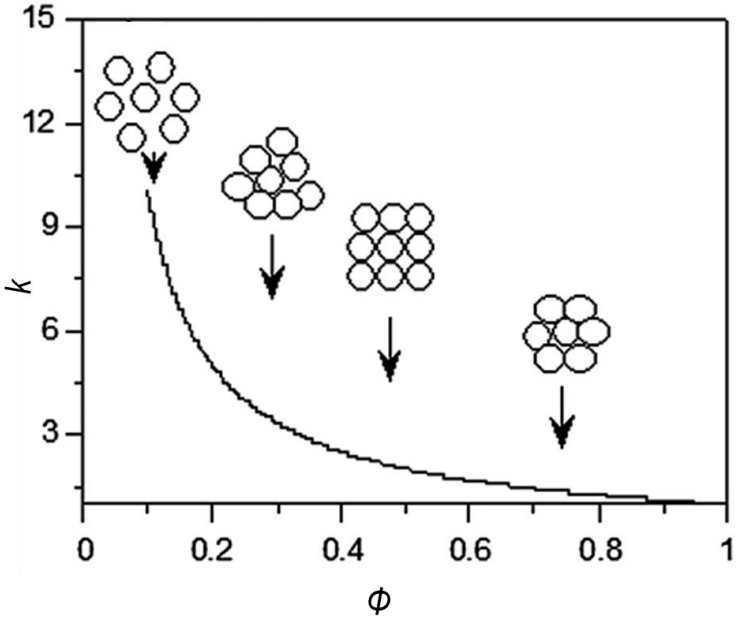

Figure 5.23 Excess thermal conductivity enhancement as a function of effective volume [107]

To study the morphology of the aggregates formed during combustion of colloidal fuels, a simple droplet evaporation experiment was designed. Three suspensions of 0.4% CNP, MWNT and GNP in jet fuel were prepared as per the procedure listed in Table 5-2. For the sake of consistency, 1.5% (by weight) Span 80 was used in the base fuel in all three cases. A droplet of prepared suspension is then deployed on a new set of fibers and the fiber support ring is placed on top of a table lamp (120 V, 250 W FEIT double ended J type halogen bulb) as shown in Figure 5.24. In about 30 seconds and due to the heat from the bulb, the base fuel evaporates and the nanoparticle aggregate remains on the fiber. A main issue that might affect the morphology of aggregates is the large time scale difference between an evaporating droplet and a burning droplet. However, in a combustion experiment the large portion of particles will burn or be covered by soot and hence an aggregate sample cannot be made. It is worth mentioning that it was more difficult to prepare samples of GNP aggregates; while CNP and MWNT aggregate were completely stuck to the fiber and could be transferred onto the carbon tape, GNP aggregates turned out to be very unstable and would easily detach from the fiber.

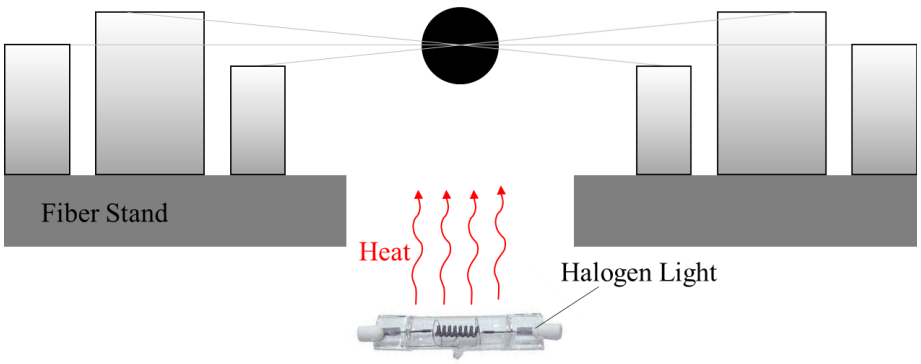

Figure 5.24 Schematic of droplet evaporation test to prepare aggregate samples

SEM images of aggregate samples are shown in Figure 5.25. It is observed that the aggregates of both CNP and MWNT are very packed while GNP aggregates are more porous. It was previously mentioned that GNP aggregates are also very loose and could easily detach from the fiber. Given the discussion about clustering effect in page 91, the loose morphology of GNP aggregates could be a reason for its high burning rate increase (7.3% at 0.1% particle loading) in spite of its lower surface area compared to MWNT. In other word, fuel fills the space between particles and enhances heat flow among them.

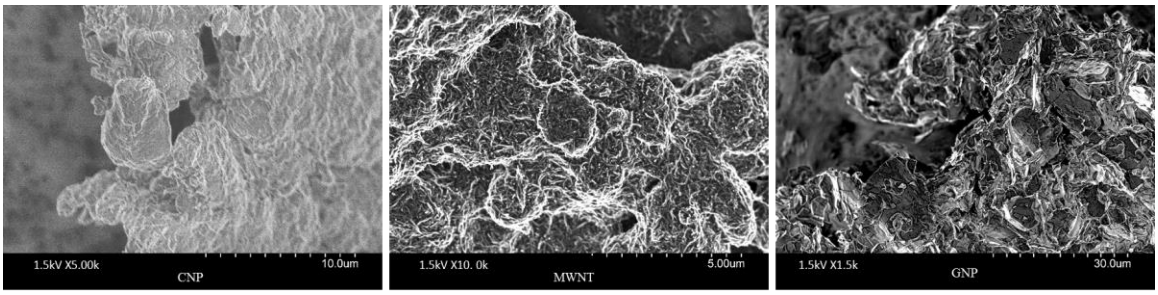

Figure 5.25 SEM images of aggregates of colloids of 0.4% nanoparticle in jet fuel

Burning time of droplets with different carbon-based nanomaterials and at different concentration has also been displayed in Figure 5.26. For both CNP and MWNT, burning time decreases towards the optimum loading and again increases at higher concentration which is consistent with burning rate data in Figures 5.15 and 5.2. For GNP, it is also expected to have a minimum burning time at 0.1% GNP loading, but instead it is observed that the burning rate continuously decreases as more particle is added. This is possibly because of droplet extinction and consequently the incomplete droplet burnout. It was previously mentioned that graphene nanoplates do not burn after droplet runs out of base fuel. Therefore, the GNP aggregate at the core of the droplet acts as a heat sink and eventually extinguishes the flame. This could be another barrier to limit the application of GNP, in spite of its superior qualities in increasing burning rate compared to other carbon-based nanomaterials examined in this work.

The SEM images of combustion residues in Figure 5.27 could also give us some information regarding combustion behavior of nanoparticle agglomerates. While the only morphology observed in the residues of CNP colloids is soot particles, MWNTs and GNPs are still available in the residues of MWNT and GNP colloids. This suggests that the CNP aggregate burns out completely via char combustion process but parts of the nanotubes, which agglomerate so quickly, form a packed aggregate and are buried unburned under a layer of soot. The situation for GNP is worse and the combustion residues are mainly graphene platelets covered with a thin layer of soot, suggesting extinction of liquid droplet before completely running out of the base fuel.

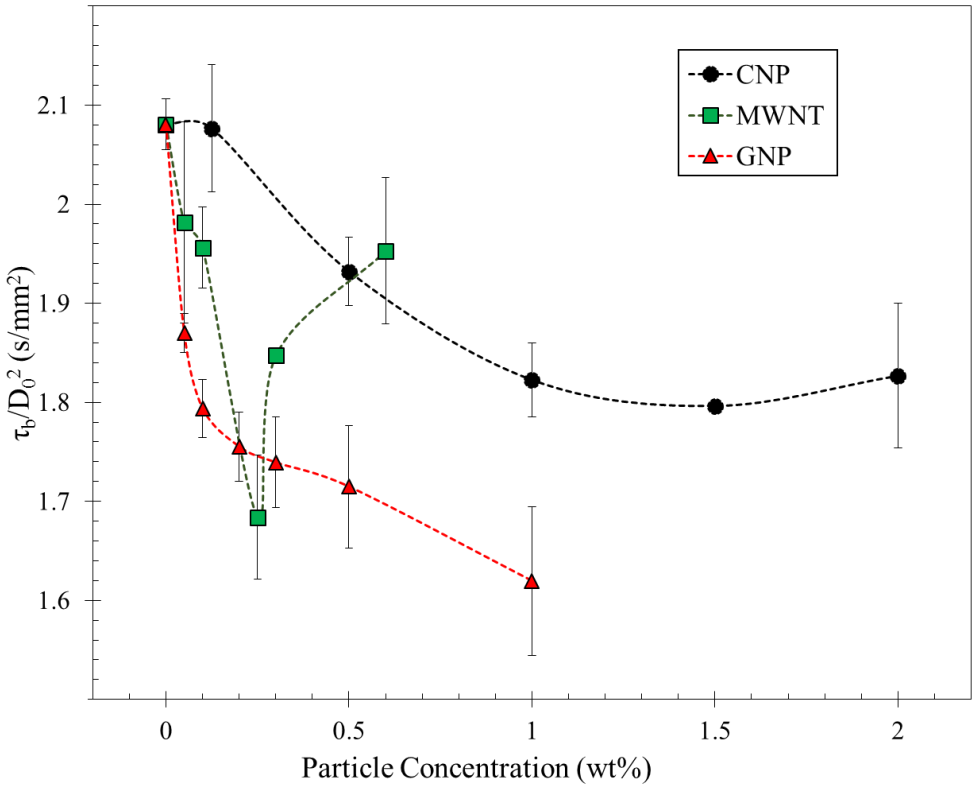

Figure 5.26 Droplet burning time as a function of particle concentration

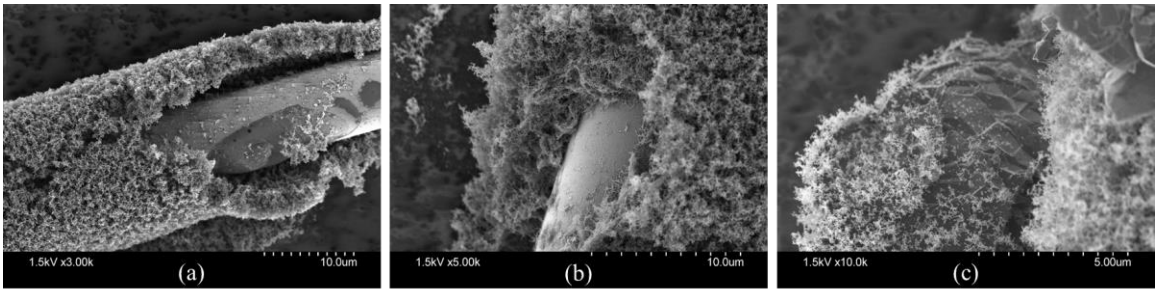

Figure 5.27 SEM images of combustion residues of (a) 0.5% CNP, (b) 0.1% MWNT and (c) 1.0% GNP in jet fuel

5.5 Conclusion and Summary

Combustion of colloidal droplets was studied experimentally to understand the effect of carbon-based nanoparticles. Carbon nanoparticles with different sizes and morphologies (Activated Nano Carbon, Multi-Walled Nanotube and Graphene Platelets) were suspended in ethanol, diesel and jet fuel at different concentrations using an ultrasonic homogenizer. In combustion of colloidal suspensions it was observed that all of the droplets, regardless of base fuel, nanoparticle type and whether or not surfactant had been

added, follow d^2-law of combustion. Furthermore, due to preferential vaporization the base fuel burn first while particles aggregate at the center of droplet and burn in the form of char combustion once the base fuel was mostly depleted. During the liquid combustion, it was observed that the droplet bulges frequently. These bulging are due to the heterogeneous nucleation of liquid fuel on nano particles and increase as the loading of nanoparticle increases. The bulging settles after particles close to the droplet surface leave it through a puffing event.

Burning rate was found to increase with the addition of nanomaterials. Unique optical and thermal properties of carbon nanomaterials is the main reason of the increase in burning rate. Due to their lower transmittance, carbon-based colloids absorb more radiative heat and at the same time improve heat conduction inside the droplet. An optimum particle loading was found for each particle type at which maximum burning rate increase was achieved. This optimum concentration was found to be 1.5%, 0.25% and 0.1% for CNP, MWNT and GNP in jet fuel suspensions, respectively. Among all three tested nanomaterials MWNTs showed a better performance by increasing burning rate more than 10% at a loading of 0.25%. GNPs also showed a promising performance by increasing burning rate more than 7% at a loading of only 0.1%. However, GNPs turned out to be noncombustible and remain unburned after the combustion. Therefore they might act as heat sink and result in flame extinction when the size of aggregates in the droplet is comparable to the base fuel content.

6 CONCLUSIONS AND FUTURE WORK

6.1 Conclusions

In this thesis, combustion dynamics of liquid droplets with polymeric and nanoparticle additives was studied experimentally. Liquid droplets with initial diameters in the range of 0.50-1.00 mm were generated using a microsyringe and ignited on a fiber supported droplet combustion configuration. The whole process (heating, ignition, combustion and extinction) were recorded using two high speed cameras at different angles. The backlit images were analyzed to obtain droplet diameter regression and hence burning rate. The high speed color movie was also used to measure the ignition and extinction time and also to see flame shape during combustion.

Polybutadiene, as a long chain polymer, was added to jet-A, diesel, n-decane, n-dodecane and n-hexadecane at different weight percentages. For all of the fuel mixtures a staged combustion representing separate combustion of base fuel and polymer additive was observed. However, in spite of hydrocarbon binary fuels which burn in only two stages, polymer added fuel burns in four stages, three of which are associated with the more volatile component (i.e. base liquid fuel): an initial steady combustion zone representing pure base fuel combustion, a strong swelling zone, and a weak swelling zone. The physics dominating these regimes could be explained as described next:

In combustion of the polymer-fuel solutions, the base fuel starts to preferentially vaporize and burn first. Hence, it could be concluded that it is the boiling point of the base fuel that controls the diffusion of species to the surface. The burning rate in this zone is very close to that of the base fuel but decreases as the initial concentration of polymer in fuel increases. The extent of this reduction is different in diesel and jet fuel solutions and diesel experiences more reduction. Through viscosity measurements it was determined that higher viscosity of pure diesel is responsible for such behavior. As the base fuel burns in the first zone and its concentration decreases, a layer of polymer is formed at the droplet surface which results in heterogeneous nucleation and bubbling. The burning rate in this stage is equal to that of former stage which means it is still the base fuel which is preferentially vaporizing and burning. Because of shear thickening effects in this regime,

these droplets never experience mass loss due to internal boiling. This is very different from most other types of multicomponent drops where the nucleate boiling regime dominates droplet mass loss. As the concentration of base fuel decreases continuously the viscosity of the droplet increases which suppresses strong swelling. This is the beginning of third stage which has very weak swellings but a higher burning rate. The increased burning rate is believed to be due to the high concentration of polymer which play a role as a thermal bridge and enhance heat transfer inside the droplet. Finally, once the base fuel is mostly depleted, the polymer starts to burn after a short low burning rate transition zone. During this transition zone (which lengthens as polymer content increases) the droplet heats up until the surface temperature reaches the vaporization temperature of the polymer.

The residual soot particles on the fibers were also analyzed by SEM microscopy. Although addition of polymer did not have any influence on the size of individual soot particles, it was observed that polymer addition results in more soot residues and larger aggregates. Three mechanism are thought to be responsible for the generation of large aggregates: polymer combustion, unburned polymer and increased viscosity. Polymers are long chains of carbon atoms that could produce significant amount of soot during combustion. In addition, some of the polymer strands might capture soot particles and make larger aggregates by binding them together. Increased viscosity could also suppress the diffusion of soot precursors to the droplet surface and increases the formation of soot during polymer combustion.

Combustion of nanofluid-type droplets made by suspending carbon-based nanomaterials in ethanol, diesel and jet fuel was also studied experimentally. Several swellings and puffing were observed at higher concentrations of nanoparticles due to internal heterogeneous nucleation. The addition of activated carbon nanoparticles results in a higher average burning rate and a lower extinction volume of the ethanol droplet by means of enhancing heat transfer. Heat transfer within a liquid droplet occurs in both conductive and radiative modes. Nanoparticles could significantly improve thermal conductivity via Brownian motion [70] and also act as thermal bridge [72] when particle diameter is less than 10 nm. Given the average diameter of 100 nm for carbon nanoparticles in this study, enhancement of thermal conductivity (if any) is considered to be negligible.

On the other hand, the properties of solid materials have been shown to improve when crushed into nano-sized particles [111] and act as both emitters and receptors of thermal energy. It has been also shown that CNP in ethanol suspensions absorb more radiative energy and have a much lower transmittance than pure ethanol [82] and therefore use a larger fraction of absorbed radiative energy to internally heat up the liquid droplet.

Multi-Walled Carbon Nanotubes and Graphene Nanoplates were also added to jet fuel to investigate the effect of size and morphology on combustion behavior. Given 8-15 nm diameter of nanotubes and 3-5 nm thickness of plates, enhancement of thermal conductivity could add up to the improved optical properties. Nanotubes are known to have a thermal conductivity as high as, and sometimes even more than, that of diamond (>6000 W/mK). On the other hand, GNP thickness is less than 10 nm and thus the enhancement of thermal conductivity via Brownian motion may become significant. Furthermore, the platelet morphology provides lower thermal contact resistance at lower loading levels, resulting in higher thermal conductivity versus other carbon particle and fibers. Such improved properties result in 10% increase in the burning rate of jet fuel droplets at loadings much less than required CNP loading for the same amount of burning rate increase. However, the agglomeration still remains a challenge especially in MWNT that seem to quickly form a packed aggregate which may remain partly unburned.

6.2 Future Work

The agglomeration of particles was found to be an issue in combustion of colloidal fuels. The size and morphology of nanoparticles was also found to be important parameters in their agglomeration. To improve our limited knowledge about this process it is recommended to perform simple droplet vaporization experiments to measure vaporization rate and to study the morphology of aggregates. Analytical models that take the size and shape of the particle into account are also required to be developed and be tuned with the experimental data.

Even though carbon nanoparticles increase the burning rate of liquid fuels, their own combustion as aggregates and in the form of char is a relatively slow process. If a droplet could be broken into smaller droplets, then the overall combustion time might reduce even more. Adding water to hydrocarbon fuels is known as a mechanism to induce

microexplosion and enhance atomization. Water in fuel emulsions are also known to reduce both NO_x and soot emission. Thus, adding water to colloidal suspensions and studying its combustion is another recommendation for future works in the area of droplet combustion.

Finally, fuel additives cannot be prescribed until their impact on the pollution emission is fully examined. In this study and using Scanning Electron Microscopy the morphology of soot particles and their aggregates was examined. The accumulation of soot on the fiber was also considered as a qualitative measure of soot emission in polymer in fuel solution. However, measuring combustion emissions (especially soot as one of the major pollutants in fossil fuels) in a more quantitative way is imperative. In this regard, experimental techniques such as broadband emission measurement are recommended to be employed in synchrony with other measurements in order to provide a temporal evolution of soot emission during droplet lifetime.

APPENDIX

"Solenoid.ino" that should be uploaded into the Arduino board in order to synchronize solenoids, hot wires and CCD camera:

```
#include "Timer.h"

Timer t;

int CameraEvent;
int HotwireEvent;
int SolenoidEvent;
int fr = 500; //Hz (or frame per second)
int PulseLength = 1000/(2*fr);
int tHotwireON = 4*PulseLength; //Hot wire begins 2 frames after recording starts
int tHeating = 350; //Hotwire heating time (duration) in ms
int tHotwireOFF = tHotwireON + 1.5*tHeating; //Hotwire goes off when its pulse is in the middle of LOW stage
int tSolenoidON = tHotwireON + tHeating; //Solenoid starts right when the Hotwire pulse goes LOW
int tRetraction = 10000; //Solenoid retraction time (duration) in ms
int tAllOFF = tSolenoidON + 1.5*tRetraction;

// the setup routine runs once when you press reset:

void setup()
{
  Serial.begin(9600);
  //Serial.print("Frequency=");
  //Serial.println(fr);
  //Serial.print("Pulse high/low edge lenght=");
  //Serial.println(PulseLength);
```

```
  pinMode(10, OUTPUT);
  CameraEvent = t.oscillate(10, PulseLength, HIGH); //pulse train with frequency = fr
  Serial.print("Camera start time=");
  Serial.println(millis());

  int afterCam = t.after(tHotwireON, runHotwire);
  Serial.print("Hotwire event started id=");
  Serial.println(afterCam);

  int afterHotwire = t.after(tSolenoidON, runSolenoid);

  int afterSolenoid = t.after(tHotwireOFF, stopHotwire);

  int afterAll = t.after(tAllOFF, stopCam);

}

void loop()
{
  t.update();
}

void runHotwire()
{
  pinMode(11, OUTPUT);
  HotwireEvent = t.pulse(11, tHeating, HIGH);
  Serial.print("Hotwire start time=");
  Serial.println(millis());
}
```

```
void runSolenoid()
{
  pinMode(12, OUTPUT);
  SolenoidEvent = t.pulse(12, tRetraction, HIGH);
  Serial.print("Solenoid start time=");
  Serial.println(millis());
}

void stopHotwire()
{
  t.stop(HotwireEvent);
  Serial.print("Hotwire stop time=");
  Serial.println(millis());
}

void stopCam()
{
  t.stop(SolenoidEvent);
  t.stop(CameraEvent);
  digitalWrite(10, LOW);
  Serial.print("Solenoid and Camera stop time=");
  Serial.println(millis());
}
```

REFERENCES

[1] Clerici A., and Alimonti G., 2015, "World energy resources," EPJ Web of Conferences, p. 01001.

[2] 2014, "U.S. Energy Information Administration" [Online]. Available: http://www.eia.gov/energy_in_brief/article/major_energy_sources_and_users.cfm. [Accessed: 21-Oct-2015].

[3] Annamalai K., and Ryan W., 1992, "Interactive processes in gasification and combustion. Part I: Liquid drop arrays and clouds," Progress in energy and combustion science, **18**(3), pp. 221–295.

[4] Law C. K., 1982, "Recent advances in droplet vaporization and combustion," Progress in Energy and Combustion Science, **8**(3), pp. 171–201.

[5] Williams A., 1990, Combustion of liquid fuel sprays, Butterworth-Heinemann.

[6] Wise H., and Agoston G. A., 1958, "Burning of a liquid droplet," Advances in Chemistry Series, (20), pp. 116–135.

[7] Bae J., 2005, "Experimental Observations and Analyses on the Dynamics of Isolated Spherical Droplet Flames Burning in Various Ambient Gases and Pressures," PhD dissertation, Cornell University.

[8] Lee A., and Law C. K., 1992, "An experimental investigation on the vaporization and combustion of methanol and ethanol droplets," Combustion Science and Technology, **86**(1-6), pp. 253–265.

[9] De Blas L. J. M., 1998, "Pollutant formation and interaction in the combustion of heavy liquid fuels," PhD dissertation, University College London.

[10] Green G., and Yan T., 1988, "Determination of jet fuel luminosity- A free droplet technique for assessing fuel effects on combustion performance in aviation turbines," Proceedings of the 23rd Intersociety Energy Conversion Engineering Conference, pp. 291–296.

[11] Wang C. H., Shy K. H., and Lieu L. C., 1996, "An experimental investigation on the ignition delay of fuel droplets," Combustion Science and Technology, **118**(1-3), pp. 63–78.

[12] Takei M., Tsukamoto T., and Niioka T., 1993, "Ignition of blended-fuel droplet in high-temperature atmosphere," Combustion and Flame, **93**(1), pp. 149–156.

[13] Ghamari M., and Ratner A., 2016, "Combustion characteristics of diesel and Jet-A droplets blended with polymeric additive," Fuel, **178**, pp. 63–70.

[14] "NASA Zero Gravity Research Facility" [Online]. Available: http://facilities.grc.nasa.gov/zerog/. [Accessed: 22-Oct-2015].

[15] Dryer F., 1977, "Water addition to practical combustion systems—concepts and applications," Symposium (international) on Combustion, pp. 279–295.

[16] Kadota T., and Yamasaki H., 2002, "Recent advances in the combustion of water fuel emulsion," Progress in Energy and Combustion Science, **28**(5), pp. 385–404.

[17] Weatherford Jr W., and Naegeli D. W., 1982, "Research on fire-resistant diesel fuel flammability mitigation mechanisms," AFLRL Report No. 165, U.S. Army Fuels and Lubricants Research Laboratory, Southwest Research Institute, San Antonio, Texas.

[18] Law C. K., 1981, "On the fire resistant nature of oil/water emulsions," Fuel, **60**(10), pp. 998 – 999.

[19] David R. A., Wei M. H., Liu D., Bathel B. F., Plog J. P., Ratner A., and Kornfield J. A., 2009, "Effects of pairwise, self-associating functional side groups on polymer solubility, solution viscosity, and mist control," Macromolecules, **42**(4), pp. 1380–1391.

[20] "Fire-Resistant Combustion" [Online]. Available: http://www.swri.org/4org/program/tardec/mission.htm. [Accessed: 22-Oct-2015].

[21] Godsave G., 1953, "Studies of the combustion of drops in a fuel spray—the burning of single drops of fuel," Symposium (International) on Combustion, pp. 818–830.

[22] Spalding D. B., 1953, "The combustion of liquid fuels," Symposium (international) on Combustion, pp. 847–864.

[23] Williams A., 1973, "Combustion of droplets of liquid fuels: a review," Combustion and Flame, **21**(1), pp. 1–31.

[24] Ross H. D., 2001, Microgravity combustion: fire in free fall, Academic Press.

[25] Faeth G., 1977, "Current status of droplet and liquid combustion," Progress in Energy and Combustion Science, **3**(4), pp. 191–224.

[26] Sirignano W. A., 1983, "Fuel droplet vaporization and spray combustion theory," Progress in Energy and Combustion Science, **9**(4), pp. 291–322.

[27] Chiu H. H., 2000, “Advances and challenges in droplet and spray combustion. I. Toward a unified theory of droplet aerothermochemistry,” Progress in Energy and Combustion Science, **26**(4-6), pp. 381–416.

[28] Law C. K., 2006, “Multicomponent Droplet Combustion,” Combustion Physics, Cambridge University Press, New York, pp. 585–602.

[29] Law C. K., 1978, “Internal boiling and superheating in vaporizing multicomponent droplets,” AIChE Journal, **24**(4), pp. 626–632.

[30] Lasheras J., Fernandez-Pello A., and Dryer F., 1980, “Experimental observations on the disruptive combustion of free droplets of multicomponent fuels,” Combustion Science and Technology, **22**(5-6), pp. 195–209.

[31] Wang C. H., Liu X. Q., and Law C. K., 1984, “Combustion and microexplosion of freely falling multicomponent droplets,” Combustion and Flame, **56**(2), pp. 175–197.

[32] Mikami M., and Kojima N., 2002, “An experimental and modeling study on stochastic aspects of microexplosion of binary-fuel droplets,” Proceedings of the Combustion Institute, **29**(1), pp. 551–559.

[33] Tsue M., Segawa D., Kadota T., and Yamasaki H., 1996, “Observation of sooting behavior in an emulsion droplet flame by planar laser light scattering in microgravity,” Symposium (International) on Combustion, pp. 1251–1258.

[34] Nazha M., and Crookes R., 1985, “Effect of water content on pollutant formation in a burning spray of water-in-diesel fuel emulsion,” Symposium (International) on Combustion, pp. 2001–2010.

[35] Sjogren A., 1977, “Burning of water-in-oil emulsions,” Symposium (International) on Combustion, pp. 297–305.

[36] Jacques M., Jordan J., Williams A., and Hadley-Coates L., 1977, “The combustion of water-in-oil emulsions and the influence of asphaltene content,” Symposium (International) on Combustion, pp. 307–319.

[37] Ocampo-Barrera R., Villasenor R., and Diego-Marin A., 2001, “An experimental study of the effect of water content on combustion of heavy fuel oil/water emulsion droplets,” Combustion and Flame, **126**(4), pp. 1845–1855.

[38] Law C. K., Lee C. H., and Srinivasan N., 1980, “Combustion characteristics of water-in-oil emulsion droplets,” Combustion and Flame, **37**, pp. 125–143.

[39] Avedisian C. T., and Andres R. P., 1978, "Bubble nucleation in superheated liquid—liquid emulsions," Journal of Colloid and Interface Science, **64**(3), pp. 438–453.

[40] Jackson G., and Avedisian C., 1998, "Combustion of unsupported water-in-n-heptane emulsion droplets in a convection-free environment," International Journal of Heat and Mass Transfer, **41**(16), pp. 2503–2515.

[41] Lasheras J., Yap L., and Dryer F., 1985, "Effect of the ambient pressure on the explosive burning of emulsified and multicomponent fuel droplets," Symposium (International) on Combustion, pp. 1761–1772.

[42] Watanabe H., Suzuki Y., Harada T., Matsushita Y., Aoki H., and Miura T., 2010, "An experimental investigation of the breakup characteristics of secondary atomization of emulsified fuel droplet," Energy, **35**(2), pp. 806–813.

[43] Watanabe H., Matsushita Y., Aoki H., and Miura T., 2010, "Numerical simulation of emulsified fuel spray combustion with puffing and micro-explosion," Combustion and Flame, **157**(5), pp. 839–852.

[44] Owens E. C., and Wright B. R., 1976, "Engine performance and fire-safety characteristics of water-containing diesel fuels," AFLRL Report No. 83, U.S. Army Fuels and Lubricants Research Laboratory, Southwest Research Institute, San Antonio, Texas.

[45] Wang C. H., and Law C. K., 1985, "Microexplosion of fuel droplets under high pressure," Combustion and Flame, **59**(1), pp. 53–62.

[46] Kadota T., Hiroyasu H., and OYA H., 1976, "Spontaneous ignition delay of a fuel droplet in high pressure and high temperature gaseous environments," Bulletin of JSME, **19**(130), pp. 437–445.

[47] Saitoh T., Ishiguro S., and Niioka T., 1982, "An experimental study of droplet ignition characteristics near the ignitable limit," Combustion and Flame, **48**, pp. 27–32.

[48] Bergeron C., and Hallett W., 1989, "Autoignition of single droplets of two-component liquid fuels," Combustion Science and Technology, **65**(4-6), pp. 181–194.

[49] Gong J.-S., and Fu W.-B., 2001, "A study on the effect of more volatile fuel on evaporation and ignition for emulsified oil," Fuel, **80**(3), pp. 437–445.

[50] Segawa D., Kadota T., Kohama R., and Enomoto H., 2000, "Ignition of binary mixture droplets by a propagating laminar flame," Proceedings of the Combustion Institute, **28**(1), pp. 961–968.

[51] Jeong I., and Lee K., 2008, "Auto-ignition and micro-explosion behaviors of droplet arrays of water-in-fuel emulsion," International Journal of Automotive Technology, **9**(6), pp. 735–740.

[52] Jeong I., Lee K.-H., and Kim J., 2008, "Characteristics of auto-ignition and micro-explosion behavior of a single droplet of water-in-fuel," Journal of Mechanical Science and Technology, **22**(1), pp. 148–156.

[53] Awasthi I., Pope D. N., and Gogos G., 2014, "Effects of the ambient temperature and initial diameter in droplet combustion," Combustion and Flame, pp. 1883–1899.

[54] Hara H., and Kumagai S., 1994, "The effect of initial diameter on free droplet combustion with spherical flame," Symposium (International) on Combustion, pp. 423–430.

[55] Nakaya S., Fujishima K., Tsue M., Kono M., and Segawa D., 2012, "Effects of droplet diameter on instantaneous burning rate of isolated fuel droplets in argon-rich or carbon dioxide-rich ambiences under microgravity," Proceedings of the Combustion Institute, pp. 1601–1608.

[56] Oliver D., and Bakhtiyarov S., 1983, "Drag reduction in exceptionally dilute polymer solutions," Journal of Non-Newtonian Fluid Mechanics, **12**(1), pp. 113–118.

[57] Ram A., Finkelstein E., and Elata C., 1967, "Reduction of friction in oil pipelines by polymer additives," Industrial & Engineering Chemistry Process Design and Development, **6**(3), pp. 309–313.

[58] Chao K., Child C., Grens E., and Williams M., 1984, "Antimisting action of polymeric additives in jet fuels," AIChE Journal, **30**(1), pp. 111–120.

[59] Kashiwagi T., 1994, "Polymer combustion and flammability—role of the condensed phase," Symposium (International) on Combustion, pp. 1423–1437.

[60] Yang J. C., Hamins A., and Donnelly M. K., 2000, "Reduced gravity combustion of thermoplastic spheres," Combustion and Flame, **120**(1), pp. 61–74.

[61] Saito T., and Iwama A., 1975, "Combustion of polymer fuel-spheres at elevated pressures," Bulletin of the Chemical Society of Japan, **48**(1), pp. 175–183.

[62] Panagiotou T., and Levendis Y., 1994, “A study on the combustion characteristics of PVC, poly (styrene), poly (ethylene), and poly (propylene) particles under high heating rates,” Combustion and Flame, **99**(1), pp. 53–74.

[63] Waibel R. T., and Essenhigh R. H., 1973, “Combustion of thermoplastic polymer particles in various oxygen atmospheres: comparison of theory and experiment,” Symposium (International) on Combustion, pp. 1413–1420.

[64] Raghunandan B. N., and Mukunda H. S., 1977, “Combustion of polystyrene spheres in air,” Fuel, **56**(3), pp. 271–276.

[65] Solomon Y., Natan B., and Cohen Y., 2009, “Combustion of gel fuels based on organic gellants,” Combustion and Flame, **156**(1), pp. 261–268.

[66] Mishra D., Patyal A., and Padhwal M., 2011, “Effects of gellant concentration on the burning and flame structure of organic gel propellant droplets,” Fuel, **90**(5), pp. 1805–1810.

[67] Liu Z., Hu X., He Z., and Wu J., 2012, “Experimental study on the combustion and microexplosion of freely falling gelled unsymmetrical dimethylhydrazine (UDMH) fuel droplets,” Energies, **5**(8), pp. 3126–3136.

[68] Choi S. U. S., and Eastman J. A., 1995, “Enhancing thermal conductivity of fluids with nanoparticles,” International Mechanical Engineering Congress and Exposition, ASME, pp. 99–106.

[69] Choi S. U., 2009, “Nanofluids: from vision to reality through research,” Journal of Heat Transfer, **131**(3), p. 033106.

[70] Jang S. P., and Choi S. U., 2004, “Role of Brownian motion in the enhanced thermal conductivity of nanofluids,” Applied Physics Letters, **84**(21), pp. 4316–4318.

[71] Prasher R., Bhattacharya P., and Phelan P. E., 2005, “Thermal conductivity of nanoscale colloidal solutions (nanofluids).,” Physical Review Letters, **94**(2), p. 025901.

[72] Yu W., and Choi S., 2004, “The role of interfacial layers in the enhanced thermal conductivity of nanofluids: a renovated Hamilton-Crosser model,” Journal of Nanoparticle Research, **6**(4), pp. 355–361.

[73] Xuan Y., Li Q., and Hu W., 2003, “Aggregation structure and thermal conductivity of nanofluids,” AIChE Journal, **49**(4), pp. 1038–1043.

[74] Liu G. E., and Law C. K., 1986, “Combustion of coal-water slurry droplets,” Fuel, **65**(2), pp. 171–176.

[75] Miyasaka K., and Law C. K., 1980, “Combustion and agglomeration of coal-oil mixtures in furnace environments,” Combustion Science and Technology, **24**(1-2), pp. 71–82.

[76] Sabourin J. L., Dabbs D. M., Yetter R. A., Dryer F. L., and Aksay I. A., 2009, “Functionalized graphene sheet colloids for enhanced fuel/propellant combustion.,” ACS Nano, **3**(12), pp. 3945–54.

[77] Sabourin J. L., Yetter R. A., and Parimi V. S., 2010, “Exploring the effects of nanostructured particles on liquid nitromethane combustion,” Journal of Propulsion and Power, **26**(5), pp. 1006–1015.

[78] Jones M., Li C. H., Afjeh A., and Peterson G., 2011, “Experimental study of combustion characteristics of nanoscale metal and metal oxide additives in biofuel (ethanol).,” Nanoscale Research Letters, **6**(1), p. 246.

[79] Allen C., Mittal G., Sung C.-J., Toulson E., and Lee T., 2011, “An aerosol rapid compression machine for studying energetic-nanoparticle-enhanced combustion of liquid fuels,” Proceedings of the Combustion Institute, **33**(2), pp. 3367–3374.

[80] Gan Y., and Qiao L., 2011, “Evaporation characteristics of fuel droplets with the addition of nanoparticles under natural and forced convections,” International Journal of Heat and Mass Transfer, **54**(23), pp. 4913–4922.

[81] Xu J., and Qiao L., 2013, “Radiation-Induced Droplet Breakup of Nano-Dispersed Coal-in-Water Colloidal Fuels,” AIAA/ASME/SAE/ASEE Joint Propulsion Conference, pp. 1–14.

[82] Gan Y., and Qiao L., 2012, “Optical properties and radiation-enhanced evaporation of nanofluid fuels containing carbon-based nanostructures,” Energy & Fuels, **26**(7), pp. 4224–4230.

[83] Avedisian C. T., and Jackson G. S., 2000, “Soot patterns around suspended n-heptane droplet flames in a convection-free environment,” Journal of Propulsion and Power, **16**(6), pp. 974–979.

[84] “TEMCo Industrial Power Supply: Kenthal Wire Data Sheet” [Online]. Available: http://attachments.temcoindustrialpower.com/Data_sheet/kanthal_wire_data_sheet.pdf. [Accessed: 19-Jun-2016].

[85] "National Transportation Safety Board, '2010-2011 Transportation Fatalities'" [Online]. Available: www.ntsb.gov/data/datafiles/2010_2011_stats_chart.doc. [Accessed: 27-Mar-2013].

[86] Bunn T., Slavova S., and Robertson M., 2012, "Crash and burn? Vehicle, collision, and driver factors that influence motor vehicle collision fires," Accident Analysis and Prevention, **47**, pp. 140–145.

[87] Shaw B., and Williams F., 1990, "Theory of influence of a low-volatility, soluble impurity on spherically-symmetric combustion of fuel droplets," International Journal of Heat and Mass Transfer, **33**(2), pp. 301–317.

[88] Dryer F., Rambach G., and Glassman I., 1976, "Some preliminary observations on the combustion of heavy fuels and water-in-fuel emulsions," Presented at the Central Section Meeting of the Combustion Institute, Columbus, OH.

[89] Lasheras J., Fernandez-Pello A., and Dryer F., 1979, "Initial Observations on the Free Droplet Combustion Characteristics of Water-In-Fuel Emulsions," Combustion Science and Technology, **21**(1-2), pp. 1–14.

[90] Watanabe H., Harada T., Matsushita Y., Aoki H., and Miura T., 2009, "The characteristics of puffing of the carbonated emulsified fuel," International Journal of Heat and Mass Transfer, **52**(15), pp. 3676–3684.

[91] Bae J., and Avedisian C., 2004, "Experimental study of the combustion dynamics of jet fuel droplets with additives in the absence of convection," Combustion and Flame, **137**(1), pp. 148–162.

[92] Klimek R., and Wright T., 2004, "Spotlight: Image Analysis and Object Tracking Software" [Online]. Available: http://microgravity.grc.nasa.gov/spotlight/. [Accessed: 20-Feb-2013].

[93] Yang J. C., Hamins A., and Donnelly M. K., 1999, Combustion of a polymer (PMMA) sphere in microgravity, US Department of Commerce, Technology Administration, National Institute of Standards and Technology, Building and Fire Research Laboratory, Gaithersburg, Maryland.

[94] Essenhigh R., and Dreier W., 1969, "Combustion behavior of thermoplastic polymer spheres burning in quiescent atmospheres of air," Fuel, **48**, pp. 330–342.

[95] Vargaftik N., Volkov B., and Voljak L., 1983, "International tables of the surface tension of water," Journal of Physical and Chemical Reference Data, **12**(3), pp. 817–820.

[96] Vazquez G., Alvarez E., and Navaza J. M., 1995, "Surface tension of alcohol water+ water from 20 to 50. degree. C," Journal of Chemical and Engineering Data, **40**(3), pp. 611–614.

[97] Avedisian C. T., and Fatehi M., 1988, "An experimental study of the Leidenfrost evaporation characteristics of emulsified liquid droplets," International Journal of Heat and Mass Transfer, **31**(8), pp. 1587–1603.

[98] Köylü U. O., and Faeth G., 1993, "Radiative Properties of Flame-Generated Soot," Journal of Heat Transfer, **115**(2), p. 409–417.

[99] Ghamari M., and Ratner A., 2015, "Experimental study of combustion of polymer added n-Decane and n-Dodecane droplets," 9th US National Combustion Meeting Organized by the Central States Section of the Combustion Institute (May 17-20, 2015).

[100] Ghamari M., and Ratner A., 2015, "Experimental Study of Combustion of Polymer Added n-Decane and n-Dodecane Droplets," ASME 2015 International Mechanical Engineering Congress and Exposition, pp. V08AT10A059–V08AT10A059.

[101] Sabourin J. L., Yetter R. A., Asay B. W., Lloyd J. M., Sanders V. E., Risha G. A., and Son S. F., 2009, "Effect of Nano-Aluminum and Fumed Silica Particles on Deflagration and Detonation of Nitromethane," Propellants, Explosives, Pyrotechnics, **34**(5), pp. 385–393.

[102] Tyagi H., Phelan P. E., Prasher R., Peck R., Lee T., Pacheco J. R., and Arentzen P., 2008, "Increased hot-plate ignition probability for nanoparticle-laden diesel fuel," Nano Letters, **8**(5), pp. 1410–1416.

[103] Gan Y., and Qiao L., 2011, "Combustion characteristics of fuel droplets with addition of nano and micron-sized aluminum particles," Combustion and Flame, **158**(2), pp. 354–368.

[104] Urban B. D., Kroenlein K., Kazakov A., Dryer F. L., Yozgatligil A., Choi M. Y., Manzello S. L., Lee K. O., and Dobashi R., 2004, "Sooting behavior of ethanol droplet combustion at elevated pressures under microgravity conditions," Microgravity-Science and Technology, **15**(3), pp. 12–18.

[105] Chen H., Ding Y., and Tan C., 2007, "Rheological behaviour of nanofluids," New journal of physics, **9**(10), p. 367.

[106] Kim S., Bang I. C., Buongiorno J., and Hu L., 2007, "Surface wettability change during pool boiling of nanofluids and its effect on critical heat flux," International Journal of Heat and Mass Transfer, **50**(19), pp. 4105–4116.

[107] Eastman J. A., Phillpot S., Choi S., and Keblinski P., 2004, "Thermal transport in nanofluids," Annu. Rev. Mater. Res., **34**, pp. 219–246.

[108] Kim P., Shi L., Majumdar A., and McEuen P., 2001, "Thermal transport measurements of individual multiwalled nanotubes," Physical Review Letters, **87**(21), pp. 215502/1–215502/4.

[109] Berber S., Kwon Y.-K., and Tománek D., 2000, "Unusually high thermal conductivity of carbon nanotubes," Physical Review Letters, **84**(20), pp. 4613–4616.

[110] Wang B.-X., Zhou L.-P., and Peng X.-F., 2003, "A fractal model for predicting the effective thermal conductivity of liquid with suspension of nanoparticles," International Journal of Heat and Mass Transfer, **46**(14), pp. 2665–2672.

[111] Ichinose N., Ozaki Y., and Kashu S., 1992, "Fundamentals of Superfine Particles," Superfine Particle Technology, Springer Science & Business Media, pp. 1–20.